PROBING SIGNS OF NEW PHYSICS AT LOW ENERGIES: THE NEUTRINO CASE

A THESIS SUBMITTED TO
THE GRADUATE SCHOOL OF NATURAL AND APPLIED SCIENCES
OF
MIDDLE EAST TECHNICAL UNIVERSITY

BY

ALTUĞ ELPE

IN PARTIAL FULFILLMENT OF THE REQUIREMENTS
FOR
THE DEGREE OF DOCTOR OF PHILOSOPHY
IN
PHYSICS

JANUARY 2023

Approval of the thesis:

PROBING SIGNS OF NEW PHYSICS AT LOW ENERGIES: THE NEUTRINO CASE

submitted by **ALTUĞ ELPE** in partial fulfillment of the requirements for the degree of **Doctor of Philosophy in Physics Department, Middle East Technical University** by,

Prof. Dr. Halil Kalıpçılar
Dean, Graduate School of **Natural and Applied Sciences**　——————————

Prof. Dr. Seçkin Kürkcüoğlu
Head of Department, **Physics**　——————————

Prof. Dr. İsmail Turan
Supervisor, **Physics, METU**　——————————

Assoc. Prof. Dr. Levent Selbuz
Co-supervisor, **Physics Engineering, Ankara University**　——————————

Examining Committee Members:

Prof. Dr. Orhan Çakır
Physics, Ankara University　——————————

Prof. Dr. İsmail Turan
Physics, METU　——————————

Prof. Dr. İnanç Şahin
Physics, Ankara University　——————————

Prof. Dr. Altuğ Özpineci
Physics, METU　——————————

Prof. Dr. Tahmasib M. Aliev
Physics, METU　——————————

Date: 27.01.2023

I hereby declare that all information in this document has been obtained and presented in accordance with academic rules and ethical conduct. I also declare that, as required by these rules and conduct, I have fully cited and referenced all material and results that are not original to this work.

Name, Surname: Altuğ Elpe

Signature   :

ABSTRACT

PROBING SIGNS OF NEW PHYSICS AT LOW ENERGIES: THE NEUTRINO CASE

Elpe, Altuğ

Ph.D., Department of Physics

Supervisor: Prof. Dr. İsmail Turan

Co-Supervisor: Assoc. Prof. Dr. Levent Selbuz

January 2023, 99 pages

Neutrinos have a special place in particle physics. They are spin-1/2, electrically neutral, nearly massless, and very weakly interacting particles. Properties of weak interactions can be conveniently studied through neutrinos. They are assumed to be sensitive to new physics effects. Moreover, searching for new physics at low energies has its motivations based on the null results about new physics at high energies coming out of Hadron Colliders' data. One of the favorite signs of new physics at low energies would be the so-called dark sector, which would show some sizable effects in neutrino scattering experiments. This thesis analyzes Abelian dark sector scenarios embedded into the two-Higgs doublet models through the Coherent Elastic Neutrino-Nucleus Scattering experiment, which was first measured by the COHERENT Collaboration in 2017. The theoretical framework assumes that there is a U(1) gauge group in the dark sector with a non-zero kinetic mixing with the hypercharge field. Moreover, the scalar sector of the Standard Model is extended with a second doublet which, under certain assumptions, makes mass mixing between the dark gauge field and neutral electroweak fields possible. The COHERENT data for the CsI and liquid argon (LAr) targets are used to constraint the multi-

dimensional parameter space, spanned by the dark gauge coupling, kinetic mixing parameter, and the dark photon mass, for a total of seven different representative scenarios, which are also compared and contrasted among each other to find out about the most sensitive one to the data.

ÖZ

YENİ FİZİĞİN İZLERİNİN DÜŞÜK ENERJİLERDE ARAŞTIRILMASI: NÖTRİNO DURUMU

Elpe, Altuğ

Doktora, Fizik Bölümü

Tez Yöneticisi: Prof. Dr. İsmail Turan

Ortak Tez Yöneticisi: Doç. Dr. Levent Selbuz

Ocak 2023 , 99 sayfa

Nötrinoların parçacık fiziğinde özel bir yeri vardır. Spin-1/2, elektriksel olarak nötr, neredeyse kütlesiz ve çok zayıf etkileşen parçacıklardır. Zayıf etkileşimlerin özellikleri, nötrinolar aracılığıyla rahatlıkla incelenebilir. Yeni fizik etkilerine duyarlı oldukları varsayılmaktadır. Ayrıca, düşük enerjilerde yeni fizik arayışı, Hadron Çarpıştırıcılarının verilerinden yüksek enerjilerde yeni fizik hakkında değeri olmayan sonuçlara dayanan motivasyonlara sahiptir. Düşük enerjilerde yeni fiziğin en önemli işaretlerinden biri, nötrino saçılma deneylerinde bazı büyük etkiler göstermesi beklenen ve karanlık olarak adlandırılan sektördür. Bu tez, ilk olarak 2017'de COHERENT Collaboration tarafından ölçülen Tutarlı Elastik Nötrino-Çekirdek Saçılımı deneyi aracılığıyla iki Higgs ikili modellerine gömülü Abelyen karanlık sektör senaryolarını analiz eder. Teorik çerçeve hiperyük alanı ile kinetik karışıma giren bir karanlık sektör U(1) ayar alanı varsayar. Ayrıca, Standart Modelin skaler sektörü, belirli varsayımlar altında karanlık ayar alanı ile nötr elektrozayıf alanlar arasında kütle karışımını mümkün kılan ikinci bir ikili ile genişletilir. CsI ve sıvı argon (LAr)

hedefleri için COHERENT verileri, toplam yedi farklı temsili senaryo için karanlık çiftlenim sabiti, kinetik karışım parametresi ve karanlık foton kütlesi tarafından yayılan çok boyutlu parametre uzayını kısıtlamak için kullanılır. Verilere en duyarlı olanı bulmak için bunlar da birbirleriyle karşılaştırılır.

Anahtar Kelimeler: Yeni Fizik, SMÖ, Vektör Bozon, Nötrino, COHERENT Kolaborasyonu

Dedicated to my mother

ACKNOWLEDGMENTS

I am grateful to my thesis supervisor, İsmail Turan, for his support, encouragement, and guidance throughout my thesis study. His expertise and knowledge in the field have been instrumental in shaping my research and providing me with insights that have been invaluable in my academic and personal growth. I am grateful for his availability and willingness to answer my questions, listen to my concerns, and provide feedback and suggestions.

I want to extend my gratitude to my co-advisor, Levent Selbuz, who has been collaborating with İsmail Turan's group on many projects. His help throughout my thesis study was very valuable.

I am also deeply grateful to all professors in our department, especially Tahmasib Aliev and Altuğ Özpineci, for their support in my studies. Their thoughtful critiques and suggestions have helped me refine and strengthen my work. Their willingness to engage in thoughtful discussions and debates has been an invaluable resource. Beyond their academic contributions, I also want to express my appreciation for the personal support that they have provided me.

I want to express my deepest gratitude to my family for their love, support, and encouragement throughout my academic journey. Their constant belief in me has been a source of motivation that has carried me through the most challenging times of my thesis project. I am grateful for their unwavering support, sacrifices, and encouragement, which have allowed me to pursue my dreams.

Lastly, I would like to thank all my friends, especially Esra Akyumuk, a grad student in Ismail Turan's group, for their discussions and help throughout my studies.

TABLE OF CONTENTS

LIST OF TABLES

LIST OF ABBREVIATIONS

2HDM	Two Higgs Doublet Model
BSM	Beyond the Standard Model
CEνNS	Coherent Elastic Neutrino Nucleus Scattering
CMB	Cosmic Microwave Background
DM	Dark Matter
EW	Electroweak
FCNC	Flavor Changing Neutral Currents
KM	Kinetic Mixing
NFC	Natural Flavor Conservation
PE	Photoelectron
POT	Proton on target
QED	Quantum Electrodynamics
QF	Quenching Factor
SM	Standard Model
vev	Vacuum Expectation Value

CHAPTER 1

INTRODUCTION

The Standard Model (SM) is the most valid model in existence today that describes the fundamental particles, which are the building blocks of the universe, and their fundamental interactions. It is powerful enough to explain almost all observed phenomena within the electromagnetic, weak, and strong interaction domains [1]. However, it is unable to provide a complete picture of the subatomic world. Therefore, it is considered to be an incomplete theory. The shortcomings of SM under three categories are given below.

1. Structural failures:

- One critical issue is that physicists are unable to incorporate gravity into this framework.

- Neutrino oscillations observed in 1998 by Super-Kamiokande Collaboration [6] point to the existence of neutrino masses which are not predicted by the SM.

- The vacuum of the universe has a uniform energy density that is related to its expansion. This energy is associated with the cosmological constant in General Relativity. The observed cosmological constant is small but non-zero. The Standard Model lacks a mechanism for generating a non-zero cosmological constant and provides no explanation for the origin of this energy [7].

2. Cosmological problems that the SM based models fail to explain:

- There is an excess of matter over anti-matter in the observable universe.

---

[1] As an example, see the results of regularly performed electroweak precision tests, given in Table 4.2 of [5]

Although there is a possible CP violation in the quark sector, cosmological models based solely on it are unable to explain the observed discrepancy [8].

- Cosmological observations suggest that %85 of all the material in the universe eluded our observations and have exotic futures. This material is referred to as dark matter, and there is no viable candidate for this material in the SM that fits the expected profile[9].

3. The so-called fine-tuning problems:

- There is a phase in the quark sector that leads to CP violation in strong interactions. However, no such violation is observed. This means that the phase is, or is close to zero. When a parameter is zero, physicists expect the existence of an underlying symmetry that drives that parameter to zero. SM does not provide a reason for this particular value of the parameter. This is called the Strong CP Problem [10].

- Quantum corrections from heavy particles at all energy scales contribute to the calculation of Higgs boson mass and drag it upwards. The Higgs mass should be much larger than what has been observed. It is unclear why quantum corrections do not increase the mass of the Higgs boson significantly. To make our calculations sense, the Higgs mass must be precisely adjusted so that the quantum corrections are canceled out [11].

This thesis investigates the possible interactions between the SM particles and the dark sector where a possible candidate for dark matter may also originate from.

The dark matter problem is one of the fundamental problems in cosmology and astrophysics. There is overwhelming evidence for gravitational effects caused by a non-luminous material that corresponds to the majority of the mass in the universe. Various astrophysical observations on large scale structures indicate that galaxies and clusters are surrounded by this material.

The first evidence for the existence of dark matter came from Fritz Zwicky's observations on the motions of galaxies in Coma Clusters in 1933 [12] that concluded

the gravity from visible material is insufficient to account for the galaxies' fast orbits. He coined the term "dark matter" to refer to the invisible material that should exist to hold the galaxies in the cluster. Shortly after, unexpectedly high velocities of galaxies are also observed in the Virgo cluster [13]. Similar behavior is observed within the individual galaxies for the first time in the 70s. Rubin and his collaborators measured the rotation speed of the galactic disks of Andromeda and other spiral galaxies. They observed that the speed of the luminous material at the outskirts did not decrease as expected from the galaxies' densities but maintained an approximately constant speed [14, 15], which suggests a dark matter density proportional to the distance from the galaxy center. Similar observations on other galaxies supported and expanded this finding [16].

Evidence for missing material is also obtained by another method for mass measurement, gravitational lensing. Galaxies and clusters bend the light that comes from an object behind them, acting like a lens. If the distance between two objects is known, the resulting lensing pattern can be expressed in terms of the mass distribution of the foreground object. Galaxy mass measurements are also performed by studying X-ray emissions from intergalactic gas. Gas forms clusters of high-temperature plasma that emits X-rays. Being dependent on the kinetic energy of the gas, the wavelength of this emission can be related to the gravitational potential of the galaxy cluster. A significant finding is obtained in the observation of colliding galaxies, first on Bullet Cluster. Due to collision, the intergalactic gas is observed to slow down, heat up, and emit X-rays. Compared to the mass distribution measured by gravitational lensing, the galaxy cluster mass center appeared to separate from luminous material [17, 18]. This indicates that this problem cannot be solved by only modifying gravitation theory.

Apart from galactic surveillance, cosmological observations may hint at the existence of dark matter. Our current understanding of the early universe heavily relies on the gravitational effects of non-baryonic dark matter. The Cosmic Microwave Background (CMB) radiation reveals essential information about the universe's early history and formation of large-scale structures. Small fluctuations in the temperature and density of the CMB are linked to galaxy formations, and other large-scale structures [10]. Simulations of the universe with dark matter can re-

produce the observed large-scale structure as well as the temperature and density fluctuations seen in CMB radiation [19].

A DM candidate has to satisfy a number of criteria to produce the observed effects. It has to be non-baryonic, electrically neutral, and have restricted self-interaction [20]. In order to explain the early universe, the DM might have additional constraints on its mass, production mechanism, stability, and kinetic energy depending on the cosmological model. The most researched DM candidates originate from theories motivated by solving other problems in particle physics. They include the lightest supersymmetric particles, axions, Kaluza-Klein particles, sterile neutrinos, and inert Higgs doublets [21] that come along with new mechanisms. None of these particles have been observed up until this day.

An alternative approach to the conceptualization of dark matter can be taken. The DM does not need to be described by a single particle and a single interaction. It is plausible to consider the DM as part of a larger dark sector parallel to the visible sector represented by the SM. This new sector could contain the DM, new gauge interactions, and other dark particles. There is no reason to assume the physics in the dark sector not to be extensive like the visible sector. After all, the current paradigm expects the dark matter to be produced through BSM mechanisms.

The primary interaction between the visible sector and the dark sector is gravity. If gravity is the only interaction between the sectors, the dark sector stays hidden. However, it is possible that other weak interactions between sectors exist. If signs of a new interaction in the visible sector are detected, it can be used to probe the dark sector (see Fig. 1.1). It is always possible to consider the SM particle coupling to a gauge boson from a new gauge group that also couples to dark sector particles. Moreover, this generic type of connection is not the only way to form communication between sectors. It is possible to construct gauge invariant terms that combine fields from two sectors. Possible combinations called portals; that are not suppressed by the energy scale are given in Table 1.1.

In this thesis, the vector portal scenario is examined. The dark sector particle, in this case, is known as the dark photon [22]. It is analogous to the SM photon because it arises from a U(1) symmetry and mediates a dark force. It is possible to

Table 1.1: Possible portals between the visible and dark sectors

Portal	Dark Sector particle	Operators
Vector	Dark Photon (X_μ^0)	$\epsilon Y_{\mu\nu} X^{0\mu\nu}$
Higgs	Dark Scalar (S)	$(\mu S + \lambda S^2)\phi^\dagger \phi$
Axion	Pseudo Scalar (a)	$(a/f_a)F_{\mu\nu}\tilde{F}^{\mu\nu}, (a/f_a)G_{i\mu\nu}\tilde{G}_i^{\mu\nu}, (1/f_a)\partial_\mu a\bar{\psi}\gamma^\mu\gamma^5\psi$
Neutrino	Sterile Neutrino (n)	$y_n L\phi n.$
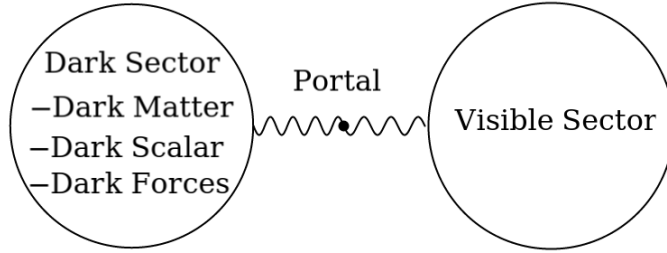
Figure 1.1: Description of dark and visible sectors communicating through a portal

form a gauge invariant term by coupling the dark vector field strength tensor with the one belonging to the weak hypercharge group $U(1)_Y$. The strength of this coupling is described by the kinetic mixing parameter $\sin\epsilon$. This parameter acts as a small perturbation to the SM, so its value is highly suppressed. Moreover, the dark photon can be massive. However, the dark sector is considered to play a role in the formation of the early universe. Models with light dark photon reproduce the observations on CMB radiation. Therefore, the dark photon mass is typically considered at most in the MeV range.

There are various approaches to detecting dark photons if they exist. The cosmological searches involve measurements of cosmic rays, looking for a characteristic excess of energy, and looking for distortions in the temperature and polarization in the CMB radiation. On the other hand, ground-based experiments allow the production and direct detection of BSM particles in the laboratory. Due to the dark photon's small mass and weak interaction, it is impossible to separate and detect it in high-energy experiments such as Large Hadron Collider. In order to detect such particles, low-energy experiments are proposed and built.

A suitable low energy phenomena for dark photon search is the coherent elastic neutrino-nucleus scattering (CEνNS). In 1974, Freedman theorized that elastic neutrino nucleus scattering occurs coherently when the incident neutrino energy is less than ≈ 50 MeV [23]. At such low energies, neutrino interacts with the nucleus as a whole, rather than with its individual constituents. In SM, the cross section for elastic scattering is two orders of magnitude larger than inelastic scattering, which makes CEνNS viable for observation. The interest in CEνNS goes beyond testing for neutrino couplings in SM and probing nuclear structure. If a new neutral current interaction mediated by a light vector boson exists, it would not be suppressed by SM interactions in this region. In spite of the fact that the earliest experimental proposal to measure CEνNS was rather old [24], it took indeed almost four decades to be able to make significant progress on the way of measuring CEνNS cross section. CEνNS was observed for the first time by the COHERENT Collaboration in 2017[2] (see Section 4.2 for details). Hence CEνNS has become one of the important probes for physics beyond the SM since then.

CHAPTER 2

REVIEW OF THE STANDARD MODEL AND ITS SCALAR SECTOR EXTENSIONS

The concepts of symmetry transformations, gauge freedom, spontaneous symmetry breaking, and the Higgs mechanism play a fundamental role in the construction of the SM. These concepts are discussed in Sec. 2.1. Then, Sec 2.2 discusses how the SM is constructed.

2.1 Spontaneous Symmetry Breaking and The Higgs Mechanism

Spontaneous symmetry breaking the Higgs mechanism plays a central role in the construction of the SM. In quantum field theories, the fundamental property of gauge freedom prevents writing mass terms for force-carrying bosons. The Higgs mechanism describes how this problem is overcome by breaking the theory's underlying symmetries.

2.1.1 Symmetries in Quantum Field Theories

A transformation is called a symmetry transformation (or simply symmetry) of a system if the transformed system is identical to the initial one [25]. In mathematical terms, a symmetry transformation preserves Lagrangian up to a total derivative.

$$\mathscr{L} \to \mathscr{L}' = U\mathscr{L} = \mathscr{L} + \partial_\mu f^\mu \tag{2.1}$$

According to Noether's first theorem, there is a conserved quantity corresponding to every continuous symmetry [26].

Two types of symmetries need to be discussed; global and local symmetries. This

7

discussion is given for a simpler model below for clarity before moving on to the SM. One of the simplest quantum field theories is the theory of a self-interacting complex scalar field, known as the ϕ^4 theory [27]

$$\mathscr{L} = \left(\partial_\mu \phi\right)^* \left(\partial^\mu \phi\right) - \mu^2 \phi^* \phi - \lambda \left(\phi^* \phi\right)^2. \tag{2.2}$$

This Lagrangian is symmetric under a global phase shift $\phi \to \phi' = e^{i\theta} \phi$.

$$\mathscr{L}' = (\partial_\mu \phi')^* (\partial^\mu \phi') - \mu^2 \phi'^* \phi' - \lambda \left(\phi'^* \phi'\right)^2 = \mathscr{L} \tag{2.3}$$

This type of transformation is called global $U(1)$ transformation, referring to 1×1 unitary matrices. Under the further inspection of the Lagrangian, it is clear that this symmetry does not hold locally, i.e., $\phi \to \phi' = e^{i\theta(x)} \phi$.

$$\begin{aligned}
\mathscr{L}' &= \left(\partial_\mu \phi'\right)^* \left(\partial^\mu \phi'\right) - \mu^2 \phi'^* \phi' - \lambda \left(\phi'^* \phi'\right)^2 \\
&= \left(\partial_\mu e^{i\theta(x)} \phi\right)^* \left(\partial^\mu e^{i\theta(x)} \phi\right) - \mu^2 \phi^* \phi - \lambda \left(\phi^* \phi\right)^2 \\
&= \left[i\left(\partial_\mu \theta(x)\right)\phi + \partial_\mu \phi\right]^* \left[i\left(\partial^\mu \theta(x)\right)\phi + \partial^\mu \phi\right] - \mu^2 \phi^* \phi - \lambda \left(\phi^* \phi\right)^2 \tag{2.4}
\end{aligned}$$

The transformation property of $\partial_\mu \phi$ prevents invariance. The same situation arises for fermionic kinetic term $\bar{\psi} \gamma^\mu \partial_\mu \psi$. The source of this behavior can be understood by examining the definition of the derivative. Derivative of ϕ in the direction of the vector n^μ is [28]

$$n^\mu \partial_\mu \phi = \lim_{\epsilon \to 0} \frac{1}{\epsilon} \left(\phi(x + \epsilon n) - \phi(x)\right) \tag{2.5}$$

Under a local phase transformations, $\phi(x + \epsilon n)$ and $\phi(x)$ have different transformation properties. In order to perform this subtraction, a factor that compensates for the difference in phase transformations needs to be introduced. This a scalar quantity $U(y, x)$, which transforms as

$$U(y, x) \to e^{i\alpha(y)} U(y, x) e^{-i\alpha(x)}. \tag{2.6}$$

$U(y, x)$ can be considered a pure phase in general. With this object, $\phi(y)$ and $U(y, x)\phi(x)$ can have the same transformation properties. This defines the covariant derivative as

$$n^\mu \partial_\mu \phi = \lim_{\epsilon \to 0} \frac{1}{\epsilon} \left(\phi(x + \epsilon n) - U(x + \epsilon n, x)\phi(x)\right) \tag{2.7}$$

8

To get the full expression, $U(y, x)$ can be expanded by separating the two points.

$$U(x + \epsilon n, x) = 1 - \mathrm{i}e\epsilon n^\mu A_\mu + \mathcal{O}(\epsilon^2) \qquad (2.8)$$

where e is an arbitrary constant. Since U is a scalar, ϵn^μ is companied by a vector field A_μ. As a result, the covariant derivative takes the form

$$D_\mu = \partial_\mu - \mathrm{i}eA_\mu \qquad (2.9)$$

By replacing ∂_μ with D_μ, a Lagrangian that is invariant under local phase transformation can be constructed.

$$\mathcal{L} = (D_\mu\phi)^* (D^\mu\phi) - \mu^2\phi^*\phi - \lambda(\phi^*\phi)^2. \qquad (2.10)$$

The new field A_μ transforms as

$$A_\mu \rightarrow A_\mu - \frac{1}{e}\partial_\mu\theta(x) \qquad (2.11)$$

so that it cancels the extra terms in Eq.(2.4). However, Eq. 2.10 is incomplete. A kinetic term for the gauge field should be added to describe its propagation [29]. To preserve the invariance, this kinetic term needs to be constructed with anti-symmetric terms,

$$\mathcal{L}_{gauge} = -\frac{1}{4}F^{\mu\nu}F_{\mu\nu} \qquad (2.12)$$

where

$$F^{\mu\nu} = \partial^\mu A^\nu - \partial^\nu A^\mu. \qquad (2.13)$$

The ϕ^4 Lagrangian becomes

$$\mathcal{L} = (D_\mu\phi)^* (D^\mu\phi) - \frac{1}{4}F^{\mu\nu}F_{\mu\nu} - \mu^2\phi^*\phi - \lambda(\phi^*\phi)^2. \qquad (2.14)$$

2.1.2 Gauge Freedom

The mentioned gauge theory plays a central role in the Higgs mechanism and general theory crafting. It is the freedom to redefine fields with superfluous degrees of freedom that ultimately have no physical consequence, and it is just a mathematical property of the model. Unlike symmetry transformations which transform into

another state with the same physical properties, gauge transformations transform into the same state [25].

Every physics student is introduced to the concept of gauge freedom in Maxwell's electromagnetism. Electric and magnetic fields are restated in terms of a four-vector $A_\mu = (V, \mathbf{A})$, where

$$\mathbf{E} = -\nabla V - \partial_t \mathbf{A}, \qquad \mathbf{B} = \nabla \times \mathbf{A}. \tag{2.15}$$

The Maxwell action,

$$S_{Maxwell} = \frac{1}{2\mu_0} \int d^4 x (\mathbf{E}^2 - \mathbf{B}^2) = \frac{1}{4\mu_0} \int d^4 x F_{\mu\nu} F^{\mu\nu}. \tag{2.16}$$

is left invariant under the following transformation

$$A_\mu(x) \rightarrow A_\mu(x) + \partial_\mu \alpha(x). \tag{2.17}$$

This is a gauge transformation. It does not affect $\mathbf{E}$ and $\mathbf{B}$ fields. Likewise, Eq. 2.11 is a gauge transformation.

Photon in vacuum has two degrees of freedom, the two perpendicular polarization states. However, A_μ, having four components, starts with four degrees of freedom. There need to be equations that relate these components. The product $p^\mu A_\mu$ is proportional to mass. This removes one degree of freedom. A second degree of freedom is removed by a procedure called gauge fixing. By choosing to work with a specific gauge, the redundancy in our description is removed, and a constraint on the gauge field is obtained. In order to describe massless photon, gauge theory is beneficial.

2.1.3 Spontaneous Symmetry Breaking

A mass term for A_μ is missing in Eq. 2.14 since a term of the form $A^\mu A_\mu$ would break the invariance. Therefore, the symmetries need to be broken somehow for gauge bosons to obtain mass. However, Lagrangian has to maintain its symmetry. There is a solution to this dilemma, as it is possible to get solutions from the Lagrangian, which does not exhibit its symmetries. In other words, a system does not always show the symmetries it is governed by. In this case, the vacuum state is not going to be invariant. This is called spontaneous symmetry breaking.

Before examining how vacuum breaks the symmetry, a quick explanation for what vacuum means in quantum field theories should be given. Energy eigenstates, to which if annihilation operator acts yields zero, are taken as the definition of vacuum [28].

$$a|\Omega\rangle = 0. \tag{2.18}$$

These states have no quanta of energy to be annihilated. The energy quanta are interpreted as particles. Then, to populate the state with particles, the creation operator is acted on the vacuum.

$$a^{\dagger}(k)|\Omega\rangle = |k\rangle \tag{2.19}$$

Thus, field excitations require a definite vacuum state.

2.1.3.1 Goldstone Theorem

Returning to the first premise, in order to show how vacuum does not hold the global symmetry in Eq.(2.2), the complex scalar ϕ field can be described in terms of two distinct fields

$$\phi(x) = \frac{1}{\sqrt{2}}\left(\phi_1(x) + i\phi_2(x)\right). \tag{2.20}$$

Then Eq.(2.2) is rewritten as

$$\mathscr{L} = \frac{1}{2}\partial_\mu\phi_1\partial^\mu\phi_1 + \frac{1}{2}\partial_\mu\phi_2\partial^\mu\phi_2 - \frac{1}{2}\mu^2(\phi_1^2 + \phi_2^2) - \frac{1}{4}\lambda(\phi_1^2 + \phi_2^2)^2. \tag{2.21}$$

Two cases can be considered; $\mu^2 > 0$ and $\mu^2 < 0$ [30]. Note that $\lambda \geq 0$ so that potential has a finite minimum.

If $\mu^2 > 0$, this describes a system of two real scalar particles with masses $\mu/\sqrt{2}$. The potential is azimuthally symmetric, and vacuum is located at $(0,0)$. The case $\mu^2 < 0$ may indicate imaginary masses at first glance, but this is not the case. The point $(0,0)$ is again an extrema as $V'(\phi) = 0$, however it is a local maxima; $V''(\phi) = -2\mu^2$. The global minima, $V(\phi) = -\frac{\lambda v^4}{4}$, is on a set of points satisfying $|\phi|^2 = \frac{v^2}{2}$, located along a circle of radius v, where v is the vacuum expectation value (vev)

$$2\langle\Omega|\phi|\Omega\rangle^2 = v^2 = -\frac{\mu^2}{\lambda}. \tag{2.22}$$

11

In order to get the particle content, a particular ground state is chosen to perturb. Without loss of generality, it can be

$$(\phi_1, \phi_2) = \left(\frac{v}{\sqrt{2}}, 0 \right). \tag{2.23}$$

Excitation around the stable minima is expressed as

$$\phi(x) = \frac{1}{\sqrt{2}} \left(v + \eta(x) + i\xi(x) \right) \tag{2.24}$$

where η and ξ are the two components of the complex field with $\langle \Omega | \eta | \Omega \rangle = \langle \Omega | \xi | \Omega \rangle = 0$. Then Eq.(2.21) can be written as

$$\mathcal{L} = \frac{1}{2} \partial_\mu \eta \partial^\mu \eta + \frac{1}{2} \partial_\mu \xi \partial^\mu \xi - \overbrace{v^2 \left(\frac{\mu^2}{2} + \frac{\lambda v^2}{4} \right)}^{\text{constant}} - v\eta \overbrace{\left(\mu^2 + \lambda v^2 \right)}^{=0}$$
$$- \overbrace{\eta^2 \left(\frac{\mu^2}{2} + \frac{3\lambda v^2}{2} \right)}^{\text{mass}} - \xi^2 \left(\frac{\mu^2}{2} + \frac{\lambda v^2}{2} \right) - \frac{\lambda}{4} \eta^4 - \lambda v \eta^3 - \frac{\lambda}{4} \xi^4 - \frac{\lambda}{2} \eta^2 \xi^2 - \lambda v \eta \xi^2. \tag{2.25}$$

After inserting Eq.(2.22), the linear term in η and the quadratic term in ξ disappears. We get

$$\mathcal{L} = \frac{1}{2} \partial_\mu \eta \partial^\mu \eta + \frac{1}{2} \partial_\mu \xi \partial^\mu \xi + \mu^2 \eta^2 - \frac{\lambda}{4} \eta^4 + \mu^2 \eta^3 - \frac{\lambda}{4} \xi^4 - \frac{\lambda}{2} \eta^2 \xi^2 + \mu^2 \eta \xi^2. \tag{2.26}$$

This describes a state of one massive and one massless particle. The outcome about the masses is expected as η describes radial excitations that go up the potential well, and ξ describes angular excitations which do not climb the potential locally. This is a case of the Goldstone theorem, which states that a massless boson exists for each spontaneously broken symmetry.

2.1.3.2 Spontaneous Symmetry Breaking of a Local Gauge Invariant Model

Although gauge freedom cannot be spontaneously broken [25], its existence affects the symmetry-breaking process. To see this, the same procedure from the previous section can be applied to Eq.(2.14). Again for $\mu^2 > 0$, it is a system of two particles of mass μ. When $\mu^2 < 0$, the minimum of the potential will be on a circle of radius

$$|\phi|^2 = -\frac{\mu^2}{\lambda} = v^2. \tag{2.27}$$

After selecting $(\phi_1, \phi_2) = \left(\frac{v}{\sqrt{2}}, 0\right)$ as the vacuum, excitations around this point can be written as

$$\phi(x) = \frac{1}{\sqrt{2}}\left(v + \eta(x) + \mathrm{i}\xi(x)\right), \tag{2.28}$$

with assuming $\langle\Omega|\eta|\Omega\rangle = \langle\Omega|\xi|\Omega\rangle = 0$. Then Eq.(2.14) becomes

$$\begin{aligned}
\mathcal{L} =& \frac{1}{2}\partial_\mu\eta\partial^\mu\eta + \frac{1}{2}\partial_\mu\xi\partial^\mu\xi - \frac{1}{4}F^{\mu\nu}F_{\mu\nu} - v^2\left(\frac{\mu^2}{2} + \frac{\lambda v^2}{4}\right) - v\eta(\mu^2 + \lambda v^2) \\
&+ \frac{1}{2}e^2v^2A^2 - \eta^2\left(\frac{\mu^2}{2} + \frac{3}{2}\lambda v^2\right) - \xi^2\left(\frac{\mu^2}{2} + \frac{\lambda v^2}{2}\right) + \frac{1}{2}e^2A^2(\eta^2 + 2v\eta + \xi^2) \\
&- \frac{\lambda}{4}(\eta^2 + \xi^2)^2 - \lambda v\eta^3 - \lambda v\eta\xi^2 + eA^\mu\xi\partial_\mu\eta + eA^\mu\eta\partial_\mu\xi + evA^\mu\partial_\mu\xi. \tag{2.29}
\end{aligned}$$

As before, inserting Eq.(2.27) cancels out the linear term in η and the mass term of ξ. After dropping the constant terms, it becomes

$$\begin{aligned}
\mathcal{L} =& \frac{1}{2}\partial_\mu\eta\partial^\mu\eta + \frac{1}{2}\partial_\mu\xi\partial^\mu\xi - \frac{1}{4}F^{\mu\nu}F_{\mu\nu} + \frac{1}{2}e^2v^2A^2 + \mu^2\eta^2 \\
&+ \frac{1}{2}e^2A^2(\eta^2 + 2v\eta + \xi^2) - \frac{\lambda}{4}(\eta^2 + \xi^2)^2 + \mu^2\eta^3 + \mu^2\eta\xi^2. \\
&+ eA^\mu\xi\partial_\mu\eta - eA^\mu\eta\partial_\mu\xi - evA^\mu\partial_\mu\xi \tag{2.30}
\end{aligned}$$

The Lagrangian now contains a mass term with $m_A^2 = \frac{v^2}{2}$ for the gauge boson in addition to the previous section. However, the procedure is not finished yet as there needs to be a clarification about degrees of freedom[27]. In the beginning, the Lagrangian had four degrees of freedom; two from massless gauge boson and two from ϕ_1 and ϕ_2. In the end, three come from massive gauge bosons and two from η and ξ. Seemingly an unphysical field appeared in the process. It is easy to find this field as it shows itself in the last term of Eq.(2.30). The term $evA^\mu\partial_\mu\xi$ describes a process in which vector particle A transforms into scalar ξ during propagation. This tells ξ acts as the longitudinal component of A. Therefore, to go on the physical eigenstate basis, one has to perform diagonalization, which would eliminate the bilinear term. In fact, in this case, the diagonalization procedure is the gauge transformation Eq.(2.11). Terms involving ξ can be rewritten as:

$$\frac{1}{2}\partial_\mu\xi\partial^\mu\xi + evA^\mu\partial_\mu\xi + \frac{1}{2}e^2v^2A^2 = \frac{1}{2}e^2v^2\left(A^\mu + \frac{1}{ev}\partial^\mu\xi\right)^2 = \frac{1}{2}e^2v^2A'^2. \tag{2.31}$$

This specific choice of $\theta = \xi/v$ is called the unitary gauge. This transformation alone does not eliminate all ξ from the Lagrangian as there still are in the interaction terms. However, recalling from Section 2.1.1, the above transformation is

companied by phase transformation for ϕ, which rotates away the remaining ξ. To simplify this calculation, Eq.(2.28) can be expressed in an equivalent form of fields h and ζ

$$\phi(x) = \frac{1}{\sqrt{2}}\big(v + \eta(x) + \mathrm{i}\xi(x)\big) = \frac{1}{\sqrt{2}}(v + h)\mathrm{e}^{\mathrm{i}\zeta/v}, \tag{2.32}$$

where $h = \eta$ and $\zeta = \xi$ in the first order due to $(v + h)(1 + \mathrm{i}\zeta) = v + h + \mathrm{i}\zeta$. This time a unitary gauge transformation with $\theta = \zeta/v$ would look like

$$\phi \to \mathrm{e}^{-\mathrm{i}\zeta/v}\phi, \qquad A_\mu \to A_\mu - \frac{1}{ev}\partial_\mu\zeta. \tag{2.33}$$

This transformation cancels out ζ, leaving ϕ with a simpler form:

$$\phi = \frac{1}{\sqrt{2}}(v + h); \tag{2.34}$$

a form that would not lead to undesired terms appearing in the Lagrangian.

$$\begin{aligned}
\mathcal{L} &= \big(D_\mu\phi\big)^*\big(D^\mu\phi\big) - \frac{1}{4}F^{\mu\nu}F_{\mu\nu} - \mu^2\phi^*\phi - \lambda\big(\phi^*\phi\big)^2 \\
&= \frac{1}{2}\partial_\mu h\partial^\mu h - \frac{1}{4}F_{\mu\nu}F^{\mu\nu} + \frac{1}{2}e^2 v^2 A^2 + \mu^2 h^2 \\
&\quad + \frac{1}{2}e^2 A^2\big(h^2 + 2vh\big) + \mu^2\Big(h^3 + \frac{1}{4}h^4\Big)
\end{aligned} \tag{2.35}$$

In the end, spontaneous symmetry breaking transformed one of the scalar fields into the longitudinal mode of the gauge boson. Without the gauge freedom, this field would end up as a massless Goldstone boson. Therefore, it is said that in the symmetry-breaking process, the gauge boson ate the Goldstone boson and gained mass. This process is called the Higgs mechanism. Here h in Eq.(2.35) is called the Higgs boson. It is massive, and examining the interaction terms shows that it has both self-interactions and interactions with the gauge boson.

2.2   Higgs Mechanism in the Standard Model

Apart from assigning masses to gauge bosons, the characteristic that weak interactions couple only left chiral fields interferes with writing mass terms for elementary particles in the Lagrangian. In this section, the idea of spontaneous symmetry breaking of a scalar theory from the previous section is applied to Standard Model by introducing a scalar doublet. The Higgs Boson, a prediction of the Higgs mechanism, was observed on July 4, 2012.

2.2.1 The Standard Model

The SM is a gauge theory of group structure $SU(3)_C \otimes SU(2)_L \otimes U(1)_Y$. The group $SU(3)_C$ is related to strong interactions, whereas $SU(2)_L \otimes U(1)_Y$ is the group structure of the Electroweak Theory (EW) (formulated by Glashow, Weinberg, and Salam), which is a unified theory of the electromagnetic and weak interactions [11]. The scope of this thesis is confined to the EW sector; therefore, only this sector is detailed below. The fermionic matter content includes leptons and quarks, organized in three families.

$$\text{Leptons} = \begin{bmatrix} \nu_e \\ e \end{bmatrix}, \begin{bmatrix} \nu_\mu \\ \mu \end{bmatrix}, \begin{bmatrix} \nu_\tau \\ \tau \end{bmatrix}, \qquad \text{Quarks} = \begin{bmatrix} u \\ d \end{bmatrix}, \begin{bmatrix} c \\ s \end{bmatrix}, \begin{bmatrix} t \\ b \end{bmatrix}.$$

Leptons include electron, muon, and tau and their related neutrinos and quarks include up, down, strange, charm, bottom, and top quarks. In both sectors, the quantum numbers of families are equal, and the only difference is in their masses. An important characteristic of weak interactions is electrically charged interaction couples only left-handed fields in a structure called V-A interactions, which is why the Higgs mechanism is needed to make fermions massive. The difference between left-handed and right-handed fermions in EW is formulated using the group $SU(2)_L$, where L refers to left-handed fields. Left-handed fields form doublets, while right-handed fields form singlets. Quark fields form

$$Q_L^\alpha = \begin{bmatrix} u_L^\alpha \\ d_L^\alpha \end{bmatrix}, \qquad u_R^\alpha, \qquad d_R^\alpha$$

where α is the family index. u, c, t are referred as up type quarks and d, s, b are referred as down type quarks. Similarly, leptons form

$$L^\alpha = \begin{bmatrix} \nu_L^\alpha \\ e_L^\alpha \end{bmatrix}, \qquad e_R^\alpha$$

where right-handed neutrinos ν_R^α are missing.

Interactions between particles formed through coupling to four gauge bosons, corresponding to three generators of SU(2) and one generator of U(1)

$$W_\mu^a, \quad B_\mu$$

Table 2.1: Quantum numbers of elementary particles under $SU(2)_L \otimes U(1)_Y$

Particles	I^3	Y	Q		I^3	Y	Q
u_L^α	$\frac{1}{2}$	$\frac{1}{6}$	$\frac{2}{3}$	u_R^α	0	$\frac{2}{3}$	$\frac{2}{3}$
d_L^α	$-\frac{1}{2}$	$\frac{1}{6}$	$-\frac{1}{3}$	d_R^α	0	$-\frac{1}{3}$	$-\frac{1}{3}$
e_L^α	$-\frac{1}{2}$	$-\frac{1}{2}$	-1	e_R^α	0	-1	-1
v_L^α	$\frac{1}{2}$	$-\frac{1}{2}$	0				

where $a = 1, 2, 3$. The EW covariant derivative is

$$D_\mu = \partial_\mu - \mathrm{i} g W_\mu^a t^a - \mathrm{i} g' Y Y_\mu, \tag{2.36}$$

where t^a and Y are generators of the related groups, and g and g' are coupling constants. Fermionic and scalar fields have weak isospin quantum numbers, $I = 0$ or $1/2$ with

$$t^a = \begin{cases} = 0 & \text{if } I = 0 \\ = \frac{1}{2}\sigma^a & \text{if } I = \frac{1}{2} \end{cases} \tag{2.37}$$

where σ^a are Pauli matrices and hypercharge $Y = Q - I^3$ where Q is the electric charge and I^3 is the third component of isospin. Quantum numbers of fermionic fields are given in Table (2.1). Under $SU(2)_L \otimes U(1)_Y$ symmetry transformations fermionic fields transform as [11]

$$Q_L^\alpha \to \exp(\mathrm{i} Y \rho) \exp\left(\mathrm{i} \frac{\sigma^a}{2} \omega^a\right) Q_L^\alpha$$
$$u_R^\alpha \to \exp(\mathrm{i} Y \rho) u_R^\alpha$$
$$d_R^\alpha \to \exp(\mathrm{i} Y \rho) d_R^\alpha \tag{2.38}$$
$$L^\alpha \to \exp(\mathrm{i} Y \rho) \exp\left(\mathrm{i} \frac{\sigma^a}{2} \omega^a\right) L^\alpha$$
$$e_R^\alpha \to \exp(\mathrm{i} Y \rho) e_R^\alpha.$$

Similarly, gauge bosons transform as (see Appendix A)

$$Y_\mu \to Y_\mu - \frac{1}{g'} \partial_\mu \rho$$
$$\widetilde{W}_\mu \to \exp\left(\mathrm{i} \frac{\sigma^a}{2} \omega^a\right) \widetilde{W} \exp\left(\mathrm{i} \frac{\sigma^a}{2} \omega^a\right)^\dagger + \frac{\mathrm{i}}{g}\left(\partial_\mu \exp\left(\mathrm{i} \frac{\sigma^a}{2} \omega^a\right)\right) \exp\left(\mathrm{i} \frac{\sigma^a}{2} \omega^a\right)^\dagger \tag{2.39}$$

where $\widetilde{W}_\mu = \frac{\sigma^a}{2} W_\mu^a$. With these, the EW Lagrangian becomes

$$\mathscr{L} = \sum_{\alpha=1}^{3} \left(\overline{Q}_L^\alpha \,\slashed{D}\, Q_L^\alpha + \overline{u}_R^\alpha \,\slashed{D}\, u_R^\alpha + \overline{d}_R^\alpha \,\slashed{D}\, d_R^\alpha + \overline{L}^\alpha \,\slashed{D}\, Q_L^\alpha + \overline{e}_R^\alpha \,\slashed{D}\, e_R^\alpha \right)$$
$$- \frac{1}{4} Y_{\mu\nu} Y^{\mu\nu} - \overbrace{\frac{1}{2} \mathrm{Tr}\left(\widetilde{W}_{\mu\nu} \widetilde{W}^{\mu\nu} \right)}^{\frac{1}{4} W_{\mu\nu}^a W^{a\mu\nu}} \tag{2.40}$$

where $\slashed{D} = D_\mu \gamma^\mu$ and $Y_{\mu\nu}$, $W_{\mu\nu}^a$ are field strength tensors of Y_μ, W_μ^a;

$$Y_{\mu\nu} = \partial_\mu Y_\nu - \partial_\nu Y_\mu$$
$$W_{\mu\nu}^a = \partial_\mu W_\nu^a - \partial_\nu W_\mu^a + f_w \epsilon^{abc} W_\mu^b W_\nu^c. \tag{2.41}$$

2.2.2 Spontaneous Symmetry Breaking in the Electroweak Theory

While generating masses for gauge bosons, one has to generate mass terms for $W^\pm$ and Z bosons while leaving photons massless. This means that after symmetry breaking, the system should still have the symmetry of QED, or $U(1)_Q$. Furthermore, three degrees of freedom for scalar fields need to be absorbed to obtain three massive bosons. To this end, EW theory is extended with a scalar sector. However to retain symmetry, only $SU(2)_L \otimes U(1)_Y$ multiples can be added. This leads to the introduction of Higgs doublet[27]

$$\phi = \begin{pmatrix} \phi^+ \\ \phi^0 \end{pmatrix} = \frac{1}{\sqrt{2}} \begin{pmatrix} \phi_1 + i\phi_2 \\ \phi_3 + i\phi_4 \end{pmatrix}. \tag{2.42}$$

which has quantum numbers $I = 1/2$ and $Y = 1$. Electric charges of both components are selected to ensure the condition on the hypercharge. The Lagrangian of the scalar sector is

$$\mathscr{L}_{\text{scalar}} = \left(D_\mu \phi \right)^\dagger \left(D^\mu \phi \right) - V(\phi). \tag{2.43}$$

Which has a potential that would spontaneously break the symmetry

$$V(\phi) = \mu^2 \left(\phi^\dagger \phi \right) + \lambda \left(\phi^\dagger \phi \right)^2, \quad \text{with} \quad \mu^2 < 0. \tag{2.44}$$

The product $\phi^\dagger \phi$ can be expanded as

$$\phi^\dagger \phi = \frac{1}{2} (\phi^{+*} \phi^+ + \phi^{0*} \phi^0) = \frac{1}{2} (\phi_1^2 + \phi_2^2 + \phi_3^2 + \phi_4^2). \tag{2.45}$$

Just like before, the vacuum is not unique. However, the vacuum should not be in the charged direction to preserve electric charge conservation. Therefore the vacuum is chosen to be at $\phi_1 = \phi_2 = \phi_4 = 0$ and $\phi_3 = v$, giving the vacuum expectation value

$$\langle\Omega|\phi|\Omega\rangle = \frac{1}{\sqrt{2}}\begin{pmatrix} 0 \\ v \end{pmatrix}, \qquad v = \sqrt{-\frac{\mu^2}{\lambda}}. \tag{2.46}$$

The theory is then developed around the vacuum with excitations h, $\xi_{1,2,3}$:

$$\phi = \begin{pmatrix} \xi_1 + i\xi_2 \\ \frac{1}{\sqrt{2}}(v+h) - i\xi_3 \end{pmatrix} = e^{\frac{2it^a\xi_a}{v}}\begin{pmatrix} 0 \\ \frac{1}{\sqrt{2}}(v+h) \end{pmatrix}. \tag{2.47}$$

After applying gauge transformation as in section Eq.(2.1.3.2), ξ_a fields disappear.

$$\phi \to e^{-\frac{2it^a\xi_a}{v}}\phi = \frac{1}{\sqrt{2}}\begin{pmatrix} 0 \\ v+h \end{pmatrix} \tag{2.48}$$

The result is symmetry breaking of form $SU(2)_L \otimes U(1)_Y \to U(1)_Q$.

2.2.3 Generating Gauge Boson Masses

Gauge boson mass terms come from the covariant derivative square term in Eq.(2.43) [30]. With ϕ given in Eq.(2.48), the relevant terms become

$$\begin{aligned}
|D^\mu\phi|^2 &\supset \left|\left(-\frac{ig}{2}t^a W_\mu^a - \frac{ig'}{2}YY_\mu\right)\frac{1}{\sqrt{2}}\begin{pmatrix} 0 \\ v \end{pmatrix}\right|^2 = \left|\frac{-iv}{2\sqrt{2}}\begin{pmatrix} gW_\mu^1 - igW_\mu^2 \\ -gW_\mu^3 + g'Y_\mu \end{pmatrix}\right|^2 \\
&= \frac{v^2}{8}\left(g^2\left(\left(W_\mu^1\right)^2 + \left(W_\mu^2\right)^2\right) + \left(-gW_\mu^3 + g'Y_\mu\right)^2\right). \tag{2.49}
\end{aligned}$$

The established $W^\pm$, Z bosons, and photon states arise from this point.

2.2.3.1 Rewriting W_μ^1 and W_μ^2 as Charged Gauge Bosons W_μ^+ and W_μ^-

The charged $W^\pm$ states are defined through charge raising and lowering operators [31]

$$t^+ = \frac{1}{2}\left(t^1 + it^2\right) = \frac{1}{2}\begin{pmatrix} 0 & 1 \\ 0 & 0 \end{pmatrix}$$

$$t^- = \frac{1}{2}\left(t^1 - it^2\right) = \frac{1}{2}\begin{pmatrix} 0 & 0 \\ 1 & 0 \end{pmatrix}. \tag{2.50}$$

In terms of $W^{1,2}$, they are expressed as

$$W_\mu^+ = \frac{1}{\sqrt{2}}\left(W_\mu^1 - iW_\mu^2\right)$$

$$W_\mu^- = \frac{1}{\sqrt{2}}\left(W_\mu^1 + iW_\mu^2\right) \tag{2.51}$$

In this mass eigenbasis, charged weak interactions couple members of weak isospin doublets.

$$\overline{Q}_L \slashed{D} Q_L = -\frac{i}{\sqrt{2}}g\begin{pmatrix} \overline{u}_L & \overline{d}_L \end{pmatrix}\begin{pmatrix} 0 & 1 \\ 0 & 0 \end{pmatrix}\begin{pmatrix} u_L \\ d_L \end{pmatrix}W^+ - \frac{i}{\sqrt{2}}g\begin{pmatrix} \overline{u}_L & \overline{d}_L \end{pmatrix}\begin{pmatrix} 0 & 0 \\ 1 & 0 \end{pmatrix}\begin{pmatrix} u_L \\ d_L \end{pmatrix}W^- + \dots$$

$$= -\frac{i}{\sqrt{2}}g\left(\overline{u}_L\gamma^\mu d_L W_\mu^+ + \overline{d}_L\gamma^\mu u_L W_\mu^-\right) + \dots \tag{2.52}$$

Returning back to Eq.(2.49), $W^{1,2}$ terms can be rewritten as

$$\frac{v^2 g^2}{8}\left(\left(W_\mu^1\right)^2 + \left(W_\mu^2\right)^2\right) = \frac{v^2 g^2}{4}\left(\left(W_\mu^+\right)^2 + \left(W_\mu^-\right)^2\right), \tag{2.53}$$

yielding the W boson mass as

$$m_{W^\pm} = \frac{vg}{2}. \tag{2.54}$$

2.2.3.2 Rewriting W_μ^3 and B_μ as Neutral Gauge Bosons Z_μ and A_μ

Next, W_μ^3 and Y_μ can be rewritten as neutral gauge bosons Z_μ and A_μ. The last term in Eq.(2.49) can be expressed as

$$\frac{v^2}{8}\left(-gW_\mu^3 + g'Y_\mu\right)^2 = \frac{v^2}{8}\begin{pmatrix} W_\mu^3 & Y_\mu \end{pmatrix}\begin{pmatrix} g^2 & -gg' \\ -gg' & g'^2 \end{pmatrix}\begin{pmatrix} W_\mu^3 \\ Y_\mu \end{pmatrix}. \tag{2.55}$$

The mass matrix needs to be diagonalized. It has two eigenvalues and eigenvectors, leading to two gauge bosons [31]

$$\lambda_1 = 0, \quad V_1 = \frac{1}{\sqrt{g^2 + g'^2}}\begin{pmatrix} g \\ g' \end{pmatrix} \rightarrow A_\mu = \frac{1}{\sqrt{g^2 + g'^2}}\left(gW_\mu^3 + g'Y_\mu\right)$$

$$\lambda_2 = g^2 + g'^2, \quad V_2 = \frac{1}{\sqrt{g^2 + g'^2}}\begin{pmatrix} g \\ -g' \end{pmatrix} \rightarrow Z_\mu = \frac{1}{\sqrt{g^2 + g'^2}}\left(gW_\mu^3 - g'Y_\mu\right). \tag{2.56}$$

In other words, there are bosons; massless photon A_μ and massive Z boson Z_μ. Inserting the expression for Z into Eq.(2.49) gives

$$m_Z = \frac{v}{2}\sqrt{g^2 + g'^2} \qquad (2.57)$$

2.2.3.3 The Weak Mixing Angle

There is a clear relation between W and Z masses Eq.(2.54), Eq.(2.57), which can be expressed in terms of trigonometric relations of some angle θ_W called Weinberg angle (or the weak mixing angle) [30]

$$m_Z = \frac{\sqrt{g^2 + g'^2}}{g} m_W = \frac{m_W}{\cos\theta_W} \qquad (2.58)$$

with

$$\cos\theta_W = \frac{g}{\sqrt{g^2 + g'^2}}, \quad \sin\theta_W = \frac{g'}{\sqrt{g^2 + g'^2}} \qquad (2.59)$$

This angle can also be interpreted as a rotation angle between bases $\left(W^3, Y\right)$ and (Z, A).

The parts involving W^3_μ and Y_μ in the EW covariant derivative Eq.(2.36) can be written in terms of Z_μ and A_μ as

$$-\mathrm{i}g\,t^3 W^3_\mu - \frac{\mathrm{i}}{2}g'Y\,Y_\mu = -\mathrm{i}\frac{gg'}{\sqrt{g^2+g'^2}}\left(t^3 + \frac{Y}{2}\right)A_\mu - \mathrm{i}\frac{1}{\sqrt{g^2+g'^2}}\left(gt^3 - g'\frac{Y}{2}\right)Z_\mu \quad (2.60)$$

which leads to the relationship between EW and QED couplings

$$e = \frac{gg'}{\sqrt{g^2 + g'^2}} = g\sin\theta_W = g'\cos\theta_W. \qquad (2.61)$$

In particle physics calculations, a commonly encountered value $\sin^2\theta_W$, is measured to have the value [11]

$$\sin^2\theta_W = 1 - \frac{m_W^2}{m_Z^2} \approx 0.2234. \qquad (2.62)$$

2.2.4 Fermion Masses

Mass terms for fermions are missing in the EW Lagrangian Eq.(2.40). Left and right chiral fields couple to each other inside the mass terms.

$$\mathcal{L}_{mass} = -mf^\dagger f = -m\left(\bar{f}_L + \bar{f}_R\right)\left(f_L + f_R\right) = -m\left(\bar{f}_L f_R + \bar{f}_R f_L\right) \qquad (2.63)$$

However, since their transformation properties are different, directly adding this term breaks the symmetry.

The Higgs mechanism can generate fermion mass terms just like it is used to generate mass terms for gauge bosons [32, 33]. If a singlet term under $SU(2)_L$ and $U(1)_Y$ can be constructed, it can be used inside EW Lagrangian. By using the Higgs doublet, such terms can be written as

$$\mathcal{L}_{\text{Yukawa}} = -y\left(\bar{f}_L \phi f_R + \bar{f}_R \widetilde{\phi} f_L\right) \tag{2.64}$$

where

$$\widetilde{\phi}^c = i\sigma^2 \phi^* = \frac{1}{\sqrt{2}} \begin{pmatrix} v + h \\ 0 \end{pmatrix}. \tag{2.65}$$

This term is known as Yukawa interaction, and the coupling y is Yukawa coupling. Not only it generates mass terms for fermions, but it also describes interactions between the Higgs field and fermions.

The EW extension in the Yukawa sector is

$$-\mathcal{L}_{\text{Yukawa}} = y'^{\alpha\beta}_e \bar{L}'^{\alpha} \phi e'^{\beta}_R + y'^{\alpha\beta}_u \bar{Q}'^{\alpha}_L \widetilde{\phi}^c u'^{\beta}_R + y'^{\alpha\beta}_d \bar{Q}'^{\alpha}_L \phi d'^{\beta}_R + \text{h.c.} \tag{2.66}$$

where the Yukawa couplings takes a matrix form $y^{\alpha\beta}_f$ due to family structure.

The primes in Eq.(2.66) indicate that fields are in interaction basis, which is explained as follows: In general, the matrices y_f are not diagonal. As a result, we obtain non-diagonal mass matrices after the EW symmetry breaking

$$m'_f = \frac{v}{\sqrt{2}} y'_f. \tag{2.67}$$

However, the mass matrices can be diagonalized with a change of basis. The basis in which the mass matrices diagonal is called the mass (or physical) basis. The states in the bases are related through unitary matrices

$$f'_L = V^f_L f_L, \quad f'_R = V^f_R f_R \tag{2.68}$$

Consequently, the Yukawa couplings transform as

$$y'_f = V^f_L y_f V^{f\dagger}_R \tag{2.69}$$

21

2.2.4.1 Lepton Masses

The EW symmetry-breaking process of the leptonic part of Eq.(2.66) is as follows:

$$
\begin{aligned}
-\mathcal{L}_{\text{Yukawa}}^{\text{lepton}} &= y_e'^{\alpha\beta}\left(\bar{L}'^{\alpha}\phi e_R'^{\beta} + \bar{e}'^{\beta}_R\bar{\phi}L'\right) \\
&= -\frac{y_e'^{\alpha\beta}}{\sqrt{2}}\left(\begin{pmatrix}\bar{v}_L^{\alpha} & \bar{e}_L'^{\alpha}\end{pmatrix}\begin{pmatrix}0\\v+h\end{pmatrix}e_R'^{\beta} + \bar{e}'^{\beta}_R\begin{pmatrix}v+h & 0\end{pmatrix}\begin{pmatrix}v_L^{\alpha}\\e_L'^{\alpha}\end{pmatrix}\right) \\
&= \frac{y_e'^{\alpha\beta}}{\sqrt{2}}(v+h)\overbrace{\left(\bar{e}'^{\alpha}_L e_R'^{\beta} + \bar{e}'^{\beta}_R e_L'^{\alpha}\right)}^{\bar{e}'^{\alpha}e'^{\beta}} \\
&= \frac{y_e'^{\alpha\beta}v}{\sqrt{2}}\bar{e}'^{\alpha}e'^{\beta} + \frac{y_e'^{\alpha\beta}v}{\sqrt{2}}h\bar{e}'^{\alpha}e'^{\beta} \\
&= \sum_{\alpha=1}^{3}\left(\frac{y_e^{\alpha\alpha}v}{\sqrt{2}}\bar{e}^{\alpha}e^{\alpha} + \frac{y_e^{\alpha\alpha}v}{\sqrt{2}}h\bar{e}^{\alpha}e^{\alpha}\right)
\end{aligned}
\tag{2.70}
$$

where two terms are the lepton mass term and lepton-Higgs interaction, respectively. The physical lepton masses are

$$
m_{l^{\alpha}} = \frac{y_e^{\alpha\alpha}v}{\sqrt{2}}
\tag{2.71}
$$

and interaction coupling is proportional to the lepton mass.

2.2.4.2 Quark Masses

The process of symmetry-breaking process in the quark sector is likewise.

$$
\begin{aligned}
-\mathcal{L}_{\text{Yukawa}}^{\text{quark}} &= y_u'^{\alpha\beta}\bar{Q}'^{\alpha}_L\widetilde{\phi}^c u_R'^{\beta} + y_d'^{\alpha\beta}\bar{Q}'^{\alpha}_L\phi d_R'^{\beta} + \text{h.c.} \\
&= \frac{y_u'^{\alpha\beta}v}{\sqrt{2}}\bar{u}'^{\alpha}u'^{\beta} + \frac{y_d'^{\alpha\beta}v}{\sqrt{2}}\bar{d}'^{\alpha}d'^{\beta} + \frac{y_u'^{\alpha\beta}v}{\sqrt{2}}h\bar{u}'^{\alpha}u'^{\beta} + \frac{y_d'^{\alpha\beta}v}{\sqrt{2}}h\bar{d}'^{\alpha}d'^{\beta} \\
&= \sum_{\alpha=1}^{3}\left(\frac{y_u^{\alpha\alpha}v}{\sqrt{2}}\bar{u}^{\alpha}u^{\alpha} + \frac{y_d^{\alpha\alpha}v}{\sqrt{2}}\bar{d}^{\alpha}d^{\alpha} + \frac{y_u^{\alpha\alpha}v}{\sqrt{2}}h\bar{u}^{\alpha}u^{\alpha} + \frac{y_d^{\alpha\alpha}v}{\sqrt{2}}h\bar{d}^{\alpha}d^{\alpha}\right)
\end{aligned}
\tag{2.72}
$$

The distinction between interaction and mass basis had no tangible effect in the lepton sector. However, it leads to quark mixing in charged weak current interactions. The weak current is

$$
-\mathcal{L}_W = \frac{g}{\sqrt{2}}\begin{pmatrix}\bar{u}'_L & \bar{c}'_L & \bar{t}'_L\end{pmatrix}\gamma^{\mu}W_{\mu}^{+}\begin{pmatrix}d'_L\\s'_L\\b'_L\end{pmatrix} + \text{h.c.}
$$

$$= \frac{g}{\sqrt{2}} \begin{pmatrix} \bar{u}_L & \bar{c}_L & \bar{t}_L \end{pmatrix} \gamma^\mu W_\mu^+ \overbrace{V_L^u V_L^{d\dagger}}^{V_{\text{CKM}}} \begin{pmatrix} d_L \\ s_L \\ b_L \end{pmatrix} + \text{h.c.} \tag{2.73}$$

where V_{CKM} is the Cabibbo–Kobayashi–Maskawa matrix.

$$V_{\text{CKM}} = V_L^u V_L^{d\dagger} = \begin{pmatrix} V_{ud} & V_{us} & V_{ub} \\ V_{cd} & V_{cs} & V_{cb} \\ V_{td} & V_{ts} & V_{tb} \end{pmatrix} \tag{2.74}$$

Its elements give the probability of transition between quark states. For example, the transition from a down quark to an up quark is described by V_{ud}, whereas the transition from an up quark to a down quark is described by V_{ud}^*.

Since it is a product of two unitary matrices, the CKM matrix is a 3×3 unitary matrix. An $n \times n$ unitary matrix can be described by $n(n-1)/2$ angles and $n(n+1)/2$ phases. In the case of the CKM matrix, five phases can be rotated away, leaving three angles and one CP- violating phase [34]. It is possible to parametrize the CKM matrix in different ways, but the common way is as follows[35]:

$$\begin{aligned} V_{\text{CKM}} &= \begin{pmatrix} 1 & 0 & 0 \\ 0 & c_{23} & s_{23} \\ 0 & -s_{23} & c_{23} \end{pmatrix} \begin{pmatrix} c_{13} & 0 & s_{13}e^{-i\delta} \\ 0 & 1 & 0 \\ -s_{13}e^{i\delta} & 0 & c_{13} \end{pmatrix} \begin{pmatrix} c_{12} & s_{12} & 0 \\ -s_{12} & c_{12} & 0 \\ 0 & 0 & 1 \end{pmatrix} \\ &= \begin{pmatrix} c_{12}c_{13} & s_{12}c_{13} & s_{13}e^{-i\delta} \\ -s_{12}c_{13} - c_{12}s_{23}s_{13}e^{i\delta} & c_{12}c_{23} - s_{12}s_{23}s_{13}e^{i\delta} & s_{23}c_{13} \\ s_{12}s_{23} - c_{12}c_{23}s_{13}e^{i\delta} & -c_{12}s_{23} - s_{12}c_{23}s_{13}e^{i\delta} & c_{23}c_{13} \end{pmatrix} \end{aligned} \tag{2.75}$$

where s_{ij} and c_{ij} are shorthand for sin and cos of the mixing angle between generations i and j.

Note that a complete review of the Higgs mechanism would involve gauge boson self-interactions, Higgs boson interactions, discussions on Higgs boson mass, and Higgs vacuum stability. However, these topics are not relevant to this thesis study; therefore, they are omitted here.

2.3 Two Higgs Doublet Models

The Higgs sector of the SM is minimal, meaning that it has the simplest possible form that generates mass terms for bosons and fermions after the electroweak symmetry breaking. However, there is no theoretical upper bound for the number of scalar doublets that can be added to the model. Therefore, in an attempt to formulate the physics beyond the SM, one might consider additional Higgs doublets.

Some of the motivations for such extensions are as follows[36]. In some cases, the addition is related to satisfying requirements from higher symmetry groups. In supersymmetric models, a Higgs doublet cannot simultaneously give mass to up type (charge 2/3) and down type (charge -1/3) quarks. Furthermore, the anomaly cancellation condition requires an additional doublet to exist. In addition to that, the strong and electroweak interactions are unified in the grand unified theories under a higher compact symmetry group. This group needs to break down to $SU(3)_C \otimes SU(2)_L \otimes U(1)_Y$, which requires a different scalar structure. This leads to additional scalar doublets in the electroweak scale.

In other cases, it is related to giving rise to particular phenomenologies. In the Peccei-Quinn model and its variations, the CP violating phase in the QCD Lagrangian can be rotated away if the Lagrangian contains two Higgs doublets. Moreover, it is possible to have CP violation in the Higgs sector in the extended scenarios. These models are investigated as a possible source of CP violation to generate baryon asymmetry in the universe.

Two Higgs Doublet Models (2HDM) are the simplest scalar sector extensions to the SM, with two identical $SU(2)_L$ doublets

$$\phi_i = \begin{pmatrix} \phi_i^+ \\ \phi_i^0 \end{pmatrix}. \tag{2.76}$$

Hence there are eight scalar degrees of freedom. During the electroweak symmetry breaking, two charged and one neutral Goldstone bosons turn into longitudinal modes of $W^\pm$ and Z bosons. Five Higgs particles remain: a charged pair $h^\pm$, two neutral scalars, and a neutral pseudoscalar [37].

The 2HDM scalar potential $V(\phi_1, \phi_2)$ can be constructed out of gauge invariant

combinations of $\phi_1^\dagger\phi_1$, $\phi_2^\dagger\phi_2$, $\phi_1^\dagger\phi_2$, and $\phi_2^\dagger\phi_1$. The renormalizability condition limits the maximum possible power of these combinations to 2. The most general potential at the tree level is [37, 36]

$$
\begin{aligned}
V^{\text{2HDM}}(\phi_1,\phi_2) = {}& m_{11}^2\phi_1^\dagger\phi_1 + m_{22}^2\phi_2^\dagger\phi_2 - \left(m_{12}^2\phi_1^\dagger\phi_2 + h.c.\right) + \frac{\lambda_1}{2}\left(\phi_1^\dagger\phi_1\right)^2 \\
& + \frac{\lambda_2}{2}\left(\phi_2^\dagger\phi_2\right)^2 + \lambda_3\left(\phi_1^\dagger\phi_1\right)\left(\phi_2^\dagger\phi_2\right) + \lambda_4\left(\phi_1^\dagger\phi_2\right)\left(\phi_2^\dagger\phi_1\right) \\
& + \left[\frac{\lambda_5}{2}\left(\phi_1^\dagger\phi_2\right)^2 + \lambda_6\left(\phi_1^\dagger\phi_1\right)\left(\phi_1^\dagger\phi_2\right) + \lambda_7\left(\phi_2^\dagger\phi_2\right)\left(\phi_1^\dagger\phi_2\right) + h.c.\right]
\end{aligned}
$$
(2.77)

where m_{11}^2, m_{22}^2, λ_1, λ_2, λ_3, and λ_4 are real and m_{12}^2, λ_5, λ_6, and λ_7 are complex parameters in general. Considering the complex conjugates, there are 14 parameters in the potential. Due to a large number of parameters, the maxima can exhibit complex characteristics. Similar to the SM, the vacuum is not unique, and there are three types of vevs in the 2HDM.

- CP-conserving

$$
\langle\phi_1\rangle = \begin{pmatrix} 0 \\ \frac{v_1}{\sqrt{2}} \end{pmatrix}, \quad \langle\phi_2\rangle = \begin{pmatrix} 0 \\ \frac{v_2}{\sqrt{2}} \end{pmatrix}
$$
(2.78)

- CP-violating (where vevs have a relative phase)

$$
\langle\phi_1\rangle = \begin{pmatrix} 0 \\ \frac{\bar{v}_1 e^{i\theta}}{\sqrt{2}} \end{pmatrix}, \quad \langle\phi_2\rangle = \begin{pmatrix} 0 \\ \frac{\bar{v}_2}{\sqrt{2}} \end{pmatrix}
$$
(2.79)

- Charge violating

$$
\langle\phi_1\rangle = \frac{1}{\sqrt{2}}\begin{pmatrix} \alpha \\ v_1' \end{pmatrix}, \quad \langle\phi_2\rangle = \frac{1}{\sqrt{2}}\begin{pmatrix} 0 \\ v_2' \end{pmatrix}
$$
(2.80)

with $v_1^2 + v_2^2 = v^2 = 246\,\text{GeV}^2$.

In the 2HDM applications, the potential is not necessarily considered in its most general form. Different versions of 2HDM applications have several simplifying assumptions to exhibit different characteristics. In general, both doublets couple to both $I_3 = 1/2$ and $-1/2$ fermions. After EW symmetry breaking, the Yukawa interaction [36]

$$
\mathcal{L}_{\text{Yukawa}}^{2HDM} = -y_1^{ij}\bar{f}_L^i\phi_1 f_R^j - y_2^{ij}\bar{f}_L^i\phi_2 f_R^j + h.c.
$$
(2.81)

25

leads to a mass matrix of the form

$$M^{ij} = v_1 y_1^{ij} \bar{f}^i f^j + v_2 y_2^{ij} \bar{f}^i f^j. \tag{2.82}$$

The Yukawa matrices y_1 and y_2 are not necessarily simultaneously diagonalizable; hence, the Yukawa interactions are not flavor diagonal. As a result, neutral Higgs bosons mediate flavor-changing interactions at the tree level [38]. Although flavor-changing neutral currents (FCNC) can be viable inside models with certain assumptions, they generally face phenomenological difficulties and are excluded from the models. Glashow-Weinberg-Pashcos theorem [39, 40] shows that it is possible to remove FCNC if fermions of particular electric charge couple only to a single doublet in the Yukawa term. This is achieved by introducing a discrete Z_2 symmetry on both scalars and fermions. This symmetry is implemented by assigning each particle a Z_2 charge, ± 1. It is known as the Natural Flavor Conservation (NFC) criterion. The scalars have different parity

$$\phi_1 \rightarrow -\phi_1, \quad \phi_2 \rightarrow \phi_2 \tag{2.83}$$

which prevents the transition $\phi_1 \leftrightarrow \phi_2$ and implies $m_{12} = \lambda_6 = \lambda_7 = 0$. However, the removal of FCNC can also be achieved by letting m_{12} to be non-zero, which softly breaks the Z_2 symmetry. Depending on assumptions on the other parameters, keeping the parameter m_{12} leads to various phenomenological outcomes [41].

In addition, the CP violation is generally excluded in 2HDM applications. Since all fields are scalar in Eq.(2.77), the invariance depends on doublets behavior under charge conjugation. The Higgs doublets transform as $\psi_i \rightarrow e^{i\eta_c^i}\psi_i^*$ under charge conjugation. Therefore, the gauge invariant combination transforms as $\psi_i^\dagger \psi_j \rightarrow e^{i\left(\eta_c^i - \eta_c^j\right)}\psi_j^\dagger \psi_i$. If there is no relative phase, $\eta_c^i = \eta_c^j$, the CP violation in Eq.(2.77) results from complex coefficients. Therefore all coefficients are assumed to be real.

The most general FNC 2HDM scalar potential is [41]

$$\begin{aligned}
V_{NFC}^{\text{2HDM}}(\phi_1, \phi_2) = {} & m_{11}^2 \phi_1^\dagger \phi_1 + m_{22}^2 \phi_2^\dagger \phi_2 - \left(m_{12}^2 \phi_1^\dagger \phi_2 + h.c.\right) + \frac{\lambda_1}{2}\left(\phi_1^\dagger \phi_1\right)^2 \\
& + \frac{\lambda_2}{2}\left(\phi_2^\dagger \phi_2\right)^2 + \lambda_3 \left(\phi_1^\dagger \phi_1\right)\left(\phi_2^\dagger \phi_2\right) + \lambda_4 \left(\phi_1^\dagger \phi_2\right)\left(\phi_2^\dagger \phi_1\right) \\
& + \left[\frac{\lambda_5}{2}\left(\phi_1^\dagger \phi_2\right)^2 + \left(\phi_2^\dagger \phi_1\right)^2\right]
\end{aligned} \tag{2.84}$$

Table 2.2: Types of 2HDMs that prevents FCNC, their descriptions and Z_2 charges of the fermions

Model	Q_L	u_R	d_R	L	l_R	Description
type-I	+	-	-	+	-	all fermions couple only to ϕ_2
type-II	+	-	+	+	-	up type quarks couple to ϕ_2, and down type quarks and leptons couple to ϕ_1
lepton-specific	+	-	+	+	-	quarks couple to ϕ_2 while leptons couple to ϕ_1
flipped	+	-	-	+	+	up type quarks and leptons couple to ϕ_2, and down type quarks couple to ϕ_1

In this case, four possible ways to configure the Yukawa sector exist. They are given in Table (2.2) along with Z_2 parities assigned to the fermions [36].

The Yukawa sector takes the form

$$\mathscr{L}_{\text{Yukawa}}^{2HDM} = -\sum_{i=1}^{2} \left(\bar{Q}_L \widetilde{\psi}_i \delta_i^u u_R + \bar{Q}_L \psi_i \delta_i^d d_R + \bar{L} \psi_i \delta_i^l e_R + \text{h.c.} \right) \tag{2.85}$$

with $\delta_1^f = 0$ or $\delta_2^f = 0$ depending on the model.

CHAPTER 3

VECTOR PORTAL

3.1   A Simple $\mathrm{U}(1)_D$ Extension of the Standard Model

The simplest form for a U(1) extension for the SM, which would act as a dark sector portal, would be obtained in the case when kinetic mixing is omitted. This case would appear as SM particles interact within a new U(1) group. Lagrangian would take the form:

$$\mathscr{L}_D = -\frac{1}{4} X^0_{\mu\nu} X^{0\mu\nu} + \frac{1}{2} m_X^2 X^0_\mu X^{0\mu} + g_D J_D^\mu X^0_\mu, \tag{3.1}$$

$$J_D^\mu = q'_f \bar{\psi}_f \gamma^\mu \psi_f \tag{3.2}$$

where X^0_μ is the new gauge boson or, in this case, the dark photon and $X^0_{\mu\nu}$ is its field strength tensor, g_D is the gauge coupling, and q'_f is he quantum number of fermions under $\mathrm{U}(1)_D$. One of the possible anomaly-free options for q'_f is $q'_f = B - L$ where B is the baryon number, and L is the lepton number of the fermion (see Appendix B).

m_X is the Stueckelberg mass parameter for the gauge field X^0_μ. Particles in the visible sector gain mass through the Higgs mechanism. However, an alternative way of mass generation can be employed in $\mathrm{U}(1)_D$. One such popular way is the Stueckelberg mechanism. In this mechanism, $\mathrm{U}(1)_D$ gauge boson couples to the derivative of axionic dark scalar in an invariant form under local gauge transformations. This allows Lagrangian to be gauge invariant while still allowing gauge particles to be massive. Such Lagrangian can be expressed as

$$\mathscr{L}_{\text{Stueckelberg}} = -\frac{1}{4} X^0_{\mu\nu} X^{0\mu\nu} + \frac{1}{2} m_X^2 \left(X^0_\mu - \partial_\mu \sigma \right)^2 \tag{3.3}$$

where σ is a scalar field. This Lagrangian is invariant under gauge transformation

$$X_\mu^0 \rightarrow X_\mu^{0\prime} = X_\mu^0 + \partial_\mu \lambda$$
$$\sigma \rightarrow \sigma' = \sigma - \lambda \tag{3.4}$$

where λ is an arbitrary function of spacetime. A scalar field from the dark sector is assumed to be charged under $U(1)_D$ only so that mass term in Eq. (3.1) is obtained.

3.2   Kinetic Mixing Between $U(1)_D$ and $U(1)_Y$

Unlike in more complex groups, in the U(1) group, the field strength tensor $F^{\mu\nu}$ is already gauge invariant. Therefore, an essential property of U(1) extensions is that it is possible to write gauge invariant terms that mix field strength tensors from different groups with a simple form of $F^{\mu\nu} F'_{\mu\nu}$ field is considered along with the previously given extension.

$$\mathscr{L} = \mathscr{L}_{\text{Gauge}}^{\text{KE}} + \mathscr{L}_{\text{Gauge}}^{\text{KM+Mass}} + \mathscr{L}_{\text{Scalar}}^{\text{KE}} + \mathscr{L}_{\text{Fermion}}^{\text{KE}} + \dots$$
$$\mathscr{L}_{\text{Gauge}}^{\text{KE}} = -\frac{1}{4} W_{3\mu\nu} W_3^{\mu\nu} - \frac{1}{4} Y_{\mu\nu} Y^{\mu\nu} - \frac{1}{4} X_{\mu\nu}^0 X^{0\mu\nu} + \dots \tag{3.5}$$
$$\mathscr{L}_{\text{Gauge}}^{\text{KM+Mass}} = -\frac{1}{2} \sin\epsilon \, X_{\mu\nu}^0 Y^{\mu\nu} + \frac{1}{2} m_X^2 X_\mu^0 X^{0\mu} \tag{3.6}$$
$$\mathscr{L}_{\text{Scalar}}^{\text{KE}} = \left(D_\mu \langle \phi \rangle\right)^\dagger D^\mu \langle \phi \rangle \tag{3.7}$$
$$\mathscr{L}_{\text{Fermion}}^{\text{KE}} = \sum_i \bar{f}_i i \slashed{D} f_i \tag{3.8}$$

where Y^μ and $W_{3\mu}$ are hypercharge fields, and the third component of weak isospin field and $Y^{\mu\nu}$ and $W_3^{\mu\nu}$ are their strength tensors. The coupling between Y^μ and $X^{0\mu}$ is expressed with $\sin\epsilon$. This value is considered very small; therefore, the approximation $\sin\epsilon \simeq \epsilon$ could be used.

By keeping the kinetic mixing term as it is, the theory can be developed around the basis of the existing gauge fields, and calculations can be made accordingly. However, removing the kinetic mixing term with a change of basis is more convenient. A rotation from the initial $(Y_\mu, W_\mu^3, X_\mu^0)$ basis and a new (B_μ, W_μ^3, X_μ) basis can be

written as

$$
\begin{pmatrix} B_\mu \\ W_{3\mu} \\ X_\mu \end{pmatrix} = \begin{pmatrix} 1 & 0 & \sin\epsilon \\ 0 & 1 & 0 \\ 0 & 0 & \cos\epsilon \end{pmatrix} \begin{pmatrix} Y_\mu \\ W_{3\mu} \\ X^0_\mu \end{pmatrix}
$$

$$
\equiv V_{BX,YX^0} \cdot \begin{pmatrix} Y_\mu \\ W_{3\mu} \\ X^0_\mu \end{pmatrix}. \tag{3.9}
$$

In the new basis, the kinetic mixing term between X^0_μ and Y_μ is no longer present; however, the transformation induces new mixing among the gauge fields in the mass and interaction terms. Therefore, additional transformations are needed to obtain the mass eigenstates of the gauge bosons, which are related to symmetry breaking and mass-gaining mechanisms.

Regardless of the form of the dark sector, a symmetry breaking of the form $G_{SM} \to SU(3)_C \otimes U(1)_Q$ is present. In order to illustrate this, the covariant derivative for $G_{SM} \otimes U(1)_D$ model can be explicitly stated.

$$
\begin{aligned}
D_\mu =& \partial_\mu - \mathrm{i}g\, \boldsymbol{t} \cdot \boldsymbol{W}_\mu - \mathrm{i}g_Y Y Y_\mu - \mathrm{i}g_D Q_D X^0_\mu \\
=& \partial_\mu - \mathrm{i}g\, t_3 W_{3\mu} - \mathrm{i}g' Y Y_\mu - \mathrm{i}g_D Q_D X^0_\mu + \left[-\mathrm{i}\frac{g}{\sqrt{2}} \left(t_+ W^+_\mu + t_- W^-_\mu \right) \right] \\
=& -\mathrm{i}g\, t_3 W_{3\mu} - \mathrm{i}g' Y B_\mu - \mathrm{i}\frac{1}{\cos\epsilon} \left(-g' Y \sin\epsilon + g_D Q_D \right) X_\mu + \dots \tag{3.10}
\end{aligned}
$$

In order to give substance to the mass gaining mechanism, the Higgs field with quantum numbers $(2,1/2)$ under $SU(2)_L \otimes U(1)_Y$ with vacuum expectation value $\langle H \rangle = (0 \quad v/\sqrt{2})^T$, $v = 246\text{GeV}$ is introduced initially.

$$
\begin{aligned}
\mathscr{L}^{\text{Mass}}_{\text{Gauge}} =& \frac{1}{2} m_X^2 X^0_\mu X^{0\mu} + \left(D_\mu \langle H \rangle \right)\left(D^\mu \langle H \rangle \right)^\dagger \\
=& \frac{1}{2} m_X^2 \sec^2\epsilon\, X_\mu X^\mu \\
&+ \frac{1}{8}(g'^2 + g^2) v^2 \left(-\sin\theta_W B_\mu + \cos\theta_W W_{3\mu} + \tan\epsilon \sin\theta_W X_\mu \right)^2 \tag{3.11}
\end{aligned}
$$

where θ_W is Weinberg mixing angle, $\tan\theta_W = g'/g$. In case of X_μ's absence (or $\epsilon \to 0$), $-\sin\theta_W B_\mu + \cos\theta_W W_{3\mu}$ would normally be Z boson and the other orthogonal combination $\cos\theta_W B_\mu + \sin\theta_W W_{3\mu}$ would be the photon. Of course, the fields

obtained in the presence of X^μ are not physical, and an additional transformation is required. Next, keeping X^μ untouched, Weinberg transformation which changes the basis $(B_\mu, W_{3\mu}, X_\mu) \to (A_\mu, \widetilde{W}_{3\mu}, X_\mu)$ is performed.

$$
\begin{pmatrix} A_\mu \\ \widetilde{W}_{3\mu} \\ X_\mu \end{pmatrix} = \begin{pmatrix} \cos\theta_W & \sin\theta_W & 0 \\ -\sin\theta_W & \cos\theta_W & 0 \\ 0 & 0 & 1 \end{pmatrix} \begin{pmatrix} B_\mu \\ W_{3\mu} \\ X_\mu \end{pmatrix}
$$

$$
\equiv V_{A\widetilde{W},BW} \cdot \begin{pmatrix} B_\mu \\ W_{3\mu} \\ X_\mu \end{pmatrix}
$$

$$
= V_{A\widetilde{W},BW} \cdot V_{BX,YX^0} \cdot \begin{pmatrix} Y_\mu \\ W_{3\mu} \\ X^0_\mu \end{pmatrix}
$$

$$
\equiv V_{A\widetilde{W},YX^0} \cdot \begin{pmatrix} Y_\mu \\ W_{3\mu} \\ X^0_\mu \end{pmatrix}
$$

$$
= \begin{pmatrix} \cos\theta_W & \sin\theta_W & \sin\epsilon\cos\theta_W \\ -\sin\theta_W & \cos\theta_W & -\sin\epsilon\sin\theta_W \\ 0 & 0 & \cos\epsilon \end{pmatrix} \begin{pmatrix} Y_\mu \\ W_{3\mu} \\ X^0_\mu \end{pmatrix} \tag{3.12}
$$

Here $V_{A\widetilde{W},YX^0}$ is defined as a single transformation from the initial base to the last base. The reason that the $(A_\mu, \widetilde{W}_{3\mu}, X_\mu)$ base is not the physical base is that the mass term is free of mixings

$$
\mathscr{L}_{\text{Gauge}}^{\text{Mass}} = \frac{1}{2} m_X^2 \sec^2\epsilon\, X_\mu X^\mu
$$

$$
+ \frac{1}{2} \underbrace{\frac{1}{4}(g'^2 + g^2)v^2}_{m_{Z^0}^2} \left(-\sin\theta_W B_\mu + \cos\theta_W W_{3\mu} + \tan\epsilon\sin\theta_W X_\mu\right)^2
$$

$$
\equiv \frac{1}{2} \begin{pmatrix} A_\mu & \widetilde{W}_{3\mu} & X_\mu \end{pmatrix} \cdot \mathscr{M}_{\text{Gauge}}^2 \cdot \begin{pmatrix} A_\mu \\ \widetilde{W}_{3\mu} \\ X_\mu \end{pmatrix}
$$

$$\mathcal{M}^2_{\text{Gauge}} = \begin{pmatrix} 0 & 0 & 0 \\ 0 & m^2_{Z^0} & m^2_{Z^0} \tan\epsilon \sin\theta_W \\ 0 & m^2_{Z^0} \tan\epsilon \sin\theta_W & m^2_X \sec^2\epsilon + \left(m_{Z^0} \tan\epsilon \sin\theta_W\right)^2 \end{pmatrix} \tag{3.13}$$

In the mass mixing matrix $\mathcal{M}^2_{\text{Gauge}}$, it is seen that the photon remains massless as expected. However, mass square terms for the remaining $(\widetilde{W}_{3\mu}, X_\mu)$ fields are still not diagonal. At this point, if an orthogonal transformation is performed,

$$\begin{pmatrix} A_\mu \\ Z_\mu \\ A'_\mu \end{pmatrix} = \begin{pmatrix} 1 & 0 & 0 \\ 0 & \cos\xi & \sin\xi \\ 0 & -\sin\xi & \cos\xi \end{pmatrix} \begin{pmatrix} A_\mu \\ \widetilde{W}_{3\mu} \\ X_\mu \end{pmatrix}$$

$$\equiv V_{ZA', \widetilde{W}X} \cdot \begin{pmatrix} A_\mu \\ \widetilde{W}_{3\mu} \\ X_\mu \end{pmatrix}$$

$$= V_{ZA', \widetilde{W}X} \cdot V_{A\widetilde{W}, BW} \cdot V_{BX, YX^0} \cdot \begin{pmatrix} Y_\mu \\ W_{3\mu} \\ X^0_\mu \end{pmatrix}$$

$$\equiv V_{AZA', YWX^0} \cdot \begin{pmatrix} Y_\mu \\ W_{3\mu} \\ X^0_\mu \end{pmatrix}$$

$$= \begin{pmatrix} \cos\theta_W & \sin\theta_W & \sin\epsilon \cos\theta_W \\ -\cos\xi \sin\theta_W & \cos\xi \cos\theta_W & \sin\xi \cos\epsilon - \cos\xi \sin\epsilon \sin\theta_W \\ \sin\xi \sin\theta_W & -\sin\xi \cos\theta_W & \cos\xi \cos\epsilon + \sin\xi \sin\epsilon \sin\theta_W \end{pmatrix} \begin{pmatrix} Y_\mu \\ W_{3\mu} \\ X^0_\mu \end{pmatrix} \tag{3.14}$$

and Eq.(3.13) can be rewritten in this base. By choosing a suitable ξ angle, $\mathcal{M}^2_{\text{Gauge}}$ given in Eq. 3.13 can be diagonalized.

$$\mathcal{L}^{\text{Mass}}_{\text{Gauge}} = \frac{1}{2} \begin{pmatrix} A_\mu & Z_\mu & A'_\mu \end{pmatrix} \begin{pmatrix} 0 & 0 & 0 \\ 0 & M^2_Z & 0 \\ 0 & 0 & M^2_{A'} \end{pmatrix} \begin{pmatrix} A_\mu \\ Z_\mu \\ A'_\mu \end{pmatrix} \tag{3.15}$$

This angle choice is given by the relation

$$
\begin{pmatrix} 1 & 0 & 0 \\ 0 & \cos\xi & \sin\xi \\ 0 & -\sin\xi & \cos\xi \end{pmatrix} m_{Z^0}^2 \begin{pmatrix} 0 & 0 & 0 \\ 0 & a & b \\ 0 & b & c \end{pmatrix} \begin{pmatrix} 1 & 0 & 0 \\ 0 & \cos\xi & -\sin\xi \\ 0 & \sin\xi & \cos\xi \end{pmatrix} = \begin{pmatrix} 0 & 0 & 0 \\ 0 & M_Z^2 & 0 \\ 0 & 0 & M_{A'}^2 \end{pmatrix}, \quad (3.16)
$$

which yields $\tan 2\xi = 2b/(a-c)$ where a, b and c are elements of the matrix $\mathcal{M}_{\text{Gauge}}^2$:

$$
\begin{aligned}
a &= 1 \\
b &= \tan\epsilon \, \sin\theta_W \qquad\qquad\qquad\qquad\qquad\qquad (3.17) \\
c &= \sec^2\epsilon \, DZ + (\tan\epsilon \, \sin\theta_W)^2, \quad DZ = \left(\frac{m_X}{m_{Z^0}} \right)^2
\end{aligned}
$$

The resulting physical gauge boson masses are:

$$
\begin{aligned}
M_A^2 &= 0, \\
M_{A'}^2 &= m_X^2 \cos^2\xi \sec^2\epsilon + m_{Z^0}^2 \left[\sin\xi - \cos\xi \sin\theta_W \tan\epsilon \right]^2, \qquad (3.18) \\
M_Z^2 &= m_X^2 \sin^2\xi \sec^2\epsilon + m_{Z^0}^2 \left[\cos\xi + \sin\xi \sin\theta_W \tan\epsilon \right]^2.
\end{aligned}
$$

Due to the mixing with the dark sector, the Z boson mass expression gets contributions from dark sector and therefore, the mass of Z would change according to the values of new parameters (see Fig. 3.1). However, this mass is measured precisely with a universal fit of $M_Z = 91.1876 \pm 0.0021$ [11], so the dark sector contribution should not change this value too much. Dark sector contribution is in the eV order in the light m_X region ($m_X \leq 1$ GeV). Moreover, for the A' mass, while for large m_X dominates the mass term so that $M_{A'} \approx m_X$, and in the small m_X region, the second term in the right hand side of M_Z^2 expression is dominant (see Fig. 3.2).

In this basis, the interaction term is also modified:

$$
\begin{aligned}
\mathscr{L}_{\text{Interaction}} &\subset \sum_i \bar{f}_i i\slashed{D} f_i \\
&= \sum_i \frac{1}{2} \bar{f}_i \left(C_V^f \gamma^\mu + C_A^f \gamma^\mu \gamma^5 \right) f_i A_\mu + \frac{1}{2} \bar{f}_i \left(C_V'^f \gamma^\mu + C_A'^f \gamma^\mu \gamma^5 \right) f_i Z_\mu \\
&\quad + \frac{1}{2} \bar{f}_i \left(C_V''^f \gamma^\mu + C_A''^f \gamma^\mu \gamma^5 \right) f_i A'_\mu \\
&\equiv g' J_Y^\mu Y_\mu + g J_3^\mu W_{3\mu} + g_D J_X^\mu X_\mu^0 \\
&= \begin{pmatrix} g' J_Y^\mu & g J_3^\mu & g_D J_X^\mu \end{pmatrix} \begin{pmatrix} Y_\mu \\ W_{3\mu} \\ X_\mu^0 \end{pmatrix}
\end{aligned}
$$
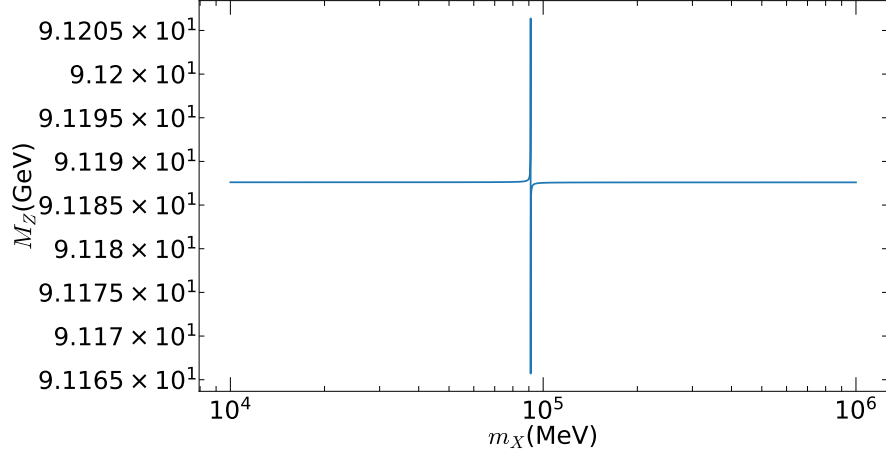
Figure 3.1: Z boson mass as a function of m_X for $\sin\epsilon = 10^{-3}$
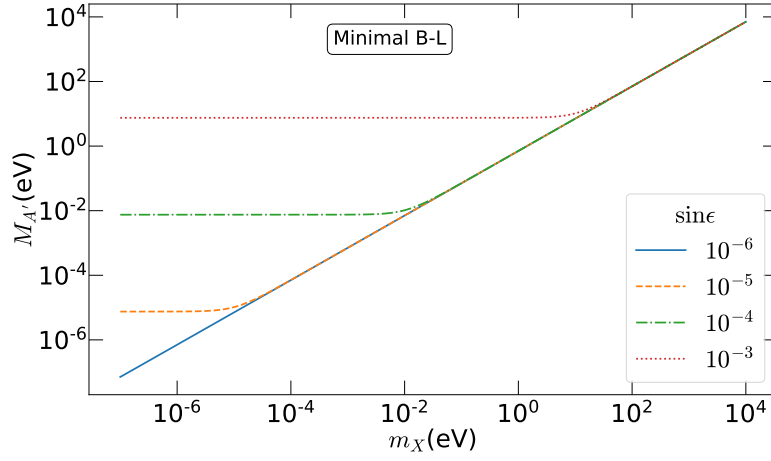
Figure 3.2: The mass of the dark photon, $M_{A'}$, as a function of m_X for various $\sin\epsilon$ in the minimal $B-L$ model
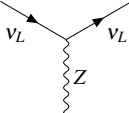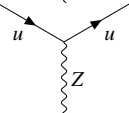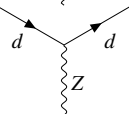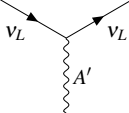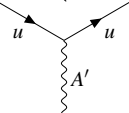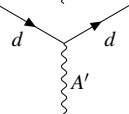
$$= \begin{pmatrix} g'J_Y^\mu & gJ_3^\mu & g_D J_X^\mu \end{pmatrix} \cdot V^{-1}_{AZA',YWX^0} \cdot \begin{pmatrix} A_\mu \\ Z_\mu \\ A'_\mu \end{pmatrix} \quad (3.19)$$

Here J_Y^μ, J_3^μ, and J_X^μ are fermion currents involving hypercharge, weak and dark forces, respectively. V^{-1}_{AZA',YWX^0} is the inverse of total transformation matrix,

$$V^{-1}_{AZA',YW_3X^0} = \begin{pmatrix} \cos\theta_W & -\frac{\sin\theta_W \cos\xi \cos\epsilon + \sin\xi \sin\epsilon}{\cos\epsilon} & \frac{\sin\theta_W \sin\xi \cos\epsilon - \cos\xi \sin\epsilon}{\cos\epsilon} \\ \sin\theta_W & \cos\xi \cos\theta_W & -\sin\xi \cos\theta_W \\ 0 & \frac{\sin\xi}{\cos\epsilon} & \frac{\cos\xi}{\cos\epsilon} \end{pmatrix}. \quad (3.20)$$

35

The photon interactions remain unchanged. The vertex factors contributing to CEνNS process are given in Table 3.1.

Table 3.1: The relevant vertex factors contributing to the CEνNS in U(1)$_D$ extended model. A shorthand notation is used for the trigonometric expressions. For example, (s_ξ, t_ϵ) stand for $(\sin\xi, \tan\epsilon)$ and similar for the others.

Vertices	$C'^{\,f}_V$	$C'^{\,f}_A$
$\nu_L \; Z \; \nu_L$	$-\dfrac{g_D s_\xi}{4 c_\epsilon} + \dfrac{e(c_\xi + s_\xi t_\epsilon s_W)}{4 c_W s_W}$	$-\dfrac{e(c_\xi + s_\xi t_\epsilon s_W)}{4 c_W s_W}$
$u \; Z \; u$	$\dfrac{g_D s_\xi}{12 c_\epsilon} + \dfrac{e c_\xi(8 s_W^2 - 3) + 5 e s_\xi t_\epsilon s_W}{12 c_W s_W}$	$-\dfrac{e(c_\xi + s_\xi t_\epsilon s_W)}{4 c_W s_W}$
$d \; Z \; d$	$\dfrac{g_D s_\xi}{12 c_\epsilon} + \dfrac{e c_\xi(4 s_W^2 - 3) + e s_\xi t_\epsilon s_W}{12 c_W s_W}$	$\dfrac{e(c_\xi + s_\xi t_\epsilon s_W)}{4 c_W s_W}$
	$C''^{\,f}_V$	$C''^{\,f}_A$
$\nu_L \; A' \; \nu_L$	$\dfrac{g_D c_\xi}{4 c_\epsilon} + \dfrac{e(s_\xi - c_\xi t_\epsilon s_W)}{4 c_W s_W}$	$\dfrac{e(s_\xi - c_\xi t_\epsilon s_W)}{4 c_W s_W}$
$u \; A' \; u$	$\dfrac{g_D c_\xi}{12 c_\epsilon} + \dfrac{e s_\xi(8 s_W^2 - 3) - 5 e c_\xi t_\epsilon s_W}{12 c_W s_W}$	$\dfrac{e(s_\xi - c_\xi t_\epsilon s_W)}{4 c_W s_W}$
$d \; A' \; d$	$\dfrac{g_D c_\xi}{12 c_\epsilon} - \dfrac{e s_\xi(4 s_W^2 - 3) - e c_\xi t_\epsilon s_W}{12 c_W s_W}$	$-\dfrac{e(s_\xi - c_\xi t_\epsilon s_W)}{4 c_W s_W}$

3.3 The Mass Mixing

Another term that can be considered in U(1) extensions is a mass mixing between the new vector mediator and the third component of the weak field, $\widetilde{W}_3^\mu$, of the form

$$\mathscr{L}_{\text{Gauge}}^{\text{MassMixing}} = \frac{1}{2} m_{\text{mix}}^2 X_\mu \widetilde{W}_3^\mu. \tag{3.21}$$

Inserting this term in a way that preserves gauge invariance would be related to the Higgs sector. If the Higgs doublet is charged under U(1)$_D$, this mixing occurs

in the electroweak symmetry-breaking procedure. However, since the anomaly-free charge options contain some combinations of baryon and lepton quantum numbers, the SM Higgs field cannot induce such a mass mixing term. Nonetheless, in the models with SM Higgs sector extended, the doublets can acquire non-zero $B - L$ values.

3.3.1 Framework of the Two Higgs Doublet Model with U(1) Extensions

The most general 2HDM Lagrangian suffers from FCNC at the tree level. To remove these currents, typically, a Z_2 symmetry is imposed on the 2HDM Lagrangian, which is discussed in Section 2.3. The Z_2 symmetry, however, is not the only way to avoid the FCNC problem. Another postulated approach to the problem is to extend the symmetry group of the Lagrangian with a U(1). Under such an extension framework, the gauge principles effectively repeat the effects of Z_2 symmetry and lead to the usual NFC 2HDM classes [41] [42]. The key criterion is that the U(1) charges of the two Higgs doublets differ. This criteria leads to distinct transformation characteristics for the doublets and simplifies the NFC scalar potential Eq.(2.84) to

$$V_{NFC}^{2\text{HDM}}(\phi_1, \phi_2) = m_{11}^2 \phi_1^\dagger \phi_1 + m_{22}^2 \phi_2^\dagger \phi_2 + \frac{\lambda_1}{2}\left(\phi_1^\dagger \phi_1\right)^2 + \frac{\lambda_2}{2}\left(\phi_2^\dagger \phi_2\right)^2$$
$$+ \lambda_3\left(\phi_1^\dagger \phi_1\right)\left(\phi_2^\dagger \phi_2\right) + \lambda_4\left(\phi_1^\dagger \phi_2\right)\left(\phi_2^\dagger \phi_1\right) \tag{3.22}$$

The fields transform under U(1)$_D$ as

$$f \to f' = e^{iq_f' \rho} f \tag{3.23}$$

where q_f' is the fermion charges under U(1)$_D$, and ρ is arbitrary spacetime dependent parameter. Once the type of Yukawa interaction is specified, the dark charges of fermions are related to each other. In this case, type-I 2HDM is chosen. Under U(1)$_D$, the Yukawa interaction transforms as

$$-\mathcal{L}_{\text{Yukawa}}^{\text{type-I}} \to -\mathcal{L}_{\text{Yukawa}}^{'\text{type-I}} = e^{i\left(-q_L' + Q_D^{\phi_2} + q_e'\right)\rho} y_e'^{\alpha\beta} \bar{L}'^\alpha \phi e_R'^\beta + e^{i\left(-q_{Q_L}' - Q_D^{\phi_2} + q_u'\right)\rho} y_u'^{\alpha\beta} \bar{Q}_L'^\alpha \tilde{\phi}^c u_R'^\beta$$
$$+ e^{i\left(-q_{Q_L}' + Q_D^{\phi_2} + q_d'\right)\rho} y_d'^{\alpha\beta} \bar{Q}_L'^\alpha \phi d_R'^\beta + \text{h.c.} \tag{3.24}$$

where $Q_D^{\phi_2}$ is the charge of the second doublet. The U(1)$_D$ invariance of this term gives the constraints

$$Q_D^{\phi_2} + q_e' - q_L' = 0,$$

$$-Q_D^{\phi_2} + q'_u - q'_{Q_L} = 0, \tag{3.25}$$
$$Q_D^{\phi_2} + q'_d - q'_{Q_L} = 0.$$

Note that, since $Q_D^{\phi_1} \neq Q_D^{\phi_2}$, the first doublet's coupling with fermions inside the Yukawa term is prohibited by gauge invariance.

3.3.1.1 Anomaly-Free Conditions in Natural Flavor Conserving Two Higgs Doublet Models

The previously discussed Minimal $B-L$ model requires additional right-handed neutrinos to satisfy anomaly-free conditions. However, in the NFC 2HDMs, it is possible to obtain anomaly cancellation without adding new fermions [1]. By combining the anomaly cancellation condition Eq.(B.7) ($q'_L = -3q'_{Q_L}$) with gauge freedom condition from Yukawa term Eq.(3.25), the charges of fields can be written in terms of q'_{u_R} and q'_{d_R}

$$
\begin{aligned}
q'_{Q_L} &= \frac{q'_{u_R} + q'_{d_R}}{2}, \\
q'_L &= -\frac{3\left(q'_{u_R} + q'_{d_R}\right)}{2}, \\
q'_{e_R} &= -\left(2q'_{u_R} + q'_{d_R}\right), \\
Q_D^{\phi_2} &= \frac{q'_{u_R} - q'_{d_R}}{2}
\end{aligned}
\tag{3.26}
$$

These charge assignments satisfy Eqs.(B.5)-(B.11). However, inserting them in the cancellation condition for $(\mathrm{U}(1)_D)^3$ triangle anomaly, Eq.(B.5), gives

$$
\begin{aligned}
&q'^3_{e_R} + 3q'^3_{u_R} + 3q'^3_{d_R} - 2q'^3_L - 6q'^3_{Q_L} \\
&= \left(-2q'_{u_R} - q'_{d_R}\right)^3 + 3q'^3_{u_R} + 3q'^3_{d_R} - 2\left(\frac{q'_{u_R} + q'_{d_R}}{2}\right)^3 - 6\left(\frac{q'_{u_R} - q'_{d_R}}{2}\right)^3 \\
&= \left(q'_{u_R} + 2q'_{d_R}\right)^3
\end{aligned}
\tag{3.27}
$$

Therefore, in the absence of new fermions, anomaly cancellation requires $q'_{u_R} = -2q'_{d_R}$.

3.3.1.2 Neutrino Masses in the Two Higgs Doublet Models

Until this point, no constraints on $Q_D^{\phi_1}$ are obtained; hence, it is arbitrary. A constraint can be obtained in a variation of this class model, which explains the neutrino masses. The neutrino masses can easily be generated by introducing a right-handed neutrino for each family of leptons. However, it is also possible to implement the seesaw mechanism within the 2HDM framework [43]. The advantage of using this mechanism is that it naturally explains the smallness of the neutrino masses. Additionally, it can be used to explain the baryon asymmetry in the universe.

In this context, three right-handed Majorana neutrinos n_R are added to the model. This changes the anomaly cancellation constraint on charges of u_R and d_R. The following relation is obtained from Eq.(B.14).

$$q'_{n_R} = -\left(q'_{u_R} + 2q'_{d_R}\right) \tag{3.28}$$

The Yukawa term needs to be examined next. However, since right-handed neutrinos are charged under $U(1)_D$, the bare Majorana mass term of the form $m_R \bar{n}_R^c n_R$ is prohibited. Instead, this coupling is achieved by introducing a massive scalar singlet ϕ_s. This addition extends the scalar potential Eq.(3.22) with the following term.

$$V_s = m_s^2 \phi_s^\dagger \phi_s + \frac{\lambda_s}{2}\left(\phi_s^\dagger \phi_s\right)^2 + \lambda_8 \phi_1^\dagger \phi_1 \phi_s^\dagger \phi_s + \lambda_9 \phi_2^\dagger \phi_2 \phi_s^\dagger \phi_s + \left(\lambda_{10} \phi_1^\dagger \phi_2 \phi_s + \text{h.c.}\right) \tag{3.29}$$

All of the terms above are invariant under $U(1)_D$ as they stand, except for the last term. This term requires $Q_D^{\phi_s} = Q_D^{\phi_1} - Q_D^{\phi_2}$ for invariance. Then the neutrino part of the Yukawa term reads

$$-\mathscr{L}_{\text{Yukawa}}^\nu = y_D^{ij} \bar{L}^i \widetilde{\phi}_2 n_R^j + y_M^{ij} \bar{n}^{ci} \phi_s n_R^j, \tag{3.30}$$

In order to generate neutrino masses through the spontaneous symmetry-breaking process, symmetry breaking of $U(1)_D$ through the scalar singlet obtaining its vacuum expectation value is assumed to happen way above the electroweak scale. At a lower energy scale, ν_2 breaks the electroweak symmetry. This process realizes the

type-I seesaw mechanism [44].

$$M_{v'} = \begin{pmatrix} \bar{v}_L & \bar{n}_R \end{pmatrix} \begin{pmatrix} 0 & m_D \\ m_D^T & m_M \end{pmatrix} \begin{pmatrix} v_L \\ n_R \end{pmatrix} \qquad (3.31)$$

The eigenvalues of $M_{v'}$ are $M_{1,2} = \frac{1}{2}\left(m_M \pm \sqrt{m_M^2 + 4m_D} \right)$. Under the assumption $m_R \gg m_D$, diagonalization yields

$$m_{v_L} = -\frac{m_D^2}{m_R}, \quad m_{n_R} = m_R \qquad (3.32)$$

where

$$m_D = \frac{y_D v_2}{2\sqrt{2}} \quad \text{and} \quad m_R = \frac{y_M v_s}{2\sqrt{2}}. \qquad (3.33)$$

Returning to the constraints on the dark charges, invariance of the first term in the neutrino Yukawa Lagrangian Eq.(3.30) is already established with the previously given constraints Eqs. (3.26, 3.28). Invariance of the second term in Eq.(3.30) requires

$$2q'_{n_R} + Q_D^{\phi_s} = 0$$
$$\text{or} \quad Q_D^{\phi_s} = 2q'_{u_R} + 4q'_{d_R}. \qquad (3.34)$$

Using the constraint from the scalar potential $Q_D^{\phi_s} = Q_D^{\phi_1} - Q_D^{\phi_2}$, the charge of the first doublet can be written as

$$Q_D^{\phi_1} = \frac{5q'_{u_R}}{2} + \frac{7q'_{d_R}}{2}. \qquad (3.35)$$

In the end, all charges under $U(1)_D$ are linked to q'_{u_R} and q'_{d_R}. In the case $q'_{u_R} = q'_{d_R} = 1/6$, we obtain the $U(1)_{B-L}$ case in the 2HDM [1]. Beyond that, a whole class of models can be generated under these constraints. A set of models leading to different phenomenology developed in [1] is given in Table 3.2.

---

[1] The charges are $1/6$ instead of $1/3$ due to our convention. A common convention is to take the covariant derivative in the form $D_\mu = \partial_\mu + ig'\frac{q'}{2}A'_\mu + ...$ In our case, the factor $1/2$ is absorbed in q'

3.3.2 Vector Portal in Two Higgs Doublet Model

A part of the Lagrangian for $U(1)_D$ extended Type-I FNC 2HDM can be expressed as follows:

$$\mathscr{L} = \mathscr{L}^{\text{KE}}_{\text{Gauge}} + \mathscr{L}^{\text{KM+Mass}}_{\text{Gauge}} + \mathscr{L}^{\text{KE}}_{\text{Scalar}} + \mathscr{L}^{\text{KE}}_{\text{Fermion}} + \cdots$$

$$\mathscr{L}^{\text{KE}}_{\text{Gauge}} = -\frac{1}{4} W_{3\mu\nu} W_3^{\mu\nu} - \frac{1}{4} Y_{\mu\nu} Y^{\mu\nu} - \frac{1}{4} X^0_{\mu\nu} X^{0\mu\nu} + \cdots \tag{3.36}$$

$$\mathscr{L}^{\text{KM+Mass}}_{\text{Gauge}} = -\frac{1}{2}\sin\epsilon \, X^0_{\mu\nu} Y^{\mu\nu} + \frac{1}{2} m_X^2 X^0_\mu X^{0\mu} \tag{3.37}$$

$$\mathscr{L}^{\text{KE}}_{\text{Scalar}} = \left(D_\mu \langle\phi_1\rangle\right)^\dagger D^\mu \langle\phi_1\rangle + \left(D_\mu \langle\phi_2\rangle\right)^\dagger D^\mu \langle\phi_2\rangle \tag{3.38}$$

$$\mathscr{L}^{\text{KE}}_{\text{Fermion}} = \sum_i \bar{f}_i i\slashed{D} f_i \tag{3.39}$$

Vacuum expectation values of the Higgs doublets have the form $v_2 = v\sin\beta$ and $v_1 = v\cos\beta$ with $v \approx 246\,\text{GeV}$. The covariant derivative of a Higgs doublet is

$$D_\mu \phi_i = \left(-ig\,t_3 W_{3\mu} - ig' Y\, Y_\mu - ig_D q_D X^0_\mu\right)\phi_i. \tag{3.40}$$

Similar to the earlier case, in order to obtain the mass eigenbasis, three rotations are performed. First, the field redefinitions $Y_\mu \to B_\mu - \tan\epsilon\, X_\mu$, $X^0_\mu \to \sec\epsilon\, X_\mu$, analogous to Eq. (3.9), removes the kinetic mixing. Eq. (3.40) takes the form

$$D_\mu \phi_i = \left(-ig\, I_H \sigma^3 W_{3\mu} - ig' Y_H \left(B_\mu - \tan\epsilon\, X_\mu\right) - ig_D Q_D^{H_i} \sec\epsilon\, X_\mu\right)\phi_i$$

$$= \left(i\frac{g}{2}\sigma^3 W_{3\mu} - i\frac{g'}{2} B_\mu - \frac{i}{\cos\epsilon}\left(-\frac{g'\sin\epsilon}{2} + g_D Q_D^{H_i}\right) X_\mu\right)\phi_i \tag{3.41}$$

$$= \begin{pmatrix} -i\frac{g}{2} W_{3\mu} - i\frac{g'}{2} B_\mu - \frac{i}{c_\epsilon}\left(-\frac{g' s_\epsilon}{2} + g_D Q_D^{H_i}\right) X_\mu & 0 \\ 0 & i\frac{g}{2} W_{3\mu} - i\frac{g'}{2} B_\mu - \frac{i}{c_\epsilon}\left(-\frac{g' s_\epsilon}{2} + g_D Q_D^{H_i}\right) X_\mu \end{pmatrix} \phi_i \tag{3.42}$$

where $Q_D^{H_i}$ is the charge of the Higgs doublet under $U(1)_D$. Inserting the vacuum expectation value

$$\langle\phi_i\rangle = \begin{pmatrix} 0 \\ \frac{v_i}{\sqrt{2}} \end{pmatrix} \tag{3.43}$$

gives

$$D_\mu \langle\phi_i\rangle = \begin{pmatrix} 0 \\ \frac{v}{\sqrt{2}}\left(i\frac{g}{2} W_{3\mu} - i\frac{g'}{2} B_\mu - \frac{i}{\cos\epsilon}\left(-\frac{g'\sin\epsilon}{2} + g_D Q_D^{H_i}\right) X_\mu\right) \end{pmatrix} \quad \text{and}$$

$$\left(D_\mu\langle\phi_i\rangle\right)^\dagger = \left(0 \quad \frac{v}{\sqrt{2}}\left(-\mathrm{i}\frac{g}{2}W_{3\mu} + \mathrm{i}\frac{g'}{2}B_\mu + \frac{\mathrm{i}}{\cos\epsilon}\left(-\frac{g'\sin\epsilon}{2} + g_D Q_D^{H_i}\right)X_\mu\right)\right). \tag{3.44}$$

Then, the kinetic energy terms of the scalar fields become

$$\left(D_\mu\langle\phi_i\rangle\right)^\dagger\left(D_\mu\langle\phi_i\rangle\right)$$

$$= -\frac{v_i^2}{2}\left(\mathrm{i}\frac{g}{2}W_{3\mu} - \mathrm{i}\frac{g'}{2}B_\mu - \frac{\mathrm{i}}{\cos\epsilon}\left(-\frac{g'\sin\epsilon}{2} + g_D Q_D^{H_i}\right)X_\mu\right)^2$$

$$= \frac{v_i^2}{8}\left(\overbrace{gW_{3\mu} - g'B_\mu}^{(c_w W_{3\mu} - s_w B_\mu)\sqrt{g^2+g'^2}} - \frac{2}{\cos\epsilon}\left(-\frac{g'\sin\epsilon}{2} + g_D Q_D^{H_i}\right)X_\mu\right)^2$$

$$= \frac{1}{8}\sqrt{g^2+g'^2}\,v_i^2\left(c_w W_{3\mu} - s_w B_\mu - \frac{2}{\cos\epsilon\sqrt{g^2+g'^2}}\left(-\frac{g'\sin\epsilon}{2} + g_D Q_D^{H_i}\right)X_\mu\right). \tag{3.45}$$

where s_w and c_w stand for sine and cosine of the Weinberg angle, respectively, and Eq. (2.59) is used in the third row. By using $\sin\theta_W = g'/\sqrt{g^2+g'^2}$ again, the X_μ term can be rewritten as

$$\frac{-2}{\cos\epsilon\sqrt{g^2+g'^2}}\left(-\frac{g'\sin\epsilon}{2} + g_D Q_D^{H_i}\right)X_\mu = \left(\sin\theta_W\tan\epsilon - \frac{2g_D}{\sqrt{g^2+g'^2}}\sec\epsilon\,Q_D^{H_i}\right)X_\mu. \tag{3.46}$$

At this point, the second basis transformation can be performed. This is the Weinberg transformation $A_\mu = \sin\theta_W W_{3\mu} + \cos\theta_W B_\mu$, $\widetilde{W}_{3\mu} = \cos\theta_W W_{3\mu} - \sin\theta_W B_\mu$, a transformation of basis $(B_\mu, W_{3\mu}, X_\mu) \to (A_\mu, \widetilde{W}_{3\mu}, X_\mu)$ described in Eq. (3.12). Using $g^2 + g'^2 = \frac{4m_{Z_0}^2}{v^2}$, Eq. (3.45) becomes

$$\left(D_\mu\langle\phi_i\rangle\right)^\dagger\left(D_\mu\langle\phi_i\rangle\right)$$

$$= \frac{1}{8}\overbrace{(g^2+g'^2)v^2}^{\frac{1}{2}m_{Z_0}^2}\,t_i\left(\overbrace{c_w W_{3\mu} - \sin\theta_W B_\mu}^{\widetilde{W}_{3\mu}} + \left(s_w\tan\epsilon - \overbrace{\frac{2g_D}{\sqrt{g^2+g'^2}}}^{\frac{g_D v}{m_{Z_0}}}\sec\epsilon\,Q_D^{H_i}\right)X_\mu\right)^2$$

$$= \frac{1}{2}m_{Z_0}^2\,t_i\left(\widetilde{W}_{3\mu} + \left(\sin\theta_W\tan\epsilon - \frac{g_D v}{m_{Z_0}}\sec\epsilon\,Q_D^{H_i}\right)X_\mu\right)^2, \quad t_i = \sin^2\beta \text{ or } \cos^2\beta \tag{3.47}$$

The gauge mass term Eq. (3.38) becomes

$$\mathscr{L}_{Gauge}^{mass} = \frac{1}{2}m_X^2\sec^2\epsilon\,X_\mu X^\mu + \sum_{i=1}^{2}\left(D_\mu\langle\phi_i\rangle\right)^\dagger\left(D_\mu\langle\phi_i\rangle\right)$$

$$= \frac{1}{2}m_X^2\sec^2\epsilon\,X_\mu X^\mu + \frac{1}{2}m_{Z_0}^2\sin^2\beta\left(\widetilde{W}_{3\mu} + \left(\sin\theta_W\tan\epsilon - \frac{g_D v}{m_{Z_0}}\sec\epsilon\,Q_D^{H_2}\right)X_\mu\right)^2$$

$$+ \frac{1}{2}m_{Z_0}^2\cos^2\beta\left(\widetilde{W}_{3\mu} + \left(\sin\theta_W\tan\epsilon - \frac{g_D v}{m_{Z_0}}\sec\epsilon\,Q_D^{H_1}\right)X_\mu\right)^2$$

$$
\begin{aligned}
=\frac{1}{2}m_{Z_0}^2 \Big\{ &\big(\sin^2\beta + \cos^2\beta\big)\widetilde{W}_{3\mu}^2 \\
&+ \sin^2\beta \overbrace{\bigg(\tan\epsilon\sin\theta_W - \frac{2g_D}{\sqrt{g'^2+g^2}}\sec\epsilon Q_D^{H_2}\bigg)}^{\widetilde{Q}_{H_2}}{}^2 X_\mu^2 \\
&+ \cos^2\beta \overbrace{\bigg(\tan\epsilon\sin\theta_W - \frac{2g_D}{\sqrt{g'^2+g^2}}\sec\epsilon Q_D^{H_1}\bigg)}^{\widetilde{Q}_{H_1}}{}^2 X_\mu^2 \\
&+ 2\bigg[\cos^2\beta\tan\epsilon\sin\theta_W - \frac{2g_D}{\sqrt{g'^2+g^2}}\sec\epsilon Q_D^{H_1} \\
&+ \sin^2\beta\,\tan\epsilon\sin\theta_W - \frac{2g_D}{\sqrt{g'^2+g^2}}\sec\epsilon Q_D^{H_2}\bigg]\widetilde{W}_{3\mu}X^\mu \Big\} \\
=\frac{1}{2}m_{Z_0}^2 \widetilde{W}_{3\mu}^2 &+ \frac{1}{2}m_{Z_0}^2\big(\cos^2\beta\,\widetilde{Q}_{H_1}^2 + \sin^2\beta\,\widetilde{Q}_{H_2}^2\big)X_\mu^2 \\
&+ \frac{1}{2}m_{Z_0}^2\big(\cos^2\beta\,\widetilde{Q}_{H_1} + \sin^2\beta\,\widetilde{Q}_{H_2}\big)2\widetilde{W}_{3\mu}X^\mu
\end{aligned}
\tag{3.48}
$$

This term can be stated in the matrix form as follows

$$
\begin{aligned}
\mathcal{L}_{\text{Gauge}}^{\text{mass}} &= \frac{1}{2}m_X^2\sec\epsilon X_\mu X^\mu + \sum_{i=1}^{2}\big(D_\mu\langle H_i\rangle\big)^\dagger D^\mu\langle H_i\rangle \\
&= \frac{1}{2}\begin{pmatrix} A_\mu & \widetilde{W}_{3\mu} & X_\mu \end{pmatrix} M_{\text{Gauge}}^2 \begin{pmatrix} A^\mu \\ \widetilde{W}_3{}^\mu \\ X^\mu \end{pmatrix}
\end{aligned}
\tag{3.49}
$$

where

$$
M_{\text{Gauge}}^2 = m_{Z_0}^2 \begin{pmatrix} 0 & 0 & 0 \\ 0 & a & b \\ 0 & b & c \end{pmatrix},
\qquad
\begin{aligned}
a &= 1 \\
b &= \cos^2\beta\,\widetilde{Q}_{H_1} + \sin^2\beta\,\widetilde{Q}_{H_2} \\
c &= \sec^2\epsilon\frac{m_{X_0}^2}{m_{Z_0}^2} + \cos^2\beta\,\widetilde{Q}_{H_1}^2 + \sin^2\beta\,\widetilde{Q}_{H_2}^2
\end{aligned}
\tag{3.50}
$$

where

$$
\widetilde{Q}_{H_i} = \tan\epsilon\sin\theta_W - \frac{2g_D}{\sqrt{g'^2+g^2}}\sec\epsilon Q_D^{H_i}.
\tag{3.51}
$$

Therefore, the third rotation should diagonalize this matrix. This transformation is equivalent to Eq. (3.16), and the rotation angle satisfies $\tan 2\xi = 2b/a - c$. The total

transformation from the initial base to the physical basis takes the form

$$
\begin{pmatrix} A_\mu \\ Z_\mu \\ A'_\mu \end{pmatrix} = \begin{pmatrix} \cos\theta_W & \sin\theta_W & \sin\epsilon\cos\theta_W \\ -\cos\xi\sin\theta_W & \cos\xi\cos\theta_W & \sin\xi\cos\epsilon - \cos\xi\sin\epsilon\sin\theta_W \\ \sin\xi\sin\theta_W & -\sin\xi\cos\theta_W & \cos\xi\cos\epsilon + \sin\xi\sin\epsilon\sin\theta_W \end{pmatrix} \begin{pmatrix} Y_\mu \\ W_{3\mu} \\ X^0_\mu \end{pmatrix}
$$

(3.52)

The corresponding eigenvalues are

$$
M_A^2 = 0,
$$
(3.53)

$$
\begin{aligned}
M_{A'}^2 = {} & m_X^2 \cos^2\xi \sec^2\epsilon + \frac{1}{4} g_D^2 v^2 \cos^2\xi \sec^2\epsilon \left[\cos^2\beta \left(Q_D^{\phi_1}\right)^2 + \sin^2\beta \left(Q_D^{\phi_2}\right)^2 \right] \\
& + g_D \, v \, m_{Z_0} \cos\xi \sec\epsilon \left(\cos^2\beta \, Q_D^{\phi_1} + \sin^2\beta \, Q_D^{\phi_2} \right) (\sin\xi - \cos\xi \sin\theta_W \tan\epsilon) \\
& + m_{Z_0}^2 (\sin\xi - \cos\xi \sin\theta_W \tan\epsilon)^2,
\end{aligned}
$$
(3.54)

$$
\begin{aligned}
M_Z^2 = {} & m_X^2 \sin^2\xi \sec^2\epsilon + \frac{1}{4} g_D^2 v^2 \sin^2\xi \sec^2\epsilon \left[\cos^2\beta \left(Q_D^{\phi_1}\right)^2 + \sin^2\beta \left(Q_D^{\phi_2}\right)^2 \right] \\
& - g_D \, v \, m_{Z_0} \sin\xi \sec\epsilon \left(\cos^2\beta \, Q_D^{\phi_1} + \sin^2\beta \, Q_D^{\phi_2} \right) (\cos\xi + \sin\xi \sin\theta_W \tan\epsilon) \\
& + m_{Z_0}^2 (\cos\xi + \sin\xi \sin\theta_W \tan\epsilon)^2.
\end{aligned}
$$
(3.55)

They correspond to squares of the masses of the photon A, dark photon A', and electroweak neutral bozon Z, respectively. The Z boson mass receives contribution due to mixing with the $U(1)_D$ gauge field X^0_μ and coupling with Higgs doublets with non-zero dark charges. Even though the Z mass is different from the SM expression for Z mass, its numerical value lies inside the SM prediction range for all parameter space except for $m_X > \mathcal{O}(\text{GeV})$.

The behavior of the dark photon mass as a function of dark sector parameter m_X for various g_D in the Two Higgs Doublet $B - L$ model is given in Fig. (3.3). The dark photon mass has a contribution from Higgs doublets, proportional to g_D, and becomes a critical parameter. When m_X becomes smaller than a critical value, the dark photon mass is only determined by the terms proportional to g_D. Therefore for fixed $\sin\epsilon$ or g_D, there will be a non-zero minimum value for the dark photon mass. Furthermore, the dark photon mass is observed to be not sensitive to $\sin\epsilon$.

Similar to the minimal case, the interactions are needed to be expressed in terms of the single transformation matrix given in Eq. (3.52). The interaction term takes
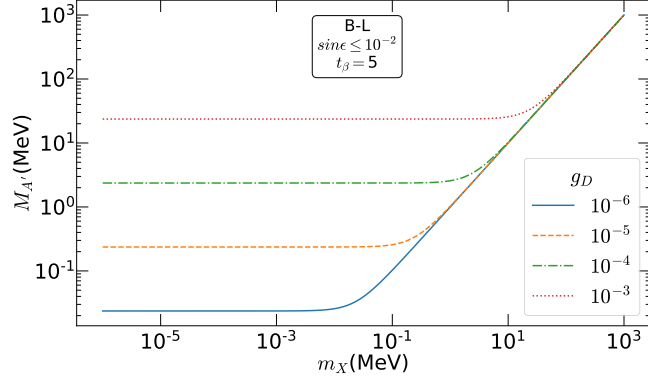
Figure 3.3: Sensitivity of the mass of the dark photon, $M_{A'}$, to the dark coupling g_D in the Two Higgs Doublet $B - L$ model

the form

$$
\begin{aligned}
\mathscr{L}_{\text{Interaction}} \subset & \sum_i \bar{f}_i \, i \slashed{D} f_i \\
= & \sum_i \frac{1}{2} \bar{f}_i \Big(C_V^f \gamma^\mu + C_A^f \gamma^\mu \gamma^5 \Big) f_i \, A_\mu + \frac{1}{2} \bar{f}_i \Big(C_V'^{\,f} \gamma^\mu + C_A'^{\,f} \gamma^\mu \gamma^5 \Big) f_i \, Z_\mu \\
& + \frac{1}{2} \bar{f}_i \Big(C_V''^{\,f} \gamma^\mu + C_A''^{\,f} \gamma^\mu \gamma^5 \Big) f_i \, A'_\mu \\
\equiv & \, g' J_Y^\mu Y_\mu + g J_3^\mu W_{3\mu} + g_D J_X^\mu X_\mu^0 \\
= & \begin{pmatrix} g' J_Y^\mu & g J_3^\mu & g_D J_X^\mu \end{pmatrix}
\begin{pmatrix} Y_\mu \\ W_{3\mu} \\ X_\mu^0 \end{pmatrix} \\
= & \begin{pmatrix} g' J_Y^\mu & g J_3^\mu & g_D J_X^\mu \end{pmatrix} \cdot V_{AZA',YWX^0}^{-1} \cdot
\begin{pmatrix} A_\mu \\ Z_\mu \\ A'_\mu \end{pmatrix}
\end{aligned}
\tag{3.56}
$$

where J_Y^μ, J_3^μ, and J_X^μ are the fermion currents involving hypercharge, weak and dark forces, respectively. V_{AZA',YWX^0}^{-1} is the inverse of the total transformation matrix. It has the same form with minimal model Eq. (3.19) in terms of model parameters, but the parameter ξ takes a different form.

$$
V_{AZA',YW_3X^0}^{-1} = \begin{pmatrix}
\cos\theta_W & -\dfrac{\sin\theta_W \cos\xi \cos\epsilon + \sin\xi \sin\epsilon}{\cos\epsilon} & \dfrac{\sin\theta_W \sin\xi \cos\epsilon - \cos\xi \sin\epsilon}{\cos\epsilon} \\[3mm]
\sin\theta_W & \cos\xi \cos\theta_W & -\sin\xi \cos\theta_W \\[3mm]
0 & \dfrac{\sin\xi}{\cos\epsilon} & \dfrac{\cos\xi}{\cos\epsilon}
\end{pmatrix}.
\tag{3.57}
$$

45

In this case, some of the vertex factors take the form given in Table 3.3.

Table 3.2: Dark quantum charges of the fields under $U(1)_D$, adapted from ref. [1]. Note that there is a difference in the convention to define the covariant derivative where we use the Peskin and Schroeder convention.

Fields	u_R	d_R	Q_L	L_L	e_R	ν_R	ϕ_2	ϕ_1
Dark Charges	Q'_u	Q'_d	$\frac{Q'_u+Q'_d}{2}$	$-\frac{3(Q'_u+Q'_d)}{2}$	$-(2Q'_u+Q'_d)$	$-(Q'_u+2Q'_d)$	$\frac{Q'_u-Q'_d}{2}$	$\frac{5Q'_u+7Q'_d}{2}$
Model C	$\frac{1}{4}$	$-\frac{1}{2}$	$-\frac{1}{8}$	$\frac{3}{8}$	0	$\frac{3}{4}$	$\frac{3}{8}$	$-\frac{9}{8}$
Model D	$\frac{1}{2}$	0	$\frac{1}{4}$	$-\frac{3}{4}$	-1	$-\frac{1}{2}$	$\frac{1}{4}$	$\frac{5}{4}$
Model E	0	$\frac{1}{2}$	$\frac{1}{4}$	$-\frac{3}{4}$	$-\frac{1}{2}$	-1	$-\frac{1}{4}$	$\frac{7}{4}$
Model F	$\frac{2}{3}$	$\frac{1}{3}$	$\frac{1}{2}$	$-\frac{3}{2}$	$-\frac{5}{3}$	$-\frac{4}{3}$	$\frac{1}{6}$	$\frac{17}{6}$
Model G	$-\frac{1}{6}$	$\frac{1}{3}$	$\frac{1}{12}$	$-\frac{1}{4}$	0	$-\frac{1}{2}$	$-\frac{1}{4}$	$\frac{3}{4}$
Model $B-L$	$\frac{1}{6}$	$\frac{1}{6}$	$\frac{1}{6}$	$-\frac{1}{2}$	$-\frac{1}{2}$	$-\frac{1}{2}$	0	1
Minimal $B-L$	$\frac{1}{6}$	$\frac{1}{6}$	$\frac{1}{6}$	$-\frac{1}{2}$	$-\frac{1}{2}$	$-\frac{1}{2}$	0	$-$

Table 3.3: The relevant vertex factors contributing to the CEνNS in the two-Higgs Doublet Models extended with a dark $U(1)_D$ group. A shorthand notation is used for the trigonometric expressions. For example, (s_ξ, t_ϵ) stand for $(\sin\xi, \tan\epsilon)$ and similar for the others.

Vertices	C_V^f	C_A^f
ν_L — ν_L, Z	$-\dfrac{g_D s_\xi\left(7Q_d'+5Q_u'\right)}{8c_\epsilon} + \dfrac{e(c_\xi + s_\xi t_\epsilon s_W)}{4c_W s_W}$	$-\dfrac{g_D s_\xi\left(Q_d'-Q_u'\right)}{8c_\epsilon} - \dfrac{e(c_\xi + s_\xi t_\epsilon s_W)}{4c_W s_W}$
u — u, Z	$\dfrac{g_D s_\xi\left(Q_d'+3Q_u'\right)}{8c_\epsilon} + \dfrac{ec_\xi(8s_W^2-3)+5es_\xi t_\epsilon s_W}{12c_W s_W}$	$-\dfrac{g_D s_\xi\left(Q_d'-Q_u'\right)}{8c_\epsilon} - \dfrac{e(c_\xi + s_\xi t_\epsilon s_W)}{4c_W s_W}$
d — d, Z	$\dfrac{g_D s_\xi\left(3Q_d'+Q_u'\right)}{8c_\epsilon} + \dfrac{ec_\xi(4s_W^2-3)+es_\xi t_\epsilon s_W}{12c_W s_W}$	$\dfrac{g_D s_\xi\left(Q_d'-Q_u'\right)}{8c_\epsilon} + \dfrac{e(c_\xi + s_\xi t_\epsilon s_W)}{4c_W s_W}$

	$C_V'^f$	$C_A'^f$
ν_L — ν, A'	$\dfrac{g_D c_\xi\left(7Q_d'+5Q_u'\right)}{8c_\epsilon} + \dfrac{e(s_\xi - c_\xi t_\epsilon s_W)}{4c_W s_W}$	$-\dfrac{g_D c_\xi\left(Q_d'-Q_u'\right)}{8c_\epsilon} + \dfrac{e(s_\xi - c_\xi t_\epsilon s_W)}{4c_W s_W}$
u — u, A'	$\dfrac{g_D c_\xi\left(Q_d'+3Q_u'\right)}{8c_\epsilon} + \dfrac{es_\xi(8s_W^2-3)-5ec_\xi t_\epsilon s_W}{12c_W s_W}$	$-\dfrac{g_D c_\xi\left(Q_d'-Q_u'\right)}{8c_\epsilon} + \dfrac{e(s_\xi - c_\xi t_\epsilon s_W)}{4c_W s_W}$
d — d, A'	$\dfrac{g_D c_\xi\left(3Q_d'+Q_u'\right)}{8c_\epsilon} - \dfrac{es_\xi(4s_W^2-3)-ec_\xi t_\epsilon s_W}{12c_W s_W}$	$\dfrac{g_D c_\xi\left(Q_d'-Q_u'\right)}{8c_\epsilon} - \dfrac{e(s_\xi - c_\xi t_\epsilon s_W)}{4c_W s_W}$

CHAPTER 4

PHENOMENOLOGY

In this chapter, phenomenological study of the dark sector model through recent CEνNS observation by COHERENT Collaboration is described. In sec. 4.1, theoretical introduction for CEνNS is given. In sec. 4.2, details of the experiment conducted by COHERENT Collaboration is given. Then in sec. 4.3, this experiment is simulated and a theoretical expectation of number of events is obtained. And in sec. 4.4, statistical analysis for comparing COHERENT data with our dark sector model is discussed.

4.1 Coherent Elastic Neutrino Nucleus Scattering

In this section, the CEνNS cross sections in the SM and minimal and non-minimal vector portal models are derived.

4.1.1 CEνNS Cross Section in the Standard Model

In the SM, elastic neutrino nucleus scattering is mediated by neutral current (NC). The part of the SM Lagrangian that describes this type of interaction is [28]

$$\mathcal{L} \supset \frac{g}{c_W} J_{NC}^\alpha Z^\alpha \tag{4.1}$$

where the neutral current is

$$
\begin{aligned}
J_{NC}^\alpha = &\bar{\nu}_L \gamma^\alpha \left(\frac{1}{2}\right) \nu_L + \bar{u}_L \gamma^\alpha \left(\frac{1}{2} - \frac{2}{3} s_W^2\right) u_L + \bar{u}_R \gamma^\alpha \left(-\frac{2}{3} s_W^2\right) u_R \\
&+ \bar{d}_L \gamma^\alpha \left(-\frac{1}{2} - \frac{1}{3} s_W^2\right) d_L + \bar{d}_R \gamma^\alpha \left(\frac{1}{4} s_W^2\right) d_R + ...
\end{aligned} \tag{4.2}
$$

49

and s_w and c_w are sine and cosine of Weinberg mixing angle respectively. The values inside the parenthesizes (g_P^f) are extended forms of fermion couplings in SM. At low energies NC interaction is given by the effective Lagrangian,

$$\mathscr{L}_{NC} = \frac{G_F}{\sqrt{2}} J_{NC}^\mu J_{NC\mu}. \tag{4.3}$$

The CEνNS cross section in SM is already well established in the literature. The SM predicts a coherent elastic scattering cross section to be proportional to the weak nuclear charge, Q_W^2, which is a value close to neutron number of the nucleus. The differential CEνNS cross section is expressed with respect to the nuclear recoil energy T because it is the only measurable quantity in this phenomena. In the coherent limit where the form factor approaches to unity, differential cross sections for spin-0 and spin-1/2 targets are given by [45]:

$$\frac{d\sigma_{\text{SM}}}{dT} = \frac{G_F^2 Q_W^2 M}{4\pi} \left(1 - \frac{T}{E_\nu} - \frac{MT}{2E_\nu^2} + 2J_N \frac{T^2}{E_\nu^2} \right), \tag{4.4}$$

where G_F is the Fermi coupling constant, M is the nucleus mass, $J_N = 0, 1/2$ is the spin of the nucleus, E_ν is the incident neutrino energy and Q_W is the weak nuclear charge [46, 47] given by,

$$Q_W = (2Z + N)g_V^u + (2N + Z)g_V^d = N - (1 - 4s_W^2)Z \tag{4.5}$$

where g_V^u and g_V^d are vector couplings of u and d quarks, Z and N are the atomic and neutron number respectively. Effect of the extra T^2/E_ν^2 term appearing in the spin-$\frac{1}{2}$ case is negligible. Therefore it is convenient to work on the spin-$\frac{1}{2}$ case since more developed computational tools are available for fermionic particles. The same applies to the dark sector extended models. Calculation details are given in Appendix C

4.1.2 Dark Sector Contribution to the CEνNS Cross Section

If the dark sector is considered along with the SM, the CEνNS process is described by two diagrams, one Z exchange and one A' exchange. The total amplitude of the process receives a contribution from both diagrams. The CEνNS cross sections obtained for our models are given below. Thew details of the calculation for the minimal $B - L$ model are given In Appendix D. The calculation is similar for the

50

other cases, with the only difference being the form of currents.

Minimal $B - L$ without kinetic mixing:

$$\frac{d\sigma}{dT}\Big|^{\text{SM}+B-L\,\text{without KM}}_{spin-1/2} = \frac{F^2(q^2)M}{8\pi(2MT + m_{A'}^2)^2}\left(1 - \frac{T}{E_\nu} - \frac{MT}{2E_\nu^2} + 2J_N\frac{T^2}{E_\nu^2}\right)$$
$$\times\left[2g_{B-L}^2A^2 + \sqrt{2}G_FQ_W(2MT + m_{A'}^2)\right]^2 \tag{4.6}$$

Minimal $B - L$ with kinetic mixing:

$$\frac{d\sigma}{dT}\Big|^{\text{SM}+B-L\,\text{with KM}}_{spin-1/2} = \frac{F^2(q^2)M}{8\pi c_\epsilon^4 m_Z^4(2MT + m_{A'}^2)^2}\left(1 - \frac{T}{E_\nu} - \frac{MT}{2E_\nu^2} + 2J_N\frac{T^2}{E_\nu^2}\right)$$
$$\left[(2MT + m_{A'}^2)\left(\sqrt[4]{2}\sqrt{G_F}m_Z\left(c_\beta c_\epsilon + s_\beta s_w s_\epsilon\right) - g_{B-L}s_\beta\right)\right.$$
$$\times\left(-2Ag_{B-L}s_\beta + \sqrt[4]{2}\sqrt{G_F}m_Z\left(c_\beta c_\epsilon Q_W + s_\beta s_w s_\epsilon(A + 2Z)\right)\right)$$
$$+ m_Z^2\left(\sqrt[4]{2}\sqrt{G_F}m_Z\left(s_\beta c_\epsilon + c_\beta s_w s_\epsilon\right) + g_{B-L}c_\beta\right)$$
$$\left.\times\left(2Ag_{B-L}c_\beta + \sqrt[4]{2}\sqrt{G_F}m_Z\left(c_\beta s_w s_\epsilon(A + 2Z) + c_\epsilon s_\beta Q_W\right)\right)\right]^2$$
$$\tag{4.7}$$

where c and s are used as shorthand for cosine and sine. Kinetic mixing vanishing limit, i.e. $\epsilon, \beta \to 0$ leads to reduction to eq.(4.6) as expected. The differential cross section expression for the 2HDM instance is rather lengthy and will not be shown here.

$F(q^2)$ is the equations above are Helm-type nuclear form factor [48] and q^2 denotes the squared momentum transfer given by $q^2 = 2MT$. The Helm form factor is

$$F(q^2) = \frac{3j_1(qR_1)}{qR_1}\,e^{-qs} \tag{4.8}$$

where $j_1(x)$ is the spherical Bessel function and $q = \sqrt{q_\mu q^\mu}$ with q^2 defined above, $s \approx 0.9\,\text{fm}$ is the nuclear skin thickness and R_1 is the effective nuclear radius

$$R_1 \simeq \sqrt{R_A^2 + \frac{7}{3}\pi^2 r_0^2 - 5s^2} \tag{4.9}$$

where

$$R_A \simeq \left(1.23A^{1/3} - 0.6\right)\text{fm}, \quad r_0 \simeq 0.52\,\text{fm}. \tag{4.10}$$

Furthermore, the cross-section expressions are not different for Dirac and Majorana neutrinos. The details are given in Appendix F. This experiment can not be used to determine if the neutrinos are Majorana fermions.

4.2   The COHERENT Experiment

COHERENT is a neutrino-based fixed target experiment. Neutrino beams are produced by striking proton beams of pulse $\sim 1\ \mu$s to a Mercury target at 60 Hz, creating $\approx 5 \times 10^{20}$ collisions per day. These collisions produce π^- and π^+ as byproducts. Pions come to rest inside the target. π^- are mostly absorbed by Mercury and π^+ decays through $\pi^+ \to \mu^+ + \nu_\mu$. Two-body decay at rest results in monochromatic energy of ≈ 29.7 MeV for ν_μ, which are called prompt neutrinos. Pion decay is then followed by muon decay $\sim 2.2\ \mu$s later, through $\mu^+ \to e^+ + \bar{\nu}_\mu + \nu_e$. Energy spectra for neutrinos coming from this decay are continuous up to 52.8 MeV. $\bar{\nu}_\mu$ and ν_e are called delayed neutrinos. This process produces ~ 0.08 neutrinos of ν_μ, $\bar{\nu}_\mu$ and ν_e flavors per proton on target (POT) collision.

The produced neutrinos then collide with 14.57 kg CsI and 24 kg Liquid Argon targets located at 19 m and 27.5 m away from the Mercury target. The incoming neutrino flux depends on energy due to its production mechanism. Since the delayed ν_e and $\bar{\nu}_\mu$ beams are produced through muon decay; their energy spectrum is described by Michel spectrum [49, 50](Top panel of Fig: 4.1)

$$
\begin{aligned}
f_E^{\nu_\mu}(E_\nu) &= \delta\left(E_\nu - \frac{m_\pi^2 - m_\mu^2}{2m_\pi}\right) \\
f_E^{\bar{\nu}_\mu}(E_\nu) &= \frac{64 E_\nu^2}{m_\mu^3}\left(\frac{3}{4} - \frac{E_\nu}{m_\mu}\right) \\
f_E^{\nu_e}(E_\nu) &= \frac{192 E_\nu^2}{m_\mu^3}\left(\frac{1}{2} - \frac{E_\nu}{m_\mu}\right)
\end{aligned}
\tag{4.11}
$$

Combining it with time dependence in time $f_t^{\nu_\alpha}(t)$, given in the bottom panel in Fig. 4.1, the final form of incoming neutrino flux is obtained:

$$
f^{\nu_\alpha}(E_\nu, t) = \mathcal{N} f_E^{\nu_\alpha}(E_\nu) \times f_t^{\nu_\alpha}(t)
\tag{4.12}
$$

where $f_E^{\nu_\alpha}(E_\nu)$ and $f_t^{\nu_\alpha}(t)$ are normalized according to $\int_\Omega dx f(x) = 1$, normalization of the total flux is given by $\mathcal{N} = r N_{POT}/4\pi L^2$, L is the distance between the detector and the neutrino source, $r = 0.0848$ is the number of neutrinos per flavor created for each POT collision and the total number of POT collisions throughout
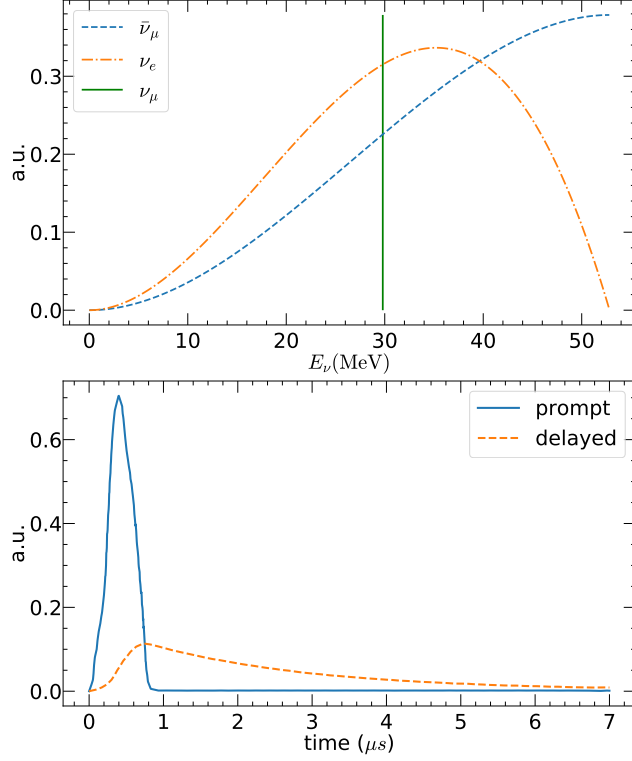
52

Figure 4.1: Energy and time-dependent distribution of incoming neutrinos.

the experiment is N_{POT}. Its value is 1.76×10^{23} for CsI 2017, 3.198×10^{23} for CsI 2022 releases and 1.37×10^{23} for LAr based experiment.

4.2.1 Energy Quenching

Nuclear recoil energy is picked up by scintillation detectors and converted into photoelectrons (PE). This conversion is parametrized with light yield $\mathscr{L}_Y$, which is the amount of PE produced per unit energy. Values provided with the data releases are as $\mathscr{L}_Y = 13.348$ PE/keVee for CsI and ~ 4.5 PE/keVee for LAr based experiment. The number of produced PE can be expressed as

$$n_{\mathrm{PE}} = \mathrm{QF}\, T\, \mathscr{L}_Y. \tag{4.13}$$

There is an important detail in Eq.(4.13). Nuclear recoil energy is primarily dissipated through secondary nuclear recoils, and only a small amount is turned into scintillation (or ionization). Quenching factor QF is the ratio of energy turned into

scintillation

$$QF = \frac{E_{ee}}{T}, \tag{4.14}$$

where the subscript ee stands for electron equivalent and E_{ee} is the equivalent energy of a recoiling electron in which the energy is dissipated through only scintillation. Suggestions for quenching factors were provided with data releases. In the 2017 study, two measurements of the quenching factor for CsI performed by the collaboration were considered, along with two previous measurements. Agreement between measurements is poor. As a pragmatic solution, a constant quenching factor $QF^{CsI} = 8.78 \pm 1.66\%$ was suggested. Later an energy-dependent model for the quenching factor was proposed in [51], which increases the accuracy of SM expectation of event rate. This model describes the scintillation in CsI by slow ions with low energy approximation to Birks' scintillation model [52] multiplied by an adiabatic factor to account for the behavior of scintillation production cut off at low nuclear recoil energy limit. Modeled quenching factor takes the form

$$QF(T) = \left[kB \cdot (dE/dr)_i \right]^{-1} \left(1 - \exp(-T/E_0) \right), \tag{4.15}$$

where $kB = 3.311 \pm 0.075 \times 10^{-3} \text{g/MeVcm}^2$ and $E_0 = 12.97 \pm 0.61 \text{ keV}$. And $(dE/dr)_i$ is the total stopping power for ions, extracted from the software SRIM-2013 [53]. Both QF suggestions for CsI were considered in the analysis in the following section.

In the 2022 study, the previously released CsI quenching factor was reassessed. A new scintillation response to nuclear recoils measurement on CsI[Na] crystal came for consideration. Quenching in the region of interest is modeled as a fourth-degree polynomial fit to five measurements mentioned above [54]

$$E_{ee} = g(T) = 0.05546T + 4.307T^2 - 111.7T^3 + 840.4T^4 \tag{4.16}$$

where detector response E_{ee} is in MeVee and nuclear recoil energy T is in MeVnr. For the LAr-based experiment, the suggested quenching factor is a linear fit [55] to world data on argon which is given in Fig 7 of [4].

$$QF^{LAr}(T) = a + bT \tag{4.17}$$

where T is in keVnr, $a = 0.246$ and $b = 7.8 \times 10^{-4} \text{keVnr}^{-1}$.

4.3 Simulating COHERENT Events

In a collision experiment, the total number of expected events is [56]

$$N_{\text{event}} = \sigma \mathscr{L} \tag{4.18}$$

where σ is cross section and $\mathscr{L}$ is integrated luminosity. In fixed-target experiments, integrated luminosity takes the form

$$\mathscr{L} = \Phi N_{\text{targ}} \tag{4.19}$$

where N_{targ} is the number of particles in the target, which can be obtained using Avogadro's number and Φ is the total number of incoming particles.

COHERENT published events in a binned histogram, counted in n_{PE} and time bins. In order to find the expected number of events in a bin, an integration of flux and differential cross section over bin limits is required. However, the integral should also account for detector effects on measurement.

4.3.1 Forward Folding

In an experiment that reports a spectrum in a binned histogram such as COHERENT, two detector effects distort and smear data in the measurement process. A response function maps the true spectrum, which is the spectrum that would have been observed without detector effects, to the measured (or reconstructed) spectrum. This function, generally published by the experimental group, is estimated using Monte Carlo methods. Using this function, either the measured data is post-processed to remove detector effects (unfolding), or a theoretical calculation is distorted and compared with the measured data (forward folding). A response function is given alongside raw measurements in all COHERENT data releases, and forward folding is the preferable approach. Details of this approach are given below.

Response function contains the two detector effects. The first effect is due to detectors' finite potential to detect signal events [57]. Acceptance of a detector refers to a region of kinematic properties in which signals are potentially detectable. As a function, it gives the fraction of signal events visible to the detector. This property

is always expressed along with another factor called detector efficiency, which is the probability of the detector responding to an event for it to be detected. This is modeled with a function that gives the fraction of signal events that pass the event selection criterion decided by the experimenters. Acceptance efficiency is the product of these two functions. Functions provided in COHERENT data releases are as follows (see Fig:4.2):

CsI 2017[58]:

Acceptance efficiency for the recoil energy spectrum is

$$\mathscr{A}(n_{\text{PE}}) = \frac{a}{1 + \exp(-k(n_{\text{PE}} - x_0))} \Theta(n_{\text{PE}}) \tag{4.20}$$

where the parameters have the following values:

$$a = 0.6655^{+0.0212}_{-0.0384},$$

$$k = 0.4942^{+0.0335}_{-0.0131},$$

$$x_0 = 10.8507^{+0.1838}_{-0.3995} \tag{4.21}$$

and $\Theta(n_{\text{PE}})$ is a modified Heavy-side step function defined as

$$\Theta(n_{\text{PE}}) = \begin{cases} 0 & n_{\text{PE}} < 5 \\ 0.5 & 5 \le n_{\text{PE}} < 6 \\ 1 & n_{\text{PE}} \ge 6 \end{cases} \tag{4.22}$$

CsI 2022[3]:

Acceptance in the energy spectrum is:

$$\mathscr{A}_{\text{PE}}(n_{\text{PE}}) = \frac{1.32045}{1 + \exp(-0.285979(n_{\text{PE}} - 10.8646))} - 0.333322 \tag{4.23}$$

Furthermore, this is the only data release with Acceptance Efficiency for the time spectrum.

$$\mathscr{A}_t(t) = \begin{cases} 1 & t < a \\ e^{-b(t-a)} & t \ge a \end{cases} \tag{4.24}$$

where

$$a = 0.52\mu s$$

$$b = 0.0494/\mu s \tag{4.25}$$

and total efficiency can be expressed as

$$\mathscr{A}(n_{\mathrm{PE}}, t) = \mathscr{A}_{\mathrm{PE}}(n_{\mathrm{PE}}) \times \mathscr{A}_t(t) \tag{4.26}$$

LAr:

A function for acceptance was not directly given. A csv file of efficiency vs. keVnr for Analysis A is given [55]. Efficiency used in Analysis B is obtained from figure 2 of [4]. If only Acceptance efficiency is considered, the expected number of events
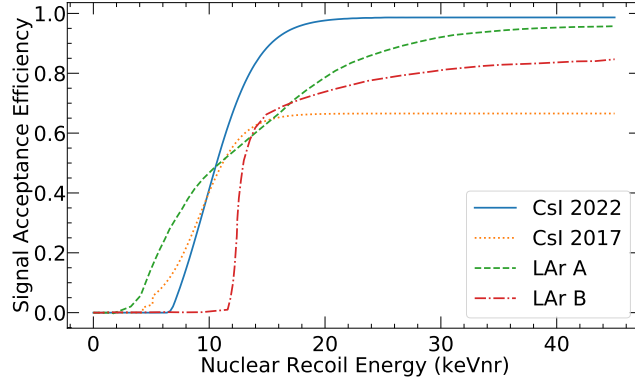

Figure 4.2: Acceptance efficiency provided along data releases for CsI 2017 [2], CsI 2022 [3] and LAr Analyses A and B [4].

in i^{th} PE and j^{th} t bin can have a simple form

$$N_{event}^{i,j} = \sum_{\alpha=\mathrm{flavor}} \sum_{\beta=\mathrm{Nucleus}} N_{targ}^{\beta} \int_{T_{\min}^i}^{T_{\max}^i} \int_{E_{\nu}^{\min}}^{E_{\nu}^{\max}} \int_{t_{\min}^j}^{t_{\max}^j} f_{\nu_\alpha}(E_\nu, t)\mathscr{A}(T, t)\left(\frac{d\sigma}{dT}\right) dt dE_\nu dT \tag{4.27}$$

The second effect is due to the finite resolution of the detectors. This smears the true energy spectrum with a resolution function. A smearing function $P(x^{\mathrm{reco}}|x^{\mathrm{true}})$ gives the probability of measuring a true value x^{true} as x^{reco}. By definition, it has the property

$$\int_{\Omega^{\mathrm{reco}}} dx^{\mathrm{reco}} P(x^{\mathrm{reco}}|x^{\mathrm{true}}) = 1 \tag{4.28}$$

In COHERENT 2022 CsI release, the energy smearing is parametrized in the following form by using the Gamma function $\Gamma(1 + b)$ [3]:

$$P(n_{\mathrm{PE}}^{\mathrm{reco}}|E_{\mathrm{ee}}^{\mathrm{true}}) = \frac{(a(1 + b))^{1+b}}{\Gamma(1 + b)} n_{\mathrm{PE}}^b e^{-a(1+b)n_{\mathrm{PE}}} \tag{4.29}$$

where parameters $a = 0.0749/E_{ee}^{\text{true}}$ and $b = 9.56 \times E_{ee}^{\text{true}}$, depends on quenched energy deposition. With this effect number of events in i^{th} PE and j^{th} time (t) bin is

$$
N_{\text{event}}^{i,j} = \sum_{\beta = \text{Nucleus}} N_{targ}^{\beta} \sum_{\alpha = \text{flavor}} \int_{T_{\min}^{i}}^{T_{\max}^{i}} \int_{E_{ee}^{\min}}^{E_{ee}^{\max}} \int_{E_{\nu}^{min}}^{E_{\nu}^{max}} \int_{t_{\min}^{j}}^{t_{\max}^{j}} dT^{\text{reco}} dE_{ee}^{\text{true}} dt dE_{\nu}
$$

$$
f_{\nu_{\alpha}}(E_{\nu}, t) \mathscr{A}_{\text{PE}}(T^{\text{reco}}) \mathscr{A}_{t}(t) P\big(n_{\text{PE}}(T^{\text{reco}}) \big| E_{ee}^{\text{true}}\big) \left(\frac{d\sigma}{dT} \Big(T^{\text{true}} \big|_{T = g^{-1}(E_{ee})} \Big) \right) \quad (4.30)
$$

Our expected event number calculated for the SM in comparison to the experimental group's and other studies are given in Table (4.1).

Table 4.1: Our calculated values for the total number of events in the SM, in comparison to the literature

Data Set	Our Study	Literature	References
CsI 2017 (constant QF)	173	173	[2]
CsI 2017 (energy dependent QF)	139	138	[54]
CsI 2022	437	431	[3]
LAr−Analysis A	128	128	[4]
LAr−Analysis B	101	101	[4]

4.4 Statistical Analysis of COHERENT Data

In this section, χ^2-fit will be adopted to study the sensitivity of COHERENT to phenomenological parameters in the framework of new physics interaction. The sensitivity analysis is based on the following form of the χ^2 function depending on a parameter set $\mathscr{P}$, which generally denotes the parameters of interest given below [2]

$$
\chi^2(\mathscr{P}) = \sum_{i = \text{bins}} \frac{\left(N_{\text{meas}}^{i} - N_{\text{exp}}^{i}(1 + \alpha) - B_{\text{on}}^{i}[1 + \beta] \right)^2}{\sigma_{\text{stat}}^2} + f_{\text{pull}}(\alpha, \sigma_{\alpha}) + f_{\text{pull}}(\beta, \sigma_{\beta}).
$$

$$(4.31)$$

where N_{meas} and N_{exp} are measured and expected number of events respectively, B_{on} is the estimated background when the beam is on, α corresponds to uncer-

tainty on the signal rate, β corresponds to uncertainty of B_{on}. χ^2 function is minimized over α and β. Here, the statistical uncertainty of the measurement is given by $\sigma_{\mathrm{stat}} = \sqrt{N_{\mathrm{meas}} + B_{\mathrm{on}} + 2B_{\mathrm{SS}}}$, where the quantity B_{SS} denotes the steady-state background. The pull terms given by the COHERENT Collaboration [2] have the form

$$f_{\mathrm{pull}}(x, \sigma_x) = \left(\frac{x}{\sigma_x}\right)^2, \quad x = \alpha, \beta \tag{4.32}$$

where σ_α and σ_β are fractional uncertainty of α and β, corresponding to 1-sigma variation. The pull term in the above form is observed to lead to unphysical results at its limiting values. This behavior was also noted in [59] and an asymmetric pull term of the form

$$f_{\mathrm{pull}}(x, \sigma_x) = \frac{2}{\sigma_x^2}\big(x - \log(x+1)\big), \tag{4.33}$$

is suggested to use. For completeness, both forms of the pull terms were used in the χ^2 calculation and comment on their effect.

Even though the scattering data were obtained in a multi-binned detector, the earlier analyses provided by COHERENT Collaboration combines all events in a single bin [2] for CsI 2017 and LAr data. This is because they created the most likelihood probability distribution function to account for both the energy spectra of the neutron background and the arrival time of neutrinos. However, a simplistic count of excess events over the background that does not benefit from this knowledge yields similar results on the total events. For this case, performing analysis on each bin separately can be preferable. Furthermore, later it is suggested to adopt a multi-bin approach by COHERENT. In the following section, analysis for both single bin and more than one multi-bin options have been performed. The χ^2 function for the single bin analysis can be obtained from Eq. (4.31) by simply using the total number of events for the signal and the background.

4.4.1 Numerical Results

In this section, both minimal $B - L$ and various 2HDMs extended by a dark $\mathrm{U}(1)_D$ gauge group are analyzed by looking at the effects of various parameters and factors in simulating CEνNS data measured by the COHERENT collaboration. $M_{A'}$,

$\sin\epsilon$, g_D, $\tan\beta$, q'_{u_R}, and q'_{d_R} are the parameters of the theoretical framework considered here. Additional factors like binning options (1PE - 1t, 9PE-1t, and 9PE-10t bins), the target used, the publication version, which are called CsI 2017, CsI 2022, LAr A, and LAr B, selection of quenching factor and pull term. There are, in total, seven chosen representative scenarios for 2HDMs, obtained by fixing $\left(q'_{u_R}, q'_{d_R}\right)$ values. Considering the number of parameters, factors, and models mentioned above, it would not be feasible to present all possible plots here. Instead, plots of two distributions for each model in the $\left(g_D, \sin\epsilon\right)$ and $\left(g_D, M_{A'}\right)$ parameter spaces, varying one factor at a time are given.

The results given in Fig. (4.3) have been obtained for CsI 2022 data along with provided the QF in the data release, and the χ^2 analysis has been carried out with one single bin (1PE-1t). In fact, our search has indicated that these are the circumstances where better bounds are possible compared to the case where the target is LAr and the χ^2 is minimized over multi bins (9PE-1t or 9PE-10t). This feature is not only true for the minimal $B - L$ scenario but also valid for the rest of the models considered.

In the left panel of Fig. (4.3), the exclusion curves in the $\left(g_D, \sin\epsilon\right)$ parameter space for various $M_{A'}$ values upto 1 GeV are shown for the minimal $B - L$ model. Spaces above the curves are excluded with %90 confidence level (CL). Stronger bounds are observed for lighter gauge bosons. This is expected because the new physics contribution to scattering cross section is inversely proportional to the dark photon mass. The number of CEνNS events increases for lighter dark photons, forcing the parameters g_D and $\sin\epsilon$ to be smaller.

In the right panel of Fig. (4.3), similar exclusion curves are given in the $\left(g_D, M_{A'}\right)$ parameter space for various $\sin\epsilon$, including no kinetic mixing scenario, is given with %90 CL. The sensitivity to the kinetic mixing parameters starts around $M_{A'} = 100$ MeV. Larger kinetic mixing pushes the bound on g_D to smaller values.

Figures (4.4, 4.6) verify their respective comparisons within the framework of specific models, but their results are valid in general. A characteristic that appears in the 2HDM case is the left tails in the right panels in Figures (4.4- 4.6). Due to $M_{A'}$ depending on other parameters and explicitly on g_D, the minimum mass re-
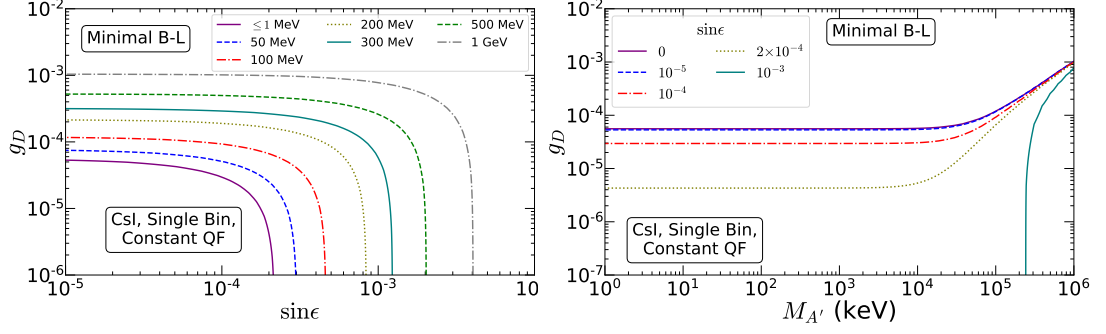
Figure 4.3: The exclusion curves in the $(g_D, \sin\epsilon)$ and $(g_D, M_{A'})$ parameter spaces for various $M_{A'}$ (left) and $\sin\epsilon$ (right) values, respectively, in the minimal $B - L$ model. Regions above the curves are excluded with %90 CL by the COHERENT data for CEνNS.

quirement (or possible values $M_{A'}$ can obtain, see Fig. (3.3) and the accompanying discussion) determines the boundary of the excluded part in this end. In the heavier dark photon region, the COHERENT data take over and give more stringent bounds.
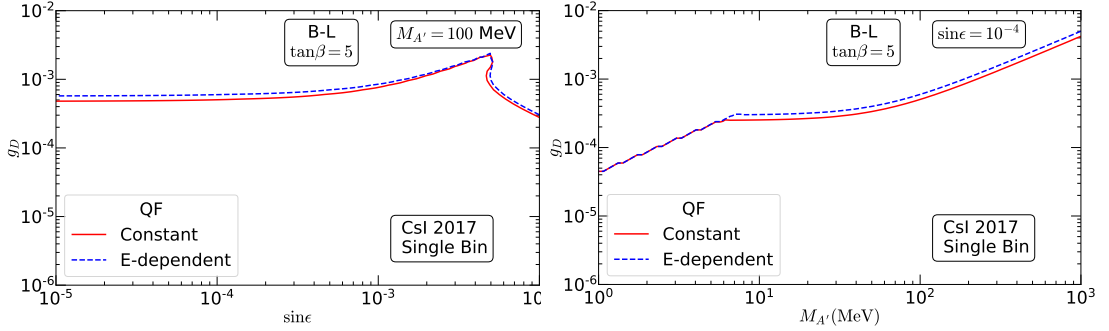

Figure 4.4: The exclusion curves in the $(g_D, \sin\epsilon)$ parameter space for $M_{A'} = 100\,\text{MeV}$ (left) and $(g_D, M_{A'})$ parameter space for $\sin\epsilon = 10^{-4}$ (right) for energy independent and energy dependent quenching factors proposed for CsI 2017 relase. Regions above the curves are excluded with %90 CL by the COHERENT data for CEνNS.

Fig.(4.8) compares the exclusion regions of all the models considered so far in the $(g_D, \sin\epsilon)$ parameter space (the left panel) and in $(g_D, M_{A'})$ (the right panel). The analysis comparing the models has been performed for an intermediate dark pho-
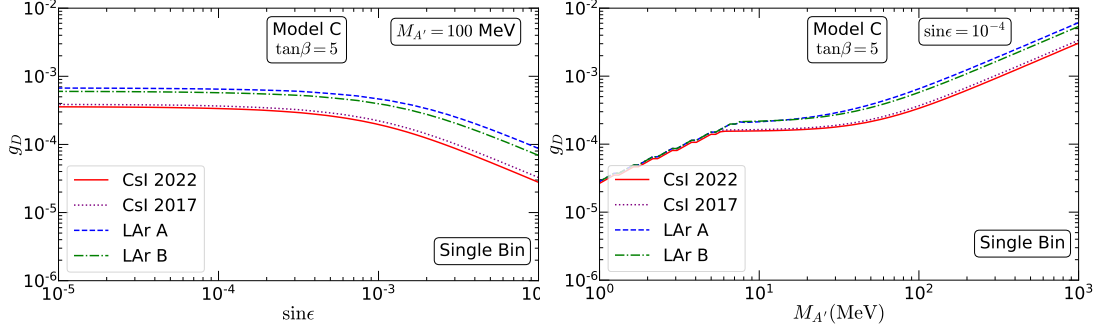
Figure 4.5: The exclusion curves in the $(g_D, \sin\epsilon)$ parameter space for $M_{A'} = 100\,\text{MeV}$ (left) and $(g_D, M_{A'})$ parameter space for $\sin\epsilon = 10^{-4}$ (right) for the sources CsI 2017, CSI 2022, LAr option A and LAr option B in the Model C. Regions above the curves are excluded with %90 CL by the COHERENT data for CEνNS.

Figure 4.6: The exclusion curves in the $(g_D, \sin\epsilon)$ parameter space for $M_{A'} = 100\,\text{MeV}$ (left) and $(g_D, M_{A'})$ parameter space for $\sin\epsilon = 10^{-4}$ (right) for the single bin (1PE-1t) and multi-bin (9PE- 1t and 9PE-10t) analyses in the Model E. Regions above the curves are excluded with %90 CL by the COHERENT data for CEνNS.

ton mass ($M_{A'} = 50\,\text{MeV}$), $\tan\beta = 5$, and for the CsI 2022 data, and single bin χ^2 configuration. For the most part, the sensitivity to the value of the parameter β disappears at $\tan\beta \geq 5$, and the choice of value does not play a significant role. The exclusion curves for the minimal $B - L$ model are given in Fig. (4.8) for comparison. In the left panel, the Minimal $B - L$ Model seems to have the most stringent bound in the entire region across all models. The behavior of models in the MeV dark photon mass range can be seen in the right panel. For the most part, the minimal $B - L$ model has the most stringent exclusion bound except for $M_{A'} \approx$ few MeV region. Model F seems most sensitive to sub-MeV dark photon mass.
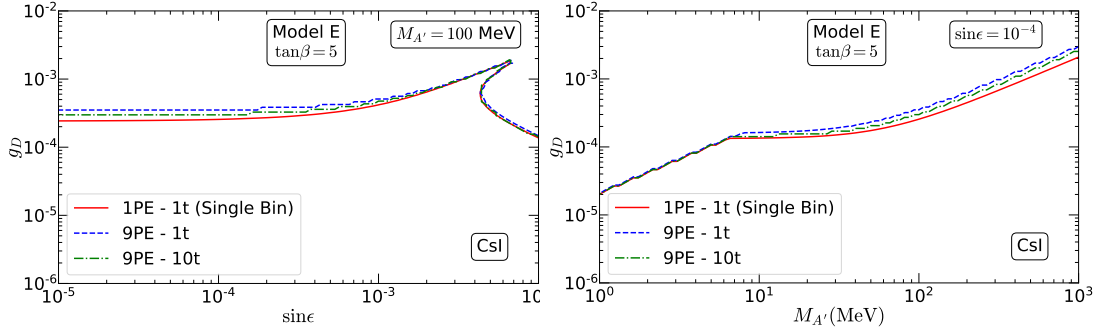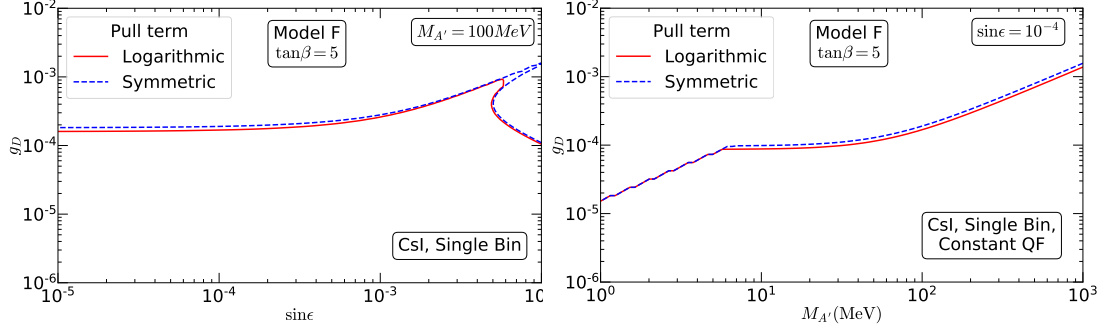
Figure 4.7: The exclusion curves in the $(g_D, \sin\epsilon)$ parameter space for $M_{A'} = 100$ MeV (left) and $(g_D, M_{A'})$ parameter space for $\sin\epsilon = 10^{-4}$ (right) for analyses done with symmetric and logarithmic pull terms. Regions above the curves are excluded with %90 CL by the COHERENT data for CEνNS.
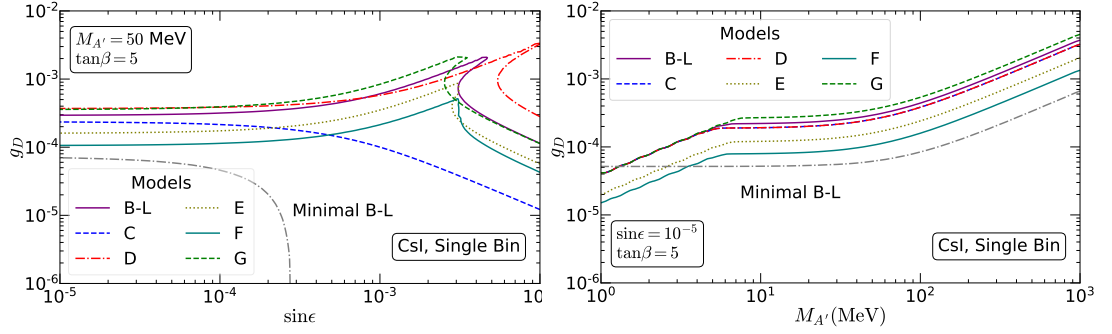

Figure 4.8: The exclusion curves in the $(g_D, \sin\epsilon)$ parameter space for $M_{A'} = 50$ MeV (left) and $(g_D, M_{A'})$ parameter space for $\sin\epsilon = 10^{-5}$ for all the models considered. Regions above the curves are excluded with %90 CL by the COHERENT data for CEνNS.

In addition to analyzing the experimental constraints of COHERENT data for CEνNS on parameter spaces of the minimal $B-L$ model and various representative 2HDM, one can analyze the effect of variation of free dark charges q'_{u_R} and q'_{d_R}, leading to different models than listed in Table 3.2. Inclusions determined from CsI 2022 data with %90 CL in the $\left(q'_{u_R}, q'_{d_R}\right)$ parameter space with respect to variation of the other parameters of 2HDM are given in Fig. (4.9). In the top left panel, the inner light blue region is the allowed region by COHERENT data for the given parameters. The encompassing yellow region is the region of the parameter space where 100 MeV dark photon is possible. Outside this region, dark photon mass has to be

greater. The sensitivity to $\tan\beta$ is shown on the top right panel. The previous argument on sensitivity loss for high values of $\tan\beta$ can be repeated here. Inclusion regions for $\tan\beta = 5$, 20 or any higher value are inseparable. In the lower row, the allowed regions are indicated for various g_D values on the left panel and various $M_{A'}$ values on the right panel. The size of the allowed region has effected significantly by varying g_D, which is somehow less pronounced for the variation of the dark photon mass.
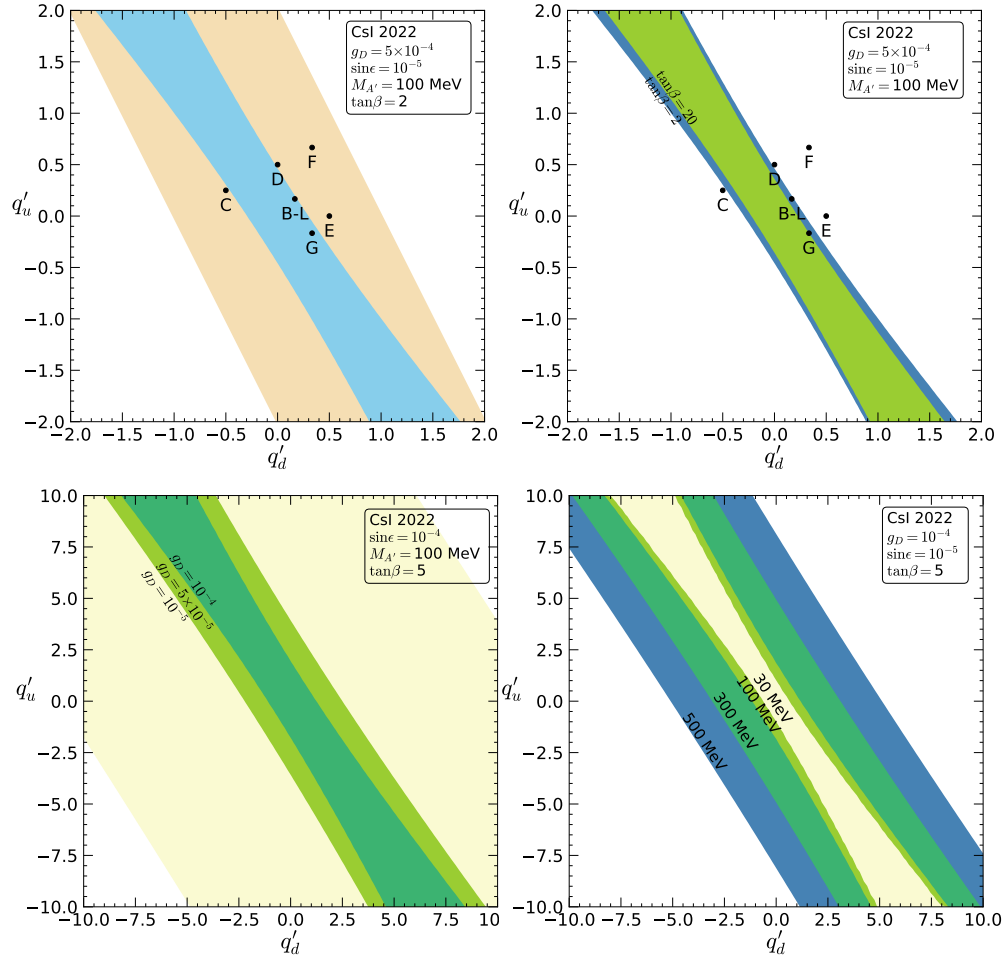
Figure 4.9: Allowed %90 CL regions for the dark charges q'_{u_R} and q'_{d_R} for the CsI target. In the upper row, $g_D = 5 \times 10^{-4}$, $\sin\epsilon = 10^{-5}$, and $M_{A'} = 100$ MeV are chosen with $\tan\beta = 2$ (upper left) and for two different $\tan\beta$ values (upper right). The $\left(q'_{u_R}, q'_{d_R}\right)$ values of all the 2HDMs extend with U(1)$_D$ are marked on the graphs given the upper row. In the lower row, $\tan\beta = 5$ with $\sin\epsilon = 10^{-4}$ and $M_{A'} = 100$ MeV for various g_D (lower left) and $\sin\epsilon = 10^{-5}$ and $g_D = 10^{-4}$ for various $M_{A'}$ (lower right). The shaded regions are allowed by the COHERENT data for CEνNS.

CHAPTER 5

CONCLUSION

The dark matter problem can be conceptualized with a dark sector parallel to the visible sector, with numerous particles interacting via gauge bosons. After all, the visible sector is full of particles and has rich and interesting physics, and the same could be possible for the dark sector. This thesis analyzes $U(1)_D$ group extension to SM as a dark sector model alongside a scalar extension in the visible scalar sector. The new gauge boson that arises with this group is called a dark photon. It can act as a portal between two sectors. In the simplest case, the dark photon would act as the mediator of the fifth force that couples to both SM and dark sector particles. Furthermore, as a property of the $U(1)$ group, the dark photon can still connect the two sectors even if it does not couple to SM particles directly. This is achieved via kinetically mixing the $U(1)_D$ gauge field with the electroweak hypercharge field, which has no precedent in SM. This mixing results in dark photon and neutral electroweak bosons turning into each other during propagation. However, it is not convenient to work on the original basis. The kinetic mixing term is rotated away with a transformation that alters the field definitions of dark photon and SM gauge bosons. Another possible connection between sectors is via a mass mixing between dark photon and Z boson. This mixing can be observed in cases where the visible scalar sector is modified. If the Higgs field is also charged under this new gauge group $U(1)_D$, the mixing, as mentioned earlier, occurs after electroweak symmetry breaking. However, this case has a problem since there are few anomaly-free options for the charge of the new group. These are some combinations of baryon and lepton quantum numbers, and in this thesis, the $q_D = B - L$ case is selected. Mass mixing can not occur in this framework since the SM Higgs field's baryon, and lepton quantum numbers are zero. Nonetheless, in the models

where the SM Higgs sector is extended, this charge could be non-zero, and mass mixing can emerge. This study chooses a specific 2HDM model as the Higgs sector expansion.

In Chapter 2, a general review of SM, the Higgs mechanism, and how this mechanism is applied in the context of SM is given. The EW Lagrangian is extended with a scalar sector where a complex scalar doublet called Higgs doublet is present. Due to the form of the potential, the Higgs vacuum is infinitely degenerate and requires selecting a specific point before seeing the particle content of the model. This selection of vacuum spontaneously breaks the EW symmetry, which results in mass terms for both gauge bosons and fermions. However, there is no theoretical cap on the number of scalar fields, and the SM Higgs sector can be expanded. A specific type-I 2HDM was discussed along with the Higgs fields charge configurations.

In Chapter 3, $U(1)_D$ extension to both SM and 2HDM are studied. In the SM extension case charge associated with the new gauge group is selected to be $B-L$; hence this case is called the minimal $B-L$ model within the context of this thesis. Three field redefinitions are performed. In sequential order, they remove the kinetic mixing, perform the Weinberg transformation, and diagonalize the gauge boson mass matrix. The resulting photon and Z boson expressions differ from their SM counterparts, but the masses and interactions are similar. The resulting dark photon is massive, and its interactions depend on the kinetic mixing parameter. Its mass receives a contribution from visible sector neutral gauge bosons and, depending on the values of the new gauge group, can be dominated by this contribution.

Moreover, the difference in construction if the visible scalar sector is extended was studied. In the framework of the type-I 2HDM used, only the second Higgs doublet couples to the fermions. Just like previously, the $B-L$ value for this doublet is zero. However, the first doublet obtains a non-zero $B-L$ value, allowing mass mixing to occur. Other possible anomaly-free charges can be associated with $U(1)_D$. All these charges were considered in the phenomenological study provided in the end. In this case, the approach to obtaining physical is similar to before. The same three basis rotations are performed, but the rotations are modified due to the mass mixing between the dark vector boson and the Z boson. Again, the resulting photon

and Z boson behave close to their SM counterparts. The dark photon, however, has a substantial contribution proportional to dark gauge coupling to its mass. This prevents dark photon mass from dropping below the MeV range in the region of interest $g_D = 10^{-6} - 10^{-3}$. The structures of interactions are also affected by this process. The dark photon mediated interactions receive a contribution from the visible sector, and so do the visible sector interactions from the dark sector.

In Chapter 4, phenomenological study on our dark sector model was performed through the recent observation of CEνNS by COHERENT Collaboration. In SM, this interaction is mediated by the Z boson. In the energy range of this phenomenon, the differential cross section for SM neutral current interactions is two orders of magnitude greater than SM charged current interactions. This gap makes CEνNS viable for testing the validity of neutral current interactions of SM. SM predicts the cross-section of this interaction scales with the number of neutrons in the nucleus. This behavior is unique to SM and dark photon exchange contribution to the cross-section scales with atom number. In sec. 4.1.2, different cross-sections for both minimal $B - L$ and non-minimal models are given. Then, in sec. 4.2, simulation of the experiment performed by COHERENT Collaboration is discussed. The experiment counts the scattering events by detecting the recoil energy of the target nuclei. The expected number of events depends on experimental parameters provided by the collaboration, which are open to discussion in the literature. Using the equation for the expected number of events with respect to cross-section, chi-square goodness of fit analysis is performed to study the sensitivity of the dark sector parameters.

The models are sensitive to the mass of the dark photon $M_{A'}$, particularly in the MeV-GeV region, and this characteristic disappears for the so-called minimal $B - L$ model for around $M_{A'} \lesssim 1$ MeV where the exact value depends on the kinetic mixing. On the other hand, the non-minimal models exhibit different behavior in this region. The dark photon mass receives scalar sector contribution proportional to g_D. This contribution is significant regardless of the value of the kinetic mixing and produces the behavior of light-dark photon tail in the right panels in the figures (4.4) - (4.6). As a result, the minimal $B - L$ model provides the best bounds for $M_{A'} \geq 1$ MeV, whereas the other models have stronger bounds in the lighter dark

69

photon region. This might be the means to distinguish them. It is also observed that the best bounds are obtained for the single bin case (1PE-1t) for the CsI 2022 data. In the final set of plots, Fig.4.9, the allowed bands on the (q'_{u_R}, q'_{d_R}) plane have been shown, and this could be used as a reference for better assessment of the scenarios beyond the chosen representative ones listed in Table 3.2. With additional data accessible at low energies, it may be possible to better probe new physics scenarios, such as 2HDM, or perhaps to identify a critical signal that may outline the physics beyond the SM.

REFERENCES

[1] Miguel D. Campos, D. Cogollo, Manfred Lindner, T. Melo, Farinaldo S. Queiroz, and Werner Rodejohann. Neutrino Masses and Absence of Flavor Changing Interactions in the 2HDM from Gauge Principles. *JHEP*, 08:092, 2017.

[2] D Akimov, JB Albert, P An, C Awe, PS Barbeau, B Becker, V Belov, A Brown, A Bolozdynya, B Cabrera-Palmer, et al. Observation of coherent elastic neutrino-nucleus scattering. *Science*, 357(6356):1123–1126, 2017.

[3] D Akimov, P An, C Awe, PS Barbeau, B Becker, V Belov, I Bernardi, MA Blackston, C Bock, A Bolozdynya, et al. Measurement of the coherent elastic neutrino-nucleus scattering cross section on csi by coherent. *Physical Review Letters*, 129(8):081801, 2022.

[4] D Akimov, JB Albert, P An, C Awe, PS Barbeau, B Becker, V Belov, I Bernardi, MA Blackston, L Blokland, et al. First measurement of coherent elastic neutrino-nucleus scattering on argon. *Physical Review Letters*, 126(1):012002, 2021.

[5] Jens Erler and Matthias Schott. Electroweak precision tests of the standard model after the discovery of the higgs boson. *Progress in Particle and Nuclear Physics*, 106:68–119, 2019.

[6] Yoshiyuki Fukuda, T Hayakawa, E Ichihara, K Inoue, K Ishihara, Hirokazu Ishino, Y Itow, T Kajita, J Kameda, S Kasuga, et al. Evidence for oscillation of atmospheric neutrinos. *Physical review letters*, 81(8):1562, 1998.

[7] Robert Mann. *An introduction to particle physics and the standard model*. Taylor & Francis, 2010.

[8] Glennys R Farrar and ME Shaposhnikov. Baryon asymmetry of the universe in the standard model. *Physical Review D*, 50(2):774, 1994.

[9] Annika HG Peter. Dark matter: a brief review. *arXiv preprint arXiv:1201.3942*, 2012.

[10] Utpal Sarkar. *Particle and Astroparticle physics.* CRC Press, 2007.

[11] Particle Data Group, RL Workman, VD Burkert, V Crede, E Klempt, U Thoma, L Tiator, K Agashe, G Aielli, BC Allanach, et al. Review of particle physics. *Progress of theoretical and experimental physics*, 2022(8):083C01, 2022.

[12] Fritz Zwicky. Die rotverschiebung von extragalaktischen nebeln. *Helvetica physica acta*, 6:110–127, 1933.

[13] Sinclair Smith. The mass of the virgo cluster. *The Astrophysical Journal*, 83:23, 1936.

[14] Vera C Rubin and W Kent Ford Jr. Rotation of the andromeda nebula from a spectroscopic survey of emission regions. *The Astrophysical Journal*, 159:379, 1970.

[15] Vera C Rubin, W Kent Ford Jr, and Norbert Thonnard. Rotational properties of 21 sc galaxies with a large range of luminosities and radii, from ngc 4605/r= 4kpc/to ugc 2885/r= 122 kpc. *The Astrophysical Journal*, 238:471–487, 1980.

[16] Jaan Einasto. Dark matter. *Brazilian Journal of Physics*, 43(5):369–374, 2013.

[17] Douglas Clowe, Anthony Gonzalez, and Maxim Markevitch. Weak-lensing mass reconstruction of the interacting cluster 1e 0657–558: Direct evidence for the existence of dark matter. *The Astrophysical Journal*, 604(2):596, 2004.

[18] David Harvey, Richard Massey, Thomas Kitching, Andy Taylor, and Eric Tittley. The nongravitational interactions of dark matter in colliding galaxy clusters. *Science*, 347(6229):1462–1465, 2015.

[19] Volker Springel, Simon DM White, Adrian Jenkins, Carlos S Frenk, Naoki Yoshida, Liang Gao, Julio Navarro, Robert Thacker, Darren Croton, John Helly, et al. Simulating the joint evolution of quasars, galaxies and their large-scale distribution. *arXiv preprint astro-ph/0504097*, 2005.

[20] Susmita Adhikari, Arka Banerjee, Kimberly K Boddy, Francis-Yan Cyr-Racine, Harry Desmond, Cora Dvorkin, Bhuvnesh Jain, Felix Kahlhoefer, Manoj

Kaplinghat, Anna Nierenberg, et al. Astrophysical tests of dark matter self-interactions. *arXiv preprint arXiv:2207.10638*, 2022.

[21] Lars Bergström. Dark matter candidates. *New Journal of Physics*, 11(10):105006, 2009.

[22] Marco Fabbrichesi, Emidio Gabrielli, and Gaia Lanfranchi. *The Physics of the Dark Photon: A Primer*. Springer, 2021.

[23] Daniel Z Freedman. Coherent effects of a weak neutral current. *Physical Review D*, 9(5):1389, 1974.

[24] A. Drukier and Leo Stodolsky. Principles and Applications of a Neutral Current Detector for Neutrino Physics and Astronomy. *Phys. Rev. D*, 30:2295, 1984.

[25] Aron Beekman, Louk Rademaker, and Jasper van Wezel. An introduction to spontaneous symmetry breaking. *SciPost Physics Lecture Notes*, page 011, 2019.

[26] Katherine Brading and Harvey R Brown. Noether's theorems and gauge symmetries. *arXiv preprint hep-th/0009058*, 2000.

[27] VA Bednyakov, ND Giokaris, and AV Bednyakov. On the higgs mass generation mechanism in the standard model. *Physics of Particles and Nuclei*, 39(1):13–36, 2008.

[28] Michael E Peskin and Daniel V Schroeder. *An introduction to quantum field theory*. CRC press, 2018.

[29] Samoil M Bilenky and Jiři Hošek. Glashow-weinberg-salam theory of electroweak interactions and the neutral currents. *Physics Reports*, 90(2):73–157, 1982.

[30] Gautam Bhattacharyya. A pedagogical review of electroweak symmetry breaking scenarios. *Reports on Progress in Physics*, 74(2):026201, 2011.

[31] Ivo van Vulpen and I Angelozzi. The standard model higgs boson. *Part of the Lecture Particle Physics II, University of Amsterdam Particle Physics Master*, 2014, 2013.

[32] John F Donoghue, Eugene Golowich, and Barry R Holstein. *Dynamics of the standard model*. Cambridge university press, 2014.

[33] Yoshiharu Kawamura. Yukawa interactions, flavor symmetry, and non-canonical kähler potential. *Progress of Theoretical and Experimental Physics*, 2019(4):043B05, 2019.

[34] Andrija Rasin. Diagonalization of quark mass matrices and the cabibbo-kobayashi-maskawa matrix. *arXiv preprint hep-ph/9708216*, 1997.

[35] Andreas Höcker and Zoltan Ligeti. Cp violation and the ckm matrix. *Annu. Rev. Nucl. Part. Sci.*, 56:501–567, 2006.

[36] Gustavo Castelo Branco, PM Ferreira, L Lavoura, MN Rebelo, Marc Sher, and Joao P Silva. Theory and phenomenology of two-higgs-doublet models. *Physics reports*, 516(1-2):1–102, 2012.

[37] Jin-Min Yang, Yang Zhang, et al. Two-higgs-doublet models in light of current experiments: a brief review. *Communications in Theoretical Physics*, 2022.

[38] Gautam Bhattacharyya and Dipankar Das. Scalar sector of two-higgs-doublet models: A minireview. *Pramana*, 87(3):1–13, 2016.

[39] Sheldon L Glashow and Steven Weinberg. Natural conservation laws for neutral currents. *Physical Review D*, 15(7):1958, 1977.

[40] Emmanuel A Paschos. Diagonal neutral currents. *Physical Review D*, 15(7):1966, 1977.

[41] Pedro M Ferreira, Bohdan Grzadkowski, Odd Magne Ogreid, and Per Osland. Softly broken symmetries in the 2hdm–an invariant formulation. *arXiv preprint arXiv:2209.00152*, 2022.

[42] Daniel A Camargo, Alex G Dias, Tessio B de Melo, and Farinaldo S Queiroz. Neutrino masses in a two higgs doublet model with a u (1) gauge symmetry. *Journal of High Energy Physics*, 2019(4):1–38, 2019.

[43] D Cogollo, Ricardo D Matheus, Tessio B de Melo, and Farinaldo S Queiroz. Type i+ ii seesaw in a two higgs doublet model. *Physics Letters B*, 797:134813, 2019.

[44] Renata Zukanovich Funchal, Benoit Schmauch, and Gaëlle Giesen. The physics of neutrinos. *arXiv preprint arXiv:1308.1029*, 2013.

[45] Manfred Lindner, Werner Rodejohann, and Xun-Jie Xu. Coherent neutrino-nucleus scattering and new neutrino interactions. *Journal of High Energy Physics*, 2017(3):97, 2017.

[46] Kate Scholberg. Prospects for measuring coherent neutrino-nucleus elastic scattering at a stopped-pion neutrino source. *Physical Review D*, 73(3):033005, 2006.

[47] AJ Anderson, JM Conrad, E Figueroa-Feliciano, K Scholberg, and J Spitz. Coherent neutrino scattering in dark matter detectors. *Physical Review D*, 84(1):013008, 2011.

[48] J.D. Lewin and P.F. Smith. Review of mathematics, numerical factors, and corrections for dark matter experiments based on elastic nuclear recoil. *Astroparticle Physics*, 6(1):87–112, 1996.

[49] P. S. Amanik and G. C. McLaughlin. Nuclear neutron form factor from neutrino nucleus coherent elastic scattering. *J. Phys. G*, 36:015105, 2009.

[50] O. Moreno and T. W. Donnelly. Unified approach to electron and neutrino elastic scattering off nuclei with an application to the study of the axial structure. *Phys. Rev. C*, 92(5):055504, 2015.

[51] JI Collar, ARL Kavner, and CM Lewis. Response of csi [na] to nuclear recoils: Impact on coherent elastic neutrino-nucleus scattering. *Physical Review D*, 100(3):033003, 2019.

[52] John Betteley Birks. Scintillations from organic crystals: specific fluorescence and relative response to different radiations. *Proceedings of the Physical Society. Section A*, 64(10):874, 1951.

[53] James F Ziegler. Srim-2003. *Nuclear instruments and methods in physics research section B: Beam interactions with materials and atoms*, 219:1027–1036, 2004.

[54] D Akimov, P An, C Awe, PS Barbeau, B Becker, V Belov, I Bernardi, MA Blackston, C Bock, A Bolozdynya, et al. Measurement of scintillation response of csi [na] to low-energy nuclear recoils by coherent. *Journal of Instrumentation*, 17(10):P10034, 2022.

[55] D Akimov, JB Albert, P An, C Awe, PS Barbeau, B Becker, V Belov, MA Blackston, L Blokland, A Bolozdynya, et al. Coherent collaboration data release from the first detection of coherent elastic neutrino-nucleus scattering on argon. *arXiv:2006.12659*, 2020.

[56] Werner Herr and B Muratori. Concept of luminosity. 2006. `https://cds.cern.ch/record/941318`.

[57] Cesare Bini. Data analysis in particle physics, 2016. `https://www.roma1.infn.it/~bini/StatEPP_new.pdf`.

[58] D Akimov, JB Albert, P An, C Awe, PS Barbeau, B Becker, V Belov, MA Blackston, A Bolozdynya, A Brown, et al. Coherent collaboration data release from the first observation of coherent elastic neutrino-nucleus scattering. *arXiv preprint arXiv:1804.09459*, 2018.

[59] Peter B Denton and Julia Gehrlein. A statistical analysis of the coherent data and applications to new physics. *Journal of High Energy Physics*, 2021(4):1–29, 2021.

[60] Ansgar Denner, H Eck, O Hahn, and J Küblbeck. Feynman rules for fermion-number-violating interactions. *Nuclear Physics B*, 387(2):467–481, 1992.

[61] Ansgar Denner, H Eck, O Hahn, and J Küblbeck. Compact feynman rules for majorana fermions. *Physics Letters B*, 291(3):278–280, 1992.

[62] J Gluza and M Zraek. Feynman rules for majorana-neutrino interactions. *Physical Review D*, 45(5):1693, 1992.

[63] J Barranco, D Delepine, V Gonzalez-Macias, C Lujan-Peschard, and M Napsuciale. Scattering processes could distinguish majorana from dirac neutrinos. *Physics Letters B*, 739:343–347, 2014.

[64] Boris Kayser and Robert E Shrock. Distinguishing between dirac and majorana neutrinos in neutral-current reactions. *Physics Letters B*, 112(2):137–142, 1982.

Appendix A

GAUGE TRANSFORMATIONS IN THE SU(2) GROUP

The covariant derivative in an SU(2) theory is

$$D_\mu = \partial_\mu + \mathrm{i}\frac{g}{2}\boldsymbol{W}_\mu \cdot \boldsymbol{\sigma}. \tag{A.1}$$

SU(2) transformations take the forms

$$\psi \to \psi' = \left(1 + \mathrm{i}\frac{1}{2}\boldsymbol{\omega}\cdot\boldsymbol{\sigma}\right)\psi, \qquad \bar{\psi} \to \bar{\psi}' = \bar{\psi}\left(1 - \mathrm{i}\frac{1}{2}\boldsymbol{\omega}\cdot\boldsymbol{\sigma}\right) \tag{A.2}$$

and

$$D_\mu \to D'_\mu = \partial_\mu + \mathrm{i}\frac{g}{2}\boldsymbol{W}'_\mu \cdot \boldsymbol{\sigma}. \tag{A.3}$$

The condition for gauge invariance is

$$\bar{\psi}\gamma^\mu D_\mu \psi = \bar{\psi}'\gamma^\mu D'_\mu \psi'. \tag{A.4}$$

This is possible if $D_\mu\psi$ transforms just like ψ.

$$D_\mu\psi \to D'_\mu\psi' = \left(1 + \mathrm{i}\frac{g}{2}\boldsymbol{\omega}\cdot\boldsymbol{\sigma}\right)D_\mu\psi \tag{A.5}$$

Then

$$\left(\partial_\mu + \mathrm{i}\frac{g}{2}\boldsymbol{W}'_\mu\cdot\boldsymbol{\sigma}\right)\left(1 + \mathrm{i}\frac{1}{2}\boldsymbol{\omega}\cdot\boldsymbol{\sigma}\right)\psi = \left(1 + \mathrm{i}\frac{1}{2}\boldsymbol{\omega}\cdot\boldsymbol{\sigma}\right)\left(\partial_\mu + \mathrm{i}\frac{g}{2}\boldsymbol{W}_\mu\cdot\boldsymbol{\sigma}\right)\psi$$

$$\left(\partial_\mu + \mathrm{i}\frac{g}{2}\boldsymbol{W}'_\mu\cdot\boldsymbol{\sigma}\right) = \left(1 + \mathrm{i}\frac{1}{2}\boldsymbol{\omega}\cdot\boldsymbol{\sigma}\right)\left(\partial_\mu + \mathrm{i}\frac{g}{2}\boldsymbol{W}_\mu\cdot\boldsymbol{\sigma}\right)\overbrace{\left(1 + \mathrm{i}\frac{1}{2}\boldsymbol{\omega}\cdot\boldsymbol{\sigma}\right)^{-1}}^{1-\mathrm{i}\frac{1}{2}\boldsymbol{\omega}\cdot\boldsymbol{\sigma}}$$

$$\partial_\mu + \mathrm{i}\frac{g}{2}\boldsymbol{W}'_\mu\cdot\boldsymbol{\sigma} = \partial_\mu - \mathrm{i}\frac{1}{2}(\partial_\mu\boldsymbol{\omega})\cdot\boldsymbol{\sigma} + \mathrm{i}\frac{g}{2}\boldsymbol{W}_\mu\cdot\boldsymbol{\sigma} - \left(\frac{\mathrm{i}}{2}\right)^2 g(\boldsymbol{W}_\mu\cdot\boldsymbol{\sigma})(\boldsymbol{\omega}\cdot\boldsymbol{\sigma})$$

$$+ \left(\frac{\mathrm{i}}{2}\right)^2 g(\boldsymbol{\omega}\cdot\boldsymbol{\sigma})(\boldsymbol{W}_\mu\cdot\boldsymbol{\sigma}) + \mathcal{O}(\omega^2). \tag{A.6}$$

Ignoring the high order terms in ω, the last two terms can be further simplified. In index notation these are

$$\frac{g}{4}\left((W_\mu)_i \sigma_i \omega_j \sigma_j - \omega_j \sigma_j (W_\mu)_i \sigma_i\right). \tag{A.7}$$

By using the property of sigma matrices

$$\sigma_i \sigma_j - \sigma_j \sigma_i = 2i\epsilon_{ijk}\sigma_k \tag{A.8}$$

(A.7) can be written as

$$-i\frac{g}{2}\epsilon_{ijk}\omega_i (W_\mu)_j \sigma_k = -i\frac{g}{2}\left(\omega \times W_\mu\right) \cdot \sigma. \tag{A.9}$$

Inserting this in (A.6) gives

$$\partial_\mu + i\frac{g}{2}W'_\mu \cdot \sigma = \partial_\mu - i\frac{1}{2}(\partial_\mu \omega) \cdot \sigma + i\frac{g}{2}W_\mu \cdot \sigma - i\frac{g}{2}\left(\omega \times W_\mu\right) \cdot \sigma \tag{A.10}$$

and

$$W'_\mu = W_\mu - \frac{1}{g}(\partial_\mu \omega) - \left(\omega \times W_\mu\right). \tag{A.11}$$

Appendix B

ANOMALIES

In a classical theory, every continuous symmetry of a system corresponds a conserved current. In particle physics, the energy is quantized, generating to quantum fields. The quantum field theoretical equivalence to classical conservation laws are known as Ward identities. Ward identities relates the correlation functions of the conserved currents to correlation functions of the fields. However, due to the quantum corrections, identities obtained in a classical theory may not hold at the quantum level. This situation is referred as anomaly. The effects of the anomaly depends on the type of symmetry effected. The current conservation under a local symmetry plays a crucial role in gauge theories. Hence, gauge anomalies, associated with gauge currents, may lead to unrenormalizable theories and braking of the gauge invariance and must be avoided.

The anomalies are generally generated by triangle diagrams. The triangle diagrams contains a type of generator at each vertex, indicated with a Latin letter in Fig. (B.1). The amplitude of this diagram is related to
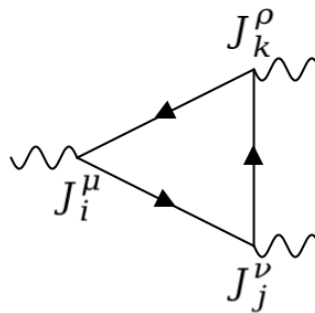

Figure B.1: Triangle diagram

$$\mathcal{M} \propto \langle \Omega | T \left[J_i^\mu J_j^\nu J_k^\rho \right] | \Omega \rangle. \tag{B.1}$$
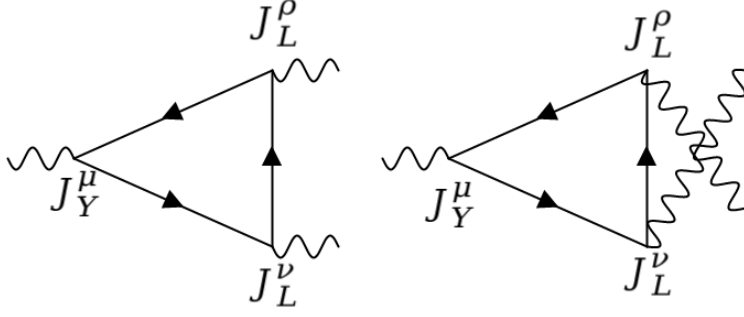
Figure B.2: Triangle diagrams with $U(1)_Y$ and $SU(2)_L$ interactions

By using Feynman rules, the amplitude can be shown to be proportional to

$$\mathscr{M} \propto \text{Tr}\left[T_{i,R}\{T_{j,R}, T_{k,R}\}\right] - \text{Tr}\left[T_{i,L}\{T_{j,L}, T_{k,L}\}\right] \tag{B.2}$$

where $T_{L,R}$ are group generators for left- and right-handed representations. The quantum corrections come from all possible current combinations of triangle diagrams. The anomaly cancellation requires that sum of diagrams from all possible fermion loops for a given group combination is zero. For example, a set of diagrams involving two $SU(2)_L$ and a $U(1)_Y$ gauge bosons (Fig.(B.2)) have the following condition

$$\begin{aligned}
\sum_{f_R}\left(I_{f_R}^3\right)^2 Y_{f_R} - \sum_{f_L}\left(I_{f_L}^3\right)^2 Y_{f_L} &= 0 \\
&= -\left(Y_{e_L} + Y_{\nu_L} + 3(Y_u + Y_d)\right) = 0 \\
&= -\left(2 \times (-1) + 3 \times 2 \times \frac{1}{3}\right) = 0
\end{aligned} \tag{B.3}$$

where the factor 3 comes from the number of color states of the quarks. The placement of the currents inside the diagrams does not effect this outcome. The ten possible combinations considered in the SM is as follows:

$$SU(3)_C^3, \ SU(3)_C^2 SU(2)_L, \ SU(3)_C^2 U(1)_Y, \ SU(3)_C SU(2)_L U(1)_Y$$
$$SU(3)_C U(1)_Y^2, \ SU(2)_L^3, \ SU(2)_L^2 U(1)_Y, \ SU(2)_L U(1)_Y^2, \ U(1)_Y^3$$

The SM by itself turns out to be anomaly-free. However, the $U(1)_D$ extension brings new anomaly-free conditions. These are

$(SU(3)_C)^2 U(1)_D$:

$$\mathscr{M} \propto \text{Tr}\left[\left\{\frac{\lambda^i}{2}\frac{\lambda^j}{2}\right\} q'_{f_R}\right] - \text{Tr}\left[\left\{\frac{\lambda^i}{2}\frac{\lambda^j}{2}\right\} q'_{f_L}\right] \tag{B.4}$$

giving

$$\sum_{\text{quarks}} q'_{f_R} - \sum_{\text{quarks}} q'_{f_L} = \left(3q'_{u_R} + 3q'_{d_R}\right) - \left(3 \times 2q'_{Q_L}\right) = 0$$

$$q'_{u_R} + q'_{d_R} - 2q'_{Q_L} = 0, \tag{B.5}$$

where $\lambda/2$ is the generator for $SU(3)_C$.

$\underline{(SU(2)_L)^2\,U(1)_D}$:

$$\mathcal{M} \propto \sum_{f_L} \left(I^3_{f_L}\right)^2 Y_{f_L} \tag{B.6}$$

giving

$$-\sum_{f_L} q'_{f_L} = -\left(2q'_L + 3 \times 2q'_{Q_L}\right) = 0$$

$$q'_L + 3q'_{Q_L} = 0, \tag{B.7}$$

$\underline{(U(1)_Y)^2\,U(1)_D}$:

$$\mathcal{M} \propto \operatorname{Tr}\left[\{Y_R, Y_R\}\, q'_R\right] - \operatorname{Tr}\left[\{Y_L, Y_L\}\, q'_L\right] \tag{B.8}$$

giving

$$\sum_{f_R} Y_R^{f_R\,2} q_R^{f_R} - \sum_{f_L} Y_R^{f_L\,2} q_R^{f_L}$$

$$= \left((-2)^2 q'_{e_R} + 3\left(\frac{4}{3}\right)^2 q'_{u_R} + 3\left(-\frac{2}{3}\right)^2\right) q'_{d_R} - \left(2(-1)^2 q'_L + 3 \times 2\left(\frac{1}{3}\right)^2 q'_{Q_L}\right) = 0$$

$$6q'_{e_R} + 8q'_{u_R} + 2q'_{d_R} - 3q'_L - q'_{Q_L} = 0, \tag{B.9}$$

$\underline{(U(1)_Y)\,U(1)_D^2}$:

$$\mathcal{M} \propto \operatorname{Tr}\left[\{q'_R, q'_R\}\, Y_{f_R}\right] - \operatorname{Tr}\left[\{q'_L, q'_L\}\, Y_{f_L}\right] \tag{B.10}$$

giving

$$\left((-2)q'^2_{e_R} + 3\left(\frac{4}{3}\right)q'^2_{u_R} + 3\left(-\frac{2}{3}\right)q'^2_{d_R}\right) - \left(2(-1)^2 q'^2_L + 3 \times 2\left(\frac{1}{3}\right)^2 q'^2_{Q_L}\right) = 0$$

$$-q'^2_{e_R} + 2q'^2_{u_R} - q'^2_{d_R} + q'^2_L - q'^2_{Q_L} = 0, \tag{B.11}$$

and lastly

$\underline{U(1)_D^3}$:

$$\mathcal{M} \propto \operatorname{Tr}\left[\{q'_R, q'_R\}\, q'_R\right] - \operatorname{Tr}\left[\{q'_L, q'_L\}\, q'_L\right] \tag{B.12}$$

83

giving

$$= \left(q'^3_{e_R} + 3q'^3_{u_R} + 3q'^3_{d_R}\right) - \left(2q'^3_L + 3 \times 2q'^3_{Q_L}\right) = 0$$

$$q'^3_{e_R} + 3q'^3_{u_R} + 3q'^3_{d_R} - 2q'^3_L - 6q'^3_{Q_L} = 0. \tag{B.13}$$

Charge configuration of any U(1) extension needs to satisfy the above conditions to be anomaly-free. According to the Adler-Bardeen theorem, once the anomalies are canceled at one loop, there are no more anomalies coming from higher diagrams. In the case $q' = B - L$, Eqs. (B.5) - (B.11) are satisfied. However, in order to satisfy Eq.(B.13), a right-handed neutrino n_R^i that do not enter weak interactions needs to added for each lepton family. The inclusion of right-handed neutrinos modify Eq.(B.13) as

$$q'^3_{n_R} + q'^3_{e_R} + 3q'^3_{u_R} + 3q'^3_{d_R} - 2q'^3_L - 6q'^3_{Q_L} = 0. \tag{B.14}$$

Appendix C

CEνNS CROSS SECTION CALCULATION IN THE STANDARD MODEL

The scattering amplitude for coherent elastic neutrino-nucleus scattering described by 4.3 is expressed as follows:

$$i\mathcal{M}_Z = -\frac{(ig)^2}{c_W^2}\left(\frac{-ig^{\alpha\beta}+i\frac{q^\alpha q^\beta}{m_Z^2}}{q^2-m_Z^2}\right)\langle \nu(p_{\nu_f})|J_{NC,\nu}^\alpha|\nu(p_{\nu_i})\rangle\langle N(p_{N_f})|J_{NC,q}^\beta|N(p_{N_i})\rangle,$$

(C.1)

where q is the momentum transfer, $J_{NC,\nu}^\alpha$ and $J_{NC,q}^\beta$ are neutrino and quark parts of the neutral current, respectively. This expression can be simplified at low energy interactions, i.e., $m_Z >> |q|$. By using the relations $m_Z c_w = m_W$ and $G_F/\sqrt{2} = g^2/8m_W^2$, C.1 becomes

$$i\mathcal{M}_Z = \frac{i8G_F}{\sqrt{2}}\langle \nu(p_{\nu_f})|J_{NC,\nu}^\alpha|\nu(p_{\nu_i})\rangle\langle N(p_{N_f})|J_{NC,q}^\alpha|N(p_{N_i})\rangle.$$

(C.2)

Since neutrinos are point-like particles, the leptonic matrix element can be written as

$$\langle \nu(p_{\nu_f})|J_{NC,\nu}^\alpha|\nu(p_{\nu_i})\rangle = \bar{u}_\nu^{s'}\gamma^\alpha\frac{1}{2}\frac{(1-\gamma^5)}{2}u_\nu^s$$

(C.3)

where u_ν^s and $\bar{u}_\nu^{s'}$ are neutrino spinors with spin indices s and s'. For hadronized states, the matrix element can be written as

$$\langle N|J_{NC,q}^\alpha|N\rangle = g_L^u\langle N|\bar{u}_L\gamma^\alpha u_L|N\rangle + g_R^u\langle N|\bar{u}_R\gamma^\alpha u_R|N\rangle$$
$$+ g_L^d\langle N|\bar{d}_L\gamma^\alpha d_L|N\rangle + g_R^d\langle N|\bar{d}_R\gamma^\alpha d_R|N\rangle$$

(C.4)

If parity symmetry for the nucleus is assumed, the following relation is obtained [45].

$$\langle N|\bar{u}_L\gamma^\alpha u_L|N\rangle = \langle N|\bar{u}_R\gamma^\alpha u_R|N\rangle,$$

85

$$\langle N|\bar{d}_L\gamma^\alpha d_L|N\rangle = \langle N|\bar{d}_R\gamma^\alpha d_R|N\rangle \tag{C.5}$$

This leads to

$$\langle N|\bar{u}\gamma^\alpha u|N\rangle = 2\langle N|\bar{u}\gamma^\alpha P_L u|N\rangle,$$
$$\langle N|\bar{d}\gamma^\alpha d|N\rangle = 2\langle N|\bar{d}\gamma^\alpha P_L d|N\rangle. \tag{C.6}$$

Since strong interactions can not distinguish u and d quarks, the matrix elements are expected to have the following forms:

$$\langle N|\bar{u}\gamma^\alpha u|N\rangle = (2Z+N)f^\alpha, \langle N|\bar{d}\gamma^\alpha d|N\rangle = (2N+Z)f^\alpha. \tag{C.7}$$

Here Z and N are numbers of proton and neutron in the nucleus and f^α is related to the form factor that can be determined from the electromagnetic properties of the nucleus, which is mediated by the electromagnetic current

$$J_{EM}^\alpha = \frac{2}{3}\bar{u}\gamma^\alpha u - \frac{1}{3}\bar{d}\gamma^\alpha d. \tag{C.8}$$

However, these properties depend on the nucleus spin. Spin-0 and spin-1/2 nucleus cases are examined below.

C.1   Spin-0 Nucleus Case

In a $U(1)$ gauge field theory, the interaction vertex involving a gauge boson and two scalar fields is proportional to the initial and final momentum of the scalar field.

$$\langle N(p_{N_f})|J_{EM}^\alpha|N(p_{N_i})\rangle = (p_{N_i} + p_{N_f})^\alpha Z F(q^2) \tag{C.9}$$

where $F(q^2)$ is the nuclear form factor. Hence the function f^α has the form

$$f^\alpha = (p_{N_i} + p_{N_f})^\alpha F(q^2) \tag{C.10}$$

Inserting Eq.(C.7) in Eq.(C.4)

$$\begin{aligned}
\langle N|J_{NC,q}^\alpha|N\rangle &= \frac{1}{2}(p_{N_i} + p_{N_f})^\alpha F(q^2) \\
&\quad \times \left[(2Z+N)(g_L^u + g_R^u) + (2N+Z)(g_L^d + g_R^d)\right] \\
&= -\frac{1}{4}(p_{N_i} + p_{N_f})^\alpha F(q^2) Q_W
\end{aligned} \tag{C.11}$$

where the weak nuclear charge Q_W is

$$Q_W = N - (1 - 4s_w^2)Z, \tag{C.12}$$

along with N and Z standing for neutron and proton numbers, respectively. Now inserting Eq.(C.11) and Eq.(C.3) in Eq.(C.2), gives the amplitude

$$i\mathcal{M}_Z^{ss'} = -\frac{i}{2\sqrt{2}}G_F Q_W F(q^2)(p_{N_i} + p_{N_f})^\alpha \bar{u}_\nu^{s'}(p_{\nu_f})\gamma^\alpha(1 - \gamma^5)u_\nu^s(p_{\nu_i}) \tag{C.13}$$

Taking amplitude square

$$|i\mathcal{M}_Z|^2 = \sum_{ss'}|i\mathcal{M}_Z^{ss'}|^2 \tag{C.14}$$

and implementing kinematic relations given in Appendix E yields

$$|i\mathcal{M}_Z|^2 = 8G_F^2 Q_W F^2(q^2)M^2 E_\nu^2\left(1 - \frac{T}{E_\nu} - \frac{MT}{2E\nu^2}\right) \tag{C.15}$$

where E_ν is the initial neutrino energy, T and M are recoil energy and mass of the nucleus. By using the relation $p_{\nu_i} \cdot q = q^2/2$, it is possible to write T in terms of other parameters[45]

$$T = \frac{2ME_\nu^2 c_\theta^2}{(M + E_\nu)^2 - E_\nu^2 c_\theta^2} \tag{C.16}$$

where c_θ is the scattering angle between initial neutrino momentum and final nucleus momentum. Maximum for T is achieved at $\theta = 0$,

$$T_{max}(E_\nu) = \frac{2E_\nu^2}{M + 2E_\nu} \tag{C.17}$$

The differential cross section in the lab frame can be written as

$$\frac{d\sigma}{dc_\theta}\bigg|_{spin-0}^{\text{SM}} = \frac{|\mathcal{M}_Z|^2}{8\pi}\frac{c_\theta(E_\nu M)^2}{[(E_\nu + M)]^2 - E_\nu^2 c_\theta^2}. \tag{C.18}$$

In the neutrino-nucleus scattering experiments, the only observable is the recoil energy of the nucleus, so it is convenient to express the differential cross section in terms of recoil energy,

$$\frac{d\sigma}{dT}\bigg|_{spin-0}^{\text{SM}} = \frac{|\mathcal{M}_Z|^2}{32\pi ME_\nu^2}. \tag{C.19}$$

Implementing the amplitude square, Eq.(C.15), gives

$$\frac{d\sigma}{dT}\bigg|_{spin-0}^{\text{SM}} = \frac{G_F^2 Q_W^2}{4\pi}M\left(1 - \frac{T}{E_\nu} - \frac{MT}{2E\nu^2}\right). \tag{C.20}$$

C.2   Spin-1/2 Nucleus Case

In the case of a spin-1/2 nucleus (C.11) is modified to

$$\langle N(p_{N_f}, r')|J_{NC}^\mu|N(p_{N_i}, r)\rangle = -\frac{1}{4}Q_W F(q^2)\bar{u}_N^{r'}(p_{N_f})\gamma^\mu u_N^r(p_{N_i}) \tag{C.21}$$

where u_N^r and $\bar{u}_N^{r'}$ are initial and final states of the nucleus. Then (C.13) is modified to

$$i\mathcal{M}_Z^{rr'ss'} = -\frac{i}{2\sqrt{2}}G_F Q_W F(q^2)[\bar{u}_N^{r'}(p_{N_f})\gamma^\mu u_N^r(p_{N_i})][\bar{u}_\nu^{s'}(p_{\nu_f})\gamma^\alpha(1-\gamma^5)u_\nu^s(p_{\nu_i})]. \tag{C.22}$$

The square of this amplitude is

$$|\mathcal{M}_Z|^2 = \sum_{ss'}\frac{1}{2}\sum_{rr'}|\mathcal{M}_Z^{r'rss'}|$$

$$=8G_F^2 Q_W F^2 M^2 E_\nu^2\left(1 - \frac{T}{E_\nu} - \frac{MT}{2E\nu^2} + \frac{T^2}{2E_\nu^2}\right) \tag{C.23}$$

and the cross section becomes

$$\frac{d\sigma}{dT}\Big|_{spin-1/2}^{SM} = \frac{G_F^2(2g_L^\nu Q_W)^2}{4\pi}M\left(1 - \frac{T}{E_\nu} - \frac{MT}{2E\nu^2} + \frac{T^2}{2E_\nu}\right). \tag{C.24}$$

Note that the cross section for both νN and $\bar{\nu} N$ scattering are equal to each other since the interaction between the nucleus and Z boson is assumed to conserve parity.

Appendix D

CEνNS CROSS SECTION CALCULATION IN THE MINIMAL $B - L$ MODEL

The amplitude for one dark photon exchange, described by the Lagrangian Eq.(3.1) is

$$i\mathcal{M}_D = -(ig_{B-L})^2 \left(\frac{-i\eta^{\alpha\beta} + \frac{iq^\alpha q^\beta}{m^2_{A'}}}{q^2 - m^2_{A'}} \right) \langle v(p_{v_f})|J^\alpha_D|v(p_{v_i})\rangle \langle N(p_{N_f})|J^\beta_D|N(p_{N_i})\rangle. \quad \text{(D.1)}$$

In this case, the expression for the leptonic matrix element is

$$\langle v(p_{v_f})|J^\alpha_D|v(p_{v_i})\rangle = \langle v(p_{v_f})|\bar{v}\gamma^\alpha v|v(p_{v_i})\rangle = \bar{u}^{s'}_v \gamma^\alpha \frac{(1-\gamma^5)}{2} u^s_v \quad \text{(D.2)}$$

The hadronic matrix element again depends on the nucleus spin. For a spin-0 nucleus, using Eq.(C.7) gives

$$\langle N|J^\beta_D|N\rangle = \frac{1}{3} \left[\langle N|\bar{u}\gamma^\beta u|N\rangle + \langle N|\bar{d}\gamma^\beta d|N\rangle \right]$$
$$= (p_{N_i} + p_{v_f})^\beta A F(q^2), \quad \text{(D.3)}$$

where A is the atom number. Hence Eq.(D.1) can be written as

$$i\mathcal{M}_D = -i\frac{g^2_{B-L}}{q^2 - m^2_{A'}} \left[(p_{N_i} + p_{v_f})^\alpha A F(q^2) \bar{u}^{s'}_v \gamma^\alpha \frac{(1-\gamma^5)}{2} u^s_v \right.$$
$$\left. + \frac{1}{m^2_{A'}}(p_{N_i} + p_{v_f}) \cdot q \, A F(q^2) q^\alpha v^{s'} \gamma^\alpha \frac{(1-\gamma^5)}{2} u^s_v \right]$$
$$= -i\frac{g^2_{B-L}}{q^2 - m^2_{A'}} A F(q^2) \bar{u}^{s'}_v \gamma^\alpha \frac{(1-\gamma^5)}{2} u^s_v$$
$$\times \left[(p_{N_i} + p_{v_f})^\alpha + \frac{q^\alpha}{m^2_{A'}(p_{N_i} + p_{v_f}) \cdot q} \right] \quad \text{(D.4)}$$

If both SM and $B - L$ interactions are considered alongside each other, both contribute to the total scattering amplitude.

$$\mathcal{M} = \mathcal{M}_Z + \mathcal{M}_D \quad \text{(D.5)}$$

The Square of this amplitude is

$$|i\mathcal{M}|^2 = \frac{4F^2(q^2)M^2E_\nu^2}{(2MT+m_{A'}^2)^2}\left(1-\frac{T}{E_\nu}-\frac{MT}{2E_\nu^2}\right)$$
$$\times\left[2g_{B-L}^2A^2+\sqrt{2}G_FQ_W(2MT+m_{A'}^2)\right]^2 \tag{D.6}$$

and the cross section is

$$\frac{d\sigma}{dT}\Big|_{spin-0}^{\text{SM}+B-L}=\frac{F^2(q^2)M}{8\pi(2MT+m_{A'}^2)^2}\left(1-\frac{T}{E_\nu}-\frac{MT}{2E_\nu^2}\right)$$
$$\times\left[2g_{B-L}^2A^2+\sqrt{2}G_FQ_W(2MT+m_{A'}^2)\right]^2 \tag{D.7}$$

When the nucleus spin is 1/2, the hadronic matrix element is

$$\langle N|J_D^\beta|N\rangle = A\,F(q^2)\bar{u}_N^{r'}(p_{N_f})\gamma^\mu u_N^r(p_{N_i}) \tag{D.8}$$

This time square of the total amplitude is

$$|i\mathcal{M}|^2 = \frac{4F^2(q^2)M^2E_\nu^2}{(2MT+m_{A'}^2)^2}\left(1-\frac{T}{E_\nu}-\frac{MT}{2E_\nu^2}+\frac{T^2}{E_\nu^2}\right)$$
$$\times\left[2g_{B-L}^2A^2+\sqrt{2}G_FQ_W(2MT+m_{A'}^2)\right]^2 \tag{D.9}$$

The cross section becomes

$$\frac{d\sigma}{dT}\Big|_{spin-1/2}^{\text{SM}+B-L}=\frac{F^2(q^2)M}{8\pi(2MT+m_{A'}^2)^2}\left(1-\frac{T}{E_\nu}-\frac{MT}{2E_\nu^2}+\frac{T^2}{E_\nu^2}\right)$$
$$\times\left[2g_{B-L}^2A^2+\sqrt{2}G_FQ_W(2MT+m_{A'}^2)\right]^2 \tag{D.10}$$

Appendix E

KINEMATIC RELATIONS FOR ELASTIC FIXED TARGET NEUTRINO COLLISIONS

In this chapter, the kinematic relations for an elastic neutrino-fixed nucleus scattering depicted in Fig.(E.1) is derived. p_{ν_i} and p_{N_i} are the initial, and p_{ν_f} and p_{N_f} are final neutrino and nucleus momenta respectively. The momentum transfer is

$$q^\mu = p_{N_f}^\mu - p_{N_i}^\mu = p_{\nu_i}^\mu - p_{\nu_f}^\mu \qquad (E.1)$$

The kinematic relations are obtained from the following combinations.

1:

$$p_{N_i}^\mu p_{N_f}^\mu = E_{N_i} E_{N_f} - \overbrace{\mathbf{p_{N_f}}}^{0} \cdot \mathbf{p_{N_i}}$$

$$p_{N_i}^\mu p_{N_f}^\mu = M(M + T) \qquad (E.2)$$

2:

$$q^{\mu 2} = (p_{N_i}^\mu - p_{N_f}^\mu)^2 = (p_{N_i}^\mu)^2 + (p_{N_f}^\mu)^2 - 2p_{N_i}^\mu p_{N_f}^\mu$$

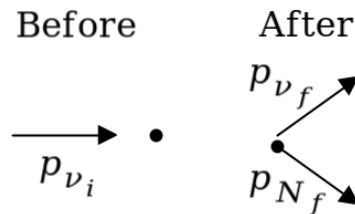$$= M^2 + M^2 - 2M(M + T)$$

$$q^{\mu 2} = -2MT \qquad (E.3)$$

Figure E.1: The process of elastic neutrino nucleus scattering

<u>3:</u>

$$q^\mu p^\mu_{N_i} = (p^\mu_{N_f} - p^\mu_{N_i}) p^\mu_{N_i} = p^\mu_{N_f} p^\mu_{N_i} - (p^\mu_{N_i})^2$$

$$= M(M+T) - M^2$$

$$q^\mu p^\mu_{v_f} = MT \tag{E.4}$$

<u>4:</u>

$$q^{\mu 2} = (p^\mu_{v_i} - p^\mu_{v_f})^2 = (p^\mu_{N_i} - p^\mu_{N_f})^2$$

$$\overbrace{(p^\mu_{v_i})^2}^{0} + \overbrace{(p^\mu_{v_f})^2}^{0} - 2p^\mu_{v_i} p^\mu_{v_f} = (p^\mu_{N_i} - p^\mu_{N_f})^2$$

$$p^\mu_{v_i} p^\mu_{v_f} = MT \tag{E.5}$$

<u>5:</u>

$$q^\mu p^\mu_{v_i} = (p^\mu_{v_i} - p^\mu_{v_f}) p^\mu_{v_i}$$

$$= \overbrace{(p^\mu_{v_i})^2}^{0} - p^\mu_{v_f} p^\mu_{v_i}$$

$$q^\mu p^\mu_{v_i} = -MT \tag{E.6}$$

<u>6:</u>

$$p^\mu_{v_i} p^\mu_{N_i} = E_v M - \overbrace{\mathbf{p_{v_i}} \cdot \mathbf{p_{N_i}}}^{0} \tag{E.7}$$

DIFFERENCE IN THE CROSS SECTION CALCULATION FOR MAJORANA AND DIRAC NEUTRINOS

In order to obtain the scattering amplitude for Majorana particles, Wick's theorem can be used. The matrix element for $\nu N \to \nu N$ scattering via Z exchange for a generic neutrino can be expressed in terms of a set of Wick contractions [60]

$$
\langle \Omega | b_N b_\nu \big(g_\nu \bar{\nu} \gamma^\mu P_L \nu \big) Z Z^\dagger \big(\bar{N} g_N \gamma^\mu N \big) b_N^\dagger b_\nu^\dagger | \Omega \rangle \Big|_{\text{possible contractions}}
$$

$$
= \langle \Omega | b_N \overbrace{b_\nu \big(g_\nu \bar{\nu} \gamma^\mu P_L \nu \big) Z Z^\dagger \big(\bar{N} g_N \gamma^\mu N \big) b_N^\dagger b_\nu^\dagger} | \Omega \rangle
$$

$$
+ \langle \Omega | b_N \overbrace{b_\nu \big(- g_\nu \bar{\nu} \gamma^\mu P_L \nu \big) Z Z^\dagger \big(\bar{N} g_N \gamma^\mu N \big) b_N^\dagger b_\nu^\dagger} | \Omega \rangle \tag{F.1}
$$

The explicit form of the free spinor fields are

$$
\psi(x) = \int \frac{d^3 k}{(2\pi)^3 2E} \sum_s \Big[b(k,s) u(k,s) e^{-ikx} + d^\dagger(k,s) v(k,s) e^{ikx} \Big]
$$

$$
\bar{\psi}(x) = \int \frac{d^3 k}{(2\pi)^3 2E} \sum_s \Big[b^\dagger(k,s) \bar{u}(k,s) e^{-ikx} + d^\dagger(k,s) \bar{v}(k,s) e^{ikx} \Big] \tag{F.2}
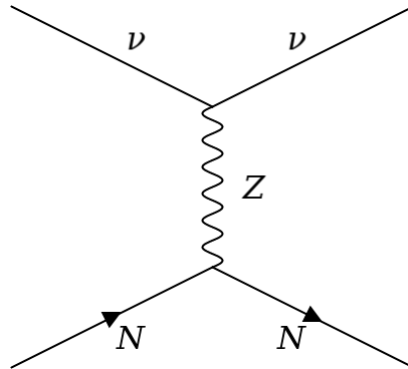$$

Figure F.1: Elastic Majorana neutrino-Nucleus via Z boson exchange

where $b^\dagger$ and $d^\dagger$ are particle and anti-particle creation, and b and d are particle and anti-particle annihilation operators respectively. u and v are spinors with momentum k and spin s. The contractions between fields and operators yield

$$
\begin{aligned}
\psi b^\dagger &= <\Omega|\psi b^\dagger|\Omega> \rightarrow u(k,s) \\
b\bar{\psi} &= <\Omega|b\bar{\psi}|\Omega> \rightarrow \bar{u}(k,s) \\
\bar{\psi}d^\dagger &= <\Omega|\bar{\psi}d^\dagger|\Omega> \rightarrow \bar{v}(k,s) \\
d\psi &= <\Omega|d\psi|\Omega> \rightarrow v(k,s)
\end{aligned}
\tag{F.3}
$$

The first set of contractions, the second line in Eq.(F.1), is the contraction set for Dirac particles and leads to the amplitude Eq.(C.22). However, the last line in Eq.(F.1) appears only for Majorana fermions. For a Dirac field, contractions $b\psi$ and $\bar{\psi}b^\dagger$ are equal to zero. However, since the particle creation operator is equal to the anti-particle creation operator for a Majorana field, these contractions are non-zero.

In order to put the form of contractions $... \bar{v}\gamma_\mu P_L v ...$, which typically appear in Majorana case, in the form given in Eq.(F.3), the definition of charge conjugate fields can be used [60, 61].

$$
\psi^c = C\bar{\psi}^T, \quad \bar{\psi}^c = -\psi^T C^{-1} \quad \text{and} \quad (\psi^c)^c = \psi
\tag{F.4}
$$

where the charge conjugate matrix C satisfies

$$
C^{-1}\gamma^{\mu T}C = -\gamma^\mu, \quad C^{-1}(\gamma^\mu\gamma^5)^T C = \gamma^\mu\gamma^5, \quad C^{-1} = C^\dagger = -C^*.
\tag{F.5}
$$

By using Eqs.(F.4, F.5), the following relation can be obtained[62].

$$
\bar{v}_i\gamma^\mu P_L v_j = v_j^T(\gamma^\mu P_L)^T \bar{v}_i^T = \bar{v}^c{}_j(-\gamma^\mu P_R)v_i^c
\tag{F.6}
$$

Further implementing the Majorana condition $v^c = v$, the contraction in the last line of Eq.(F.1) can be written as [60]

$$
\begin{aligned}
&\langle\Omega|b_N b_v\left(g_v\bar{v}\gamma^\mu P_L v\right)ZZ^\dagger\left(\bar{N}g_N\gamma^\mu N\right)b_N^\dagger b_v^\dagger|\Omega\rangle \\
&=\langle\Omega|b_N b_v\left(-g_v\bar{v}\gamma^\mu P_R v\right)ZZ^\dagger\left(\bar{N}g_N\gamma^\mu N\right)b_N^\dagger b_v^\dagger|\Omega\rangle,
\end{aligned}
\tag{F.7}
$$

which can be calculated just like the Dirac term. This leads to the Majorana neutrino version of amplitude Eq.(C.22)

$$
i\mathcal{M}_Z^{rr'ss'} = -\frac{i}{\sqrt{2}}G_F Q_W F(q^2)[\bar{u}_N^{r'}(p_{N_f})\gamma^\mu u_N^r(p_{N_i})][\bar{u}_v^{s'}(p_{v_f})(P_L - P_R)u_v^s(p_{v_i})]
$$

94

$$= \frac{\mathrm{i}}{\sqrt{2}} G_F Q_W F(q^2) [\bar{u}_N^{r'}(p_{N_f}) \gamma^\mu u_N^r(p_{N_i})][\bar{u}_\nu^{s'}(p_{\nu_f})(\gamma^\mu \gamma^5) u_\nu^s(p_{\nu_i})] \qquad \text{(F.8)}$$

This amplitude is different from the Dirac neutrino amplitude Eq.(C.22). However, neutrinos can almost be considered a chiral state due to their small mass. Therefore an additional P_L is included in the Majorana case, which equalizes the amplitude expressions [63] [64]. Although this derivation is given for Z exchange, the same procedure can be applied to the A' exchange case.

CURRICULUM VITAE

EDUCATION

■   Ph.D. in Physics   **September 2016 - January 2023**
Middle East Technical University

  – **Thesis Title:** Probing Signs of New Physics at Low Energies: The Neutrino
    Case

  – **Advisor:** Prof. Dr. Ismail Turan

■   M.Sc. in Physics   **September 2013 - September 2016**
Middle East Technical University

  – **Thesis Title:** Heavy Mesons in Heavy Quark Effective Theory

  – **Advisor:** Prof. Dr. Altuğ Özpineci

■   B.Sc. in Physics   **August 2009 - June 2013**
Middle East Technical University

  – **Graduation Project:** On the Current Situation of Gravitation Three Body Prob-
    lem

  – **Advisor:** Prof. Dr. Bayram Tekin

WORK EXPERIENCE

■   Teaching Assistant   **January 2015-ongoing**
Middle East Technical University

  Physics I & II (First-year courses for physics students)

– Recitations, tutoring and homework grading

General Physics Laboratory I & II (First-year laboratory courses for physics students)

– Course coordination, tutoring

Analytic Mechanics (Graduate level mechanics course for physics students)

– Recitations, tutoring and homework grading

RESEARCH INTERESTS

Neutrino Physics, Beyond Standard Model Physics, Flavor Physics

PUBLICATIONS

■ **A. Elpe**, E. Akyumuk, T.M. Aliev, L. Selbuz, and I. Turan, "Constraining non-minimal dark sector scenarios with the coherent neutrino scattering data," arXiv:2212.06861 [Preprint]

■ **A. Elpe**, E. Akyumuk, T.M. Aliev, L. Selbuz, and I. Turan, "Dark photon effects in the charge radius of neutrino" [In Preparation]

Schools, Workshops and Conferences

Presentations and Organizations:

■ Organizer of Hadron Physics Winter School, January 25-29 2016, Middle East Technical University (Ankara, Turkey)

■ "COHERENT Nötrino Saçılma Verileri ile Minimal Olmayan Karanlık Sektör Senaryolarının Kısıtlanması," Altuğ Elpe, İstanbul High Energy Physics Workshop, YEFIST2022, 24-25 September 2022

Attendance:

■ Ankara High Energy Physics Workshop, February 12-14 2015, Middle East Technical University (Ankara, Turkey)

- XHADRONS@ISTANBUL: International Workshop on Exotic Hadrons, September 3-5 2015 Mimar Sinan Fine Arts University (Istanbul, Turkey)

- Istanbul High Energy Physics Workshop, May 6-7 2017, Yıldız Technical University

- Quantum to Cosmos: Ideas and Applications, June 25- July 4 2019, Tusside (Gebze, Turkey)

TECHNICAL COMPUTATION, SIMULATION SKILLS

MATHEMATICA, OCTAVE, Python, TensorFlow, LaTeX